

**Development and application of WetQual-C, a mechanistic model for simulating carbon dynamics, GHG gas emissions and carbon export from wetlands**

by

Amirreza Sharifi

A dissertation submitted to the Graduate Faculty of  
Auburn University  
in partial fulfillment of the  
requirements for the Degree of  
Doctor of Philosophy

Auburn, Alabama  
May 3, 2014

Keywords: Wetland Modeling, Carbon and nutrient cycling,  
Dissolved organic carbon, Methane, Uncertainty Analysis, GLUE

Copyright 2014 by Amirreza Sharifi

Approved by

Latif Kalin, Chair, Associate professor of School of Forestry and Wildlife Sciences  
Mohamed M. Hantush, Senior research scientist, USEPA  
B. Graeme Lockaby, Professor of School of Forestry and Wildlife Sciences  
Christopher J. Anderson, Assistant professor of School of Forestry and Wildlife Sciences  
Puneet Srivastava, Professor of Biosystems Engineering

## Abstract

Wetlands possess qualities that distinguish them as the most important influencer of global carbon (C) budgets. They have the highest carbon density among all terrestrial ecosystems and are known as the greatest individual source of methane emission to the atmosphere. Because of this great influence, considerable scientific efforts have been invested in wetland models, with the objective of quantifying wetland C storage, turnover and carbon interchanges between wetland soils and atmosphere. This study, performed in three stages, was undertaken to advance the current state of wetland modeling by introducing a comprehensive mechanistic wetland carbon cycling model. In stage one, I developed and validated a process based model for carbon cycling in flooded wetlands, called WetQual-C. WetQual-C reflects various biogeochemical interactions affecting C cycling in flooded wetlands, and is capable of simulating the dynamics of organic carbon (OC) retention, OC export and greenhouse gas (GHG) emissions on the same platform. Using field collected data from a small wetland on the eastern shore of Chesapeake Bay, model performance was assessed and a thorough sensitivity and uncertainty analysis was carried out. Overall, the model performed well in capturing total organic carbon (TOC) export dynamics from the study wetland. Model results revealed that over a period of 2 years, the wetland removed or retained  $47 \pm 12\%$  of the OC carbon intake, mostly via OC decomposition and dissolved organic carbon (DOC) diffusion to sediment. In the second stage of this study, I

expanded WetQual model's spatial resolution through compartmentalization of the model, in order to capture the spatial variability of constituent concentrations in water and sediment of various zones in the wetland. The compartmental model was applied to data collected from a restored wetland in California's Central Valley during the 2007 growing season. The study wetland had a formation of a large stagnant zone at the southern end which constituted more than 50% of the wetland area. Mass balance analysis revealed that over the course of the study period, about  $23.4 \pm 3.9\%$  of the incoming total nitrogen (TN) load and  $21.1 \pm 4.4\%$  of the TOC load was removed or retained by the study wetland. It was observed that mass of all exchanges (physical and biogeochemical) regarding nitrogen and carbon cycling decreased along the activity gradient from active to passive zones of the wetland. In the third stage of this study, I further extended WetQual capabilities to simulate geochemical reactions in parts of the wetland that are not flooded (unsaturated wetland soil). To accomplish such goal, a comprehensive module for tracking soil moisture in wetland soil was implemented, and model relationships were updated to simulate geochemical reactions of nitrogen, carbon and phosphorus related constituents in unsaturated wetland soil. The developed model was applied to a small restored wetland located on Kent Island, Maryland. On average, the ponded compartment of the study wetland covered 65% of the total 1.2 ha area. Through mass balance analysis, it was revealed that denitrification in the unsaturated compartment of the study wetland was approximately 3 times higher than that of the ponded compartment ( $32.7 \pm 29.3$  kg vs.  $9.5 \pm 5.5$  kg) whereas ammonia volatilization in the unsaturated compartment was a fraction of that of ponded compartment.

## Acknowledgments

Completing this doctoral dissertation has been my most significant scientific achievement so far, and I wouldn't have been able to accomplish it without help and advice of many people. First and foremost, I'd like to express my deepest gratitude to my advisor, Dr. Latif Kalin who not only supported me scientifically, but offered me his wisdom and moral support through every step of this long expedition. My heartfelt appreciation goes to my committee member, Dr. Mohamed Hantush for his mentorship and invaluable contribution to this research. I am also thankful to other members of my dissertation advisory committee, Dr. Graeme B. Lockaby, Dr. Christopher J. Anderson and Dr. Puneet Srivastava for their support and valuable suggestions towards improving this research. My special thanks go to Dr. Sabahattin Isik for his sharing of knowledge and experience with me.

Several friends and colleagues made this journey enjoyable through their friendship and joyful conversations. My special thanks go to Rewati Niralua, Ruoyu Wang, Diane Alix, Dr. Vaishali Sharda, Navideh Noori, Hamed Majidzadeh, Dr. Sumit Sen, Flynt Barksdale, Dr. John Kush and Joseph D'Angelo for their encouragement and friendship.

I owe every bit of my success to my parents who have been a constant source of inspiration to me. They supported me through every step of my life with their passionate and unconditional love. It was through them that I learned to have high moral standards and to be sincere in my work. This dissertation is dedicated to them. My special thanks are due to my dearest brothers, Dr. Soroosh, Sadra and Sina Sharifi for being a big source of support and love for me.

Finally, and most importantly, I would like to thank my wife, Dr. Golbahar Mirhosseini, who has been my pillar of strength during this difficult endeavor. The past eight years of my life have been built upon her unwavering love, devotion, companionship and unconditional support.

*The U.S. Environmental Protection Agency through its Office of Research and Development partially funded and collaborated in the research described here under contract (EP08C000066) with Auburn University, School of Forestry and Wildlife Sciences.*

## Table of Contents

Abstract.....	ii
Acknowledgments.....	iv
List of Tables.....	xi
List of Figures.....	xii
1. Chapter 1: Introduction.....	1
1. Objectives of this study.....	3
2. Classifications of existing wetland carbon models.....	4
3. Greenhouse gas (CH <sub>4</sub> and CO <sub>2</sub> ) emission models.....	5
3.1 Allocation of available carbon substrate to microbial decomposition.....	6
3.2 Production of CO <sub>2</sub> and CH <sub>4</sub> .....	9
3.3 Aerobic and anaerobic oxidation of CH <sub>4</sub> .....	10
3.4 Transport processes governing CH <sub>4</sub> flux to atmosphere.....	11
4. Dissertation organization.....	12
2. Chapter 2: Carbon dynamics and export from flooded Wetlands: A modeling approach....	14
1. Introduction.....	15
2. Model description.....	16

2.1	Wetqual-C model.....	17
2.2	Mass balance equations .....	20
3.	Model assessment .....	31
3.1	Study area and input data.....	31
3.2	Numerical scheme verification.....	34
3.3	Uncertainty and Sensitivity assessment.....	35
4.	Results and discussion .....	41
4.1	TOC export.....	42
4.2	Methane emission.....	47
4.3	Carbon mass exchanges and exports .....	48
5.	Summary and conclusion.....	49
6.	Appendix.....	53
	Temperature dependence of reaction rates and coefficients.....	53
	Diffusive mass transfer coefficients.....	54
3.	Chapter 3: Capturing spatial variability of concentrations and reaction rates in wetland water and soil through model compartmentalization.....	56
1.	Introduction.....	57
2.	Compartmentalization approach .....	60
2.2	Updated compartmental model equations .....	70
2.3	Site description .....	75

2.4	Regression relationships for collected water quality data at the inlet .....	80
3.	Model application .....	84
4.	Model Assessment .....	86
5.	Results and discussion .....	87
5.1	Uncertainty analysis .....	88
5.2	Sensitivity Analysis .....	92
5.3	Mass balance Analysis.....	97
6.	Conclusion and summary.....	101
7.	Appendix.....	103
4.	Chapter 4: Modeling Nitrogen, Carbon and Phosphorus Dynamics in unsaturated wetland soils .....	108
1.	Introduction.....	109
2.	Modeling moisture redistribution in wetland soil.....	111
2.1	Richards Equation.....	112
2.2	Finite difference solution to Richard’s equation .....	114
2.3	Upper and lower boundary conditions.....	116
3.	Compartmentalization of unsaturated soil .....	117
4.	Updated relationships for N, P and C cycling in unsaturated wetland soil.....	121
4.1	Organic Nitrogen .....	122

4.2	Ammonia-N .....	123
4.3	NO <sub>3</sub> -N .....	123
4.4	Phosphorus.....	124
4.5	LPOC .....	124
4.6	RPOC.....	124
4.7	DOC.....	125
4.8	CH <sub>4</sub> .....	125
5.	Case study application .....	126
6.	Model Assessment .....	130
7.	Results and discussion .....	132
7.1	Soil moisture redistribution in Barnstable wetland .....	133
7.2	Sensitivity analysis .....	137
7.3	Mass balance analysis.....	141
8.	Summary and Conclusion.....	144
9.	Appendix.....	146
9.1	Intermediate nodes.....	146
9.2	Top node .....	147
9.3	Bottom node .....	149
5.	Chapter 5: Conclusions .....	151

1. Summary and Conclusions .....	151
1.1 Objective 1.....	151
1.2 Objective 2.....	152
1.3 Objective 3.....	153
2. Future research.....	154
6. References.....	156

## List of Tables

Table 1.1: Review of prominent wetland GHG emission models .....	7
Table 2.1: Wetqual-C model parameter definitions.....	25
Table 2.2: Model parameters with fixed values (i.e. constants) .....	26
Table 2.3: Model parameters considered random and their best estimates based on TOC export	39
Table 2.4: Rank correlation coefficients (%) of model outputs versus model parameters for methane emission.....	48
Table 3.1: Regression statistics and coefficient values generated by LOADEST for constituents inflowing to SJRW.....	82
Table 3.2: Average area, volume and depth of compartments C.1 to C.4 of SJRW .....	85
Table 3.3: Average model performances (MBE and Ens) for behavioral simulations based on observed and simulated concentrations .....	88
Table 3.4: Nitrogen budget in the study wetland. <sup>Y</sup> .....	97
Table 3.5: Carbon budgets in the study wetland <sup>Y</sup> .....	100
Table 4.1: Definition and dimension of new model parameters .....	126
Table 4.2: Average model performances (MBE and Ens) for behavioral simulations based on observed and simulated loadings (mass of export).....	133
Table 4.3: Assumed parameter values for Richard's equation .....	134
Table 4.4: Nitrogen budget in the study wetland.....	142
Table 4.5: Carbon budgets in the study wetland.....	144

## List of Figures

Figure 2.1: Conceptual model for carbon cycling in flooded wetlands.....	18
Figure 2.2: Study wetland and its watershed outlined by dashed lines (regenerated from Jordan et al., 2003).....	33
Figure 2.3: Top panel: Hydrology of Barnstable wetland during study period. Bottom panel: Measured concentration of TOC inflow (mg/L) to wetland over the study period. ....	35
Figure 2.4: Stepwise flowchart to GSA/GLUE methodology applied in this study.....	38
Figure 2.5: Top: Summary of the K-S test and order of sensitivities based on TOC export for the whole study period.....	44
Figure 2.6 :Model generated 95% prediction interval (P.I.) from 100,000 MC simulations versus field observations.....	45
Figure 2.7: Dotty plot exhibiting ENS vs. MBE. The relative scatterings of dots over the graph reveal non-independence of the two performance criteria.....	47
Figure 2.8: Carbon net mass exchanges and export in study wetland over year 1, year 2 and the whole simulation period.....	50
Figure 3.1: A hypothetical wetland, catalogued to a number of compartments with varying depths.....	59
Figure 3.2: A schematic plan of a compartmentalized wetland.....	61
Figure 3.3: A schematic representation of a simple wetland with 4 compartments.....	63
Figure 3.4: direction of interval advective exchanges between compartments when the water level is rising (left panel) and falling (right panel).....	64
Figure 3.5: Schematic illustration of three adjacent compartments and concept of effective diffusion/dispersion parameter.....	66
Figure 3.6: Study wetland located on west side of the San Joaquin River in California’s Central Valley.....	76
Figure 3.7: Graphical demonstration of the hydrologic regime (inflow/outflow) and volume of SJRW during growing season of 2007.....	78
Figure 3.8: Grab sample concentrations of inflowing constituents to SJRW during the study period (n=19). ....	79
Figure 3.9: Prediction intervals of regression models established for NO <sub>3</sub> -N (top) and TSS (bottom) at 95% confidence level.....	84

Figure 3.10: Compartmentalized study wetland. ....	85
Figure 3.11: Model generated 95% prediction intervals (P.I) from 100,000 MC simulations versus observed concentrations of NO <sub>3</sub> for compartments C.1 to C.4.....	89
Figure 3.12: Model generated 95% prediction intervals (P.I) from 100,000 MC simulations versus observed concentrations of TN for compartments 1 to 4. ....	90
Figure 3.13: Model generated 95% prediction intervals (P.I) from 100,000 MC simulations versus observed concentrations of TOC for compartments 1 to 4.....	91
Figure 3.14: Summary of the K-S test and order of sensitivities based on TN export for compartments C.1 to C.4 .....	94
Figure 3.15: Summary of the K-S test and order of sensitivities based on TOC export for compartments C.1 to C.4 .....	96
Figure 4.1: Schematics of a hypothetical seasonally flooded wetland .....	111
Figure 4.2: Spatial and temporal discretization of Richard’s Equation .....	116
Figure 4.3: Schematic representation for new Sat/Unsat compartmentalization scheme .....	118
Figure 4.4: Study wetland and its watershed outlined by dashed lines. ....	128
Figure 4.5: % Area covered by ponded compartment in Barnstable wetland over study period	129
Figure 4.6: Hydrology of the study wetland (inflow, outflow and average water depth in ponded compartment) in addition to inflow concentrations of TOC, NH <sub>4</sub> , NO <sub>3</sub> , TSS and inorganic P from May 1995 to May 1997.....	131
Figure 4.7: Average soil moisture content in unsaturated compartment of Barnstable wetland +daily precipitation records (top) along with average depth of water in the ponded compartment (bottom) .....	135
Figure 4.8: Simulated soil moisture profile in the banks of Barnstable wetland (top) in addition to evapotranspiration rate and precipitation records (bottom) during first two weeks of study period. ....	136
Figure 4.9: Summary of the K-S test and order of sensitivities based on NH <sub>4</sub> loading for ponded and unsaturated compartments (top) and Lumped model.....	138
Figure 4.10: Summary of the K-S test and order of sensitivities based on NO <sub>3</sub> loading for ponded and unsaturated compartments (top) and Lumped model (bottom, borrowed from Kalin et al., 2013) .....	139

Figure 4.11: Summary of the K-S test and order of sensitivities based on TOC loading for ponded and unsaturated compartments (top) and Lumped model (bottom, borrowed from Chapter 2 ) ..... 140

Figure 4.12: The procedure for selecting top boundary conditions through the iterative solution of the Richards equation (van Dam and Feddes, 2000)..... 147

## Chapter 1: Introduction

Wetlands are environments characterized with waterlogged soils and biota adapted to saturated soil conditions. They are found in almost every climate and continent (with the exception of Antarctica) and are recognized for their unique role in regulating global biogeochemical cycles (Reddy and DeLaune, 2008). In the context of global biogeochemical budgets, it is the carbon (C) cycle that wetlands influence the most. Because of high productivity and slow decomposition rates, wetlands have the highest soil carbon density among all terrestrial ecosystems (Kayranli et al., 2010). Despite covering less than 8% of the terrestrial land surface (Aselmann and Crutzen, 1989; Mitsch and Gosselink, 2007), wetlands are the greatest individual source of methane emission to the atmosphere (Walter and Heimann, 2000). Wetland methane emissions have been estimated about 100-231 Tg CH<sub>4</sub> yr<sup>-1</sup> which accounts for 17% to 40% of the global (anthropogenic + natural) methane emissions annually (Denman et al., 2007). Influence of wetlands on global carbon balance is not limited to sequestering atmospheric carbon and emitting greenhouse gasses. When hydrologically connected to surface flow, wetlands export carbon in the form of dissolved and particulate organic material (DOM and POM) to receiving waters (Reddy and DeLaune, 2008), acting as primary sources of humic substances to freshwater aquatic systems (Stern et al., 2007; Ziegler and Fogel, 2003). Much of the organic material exported from wetlands eventually reach oceans and it is estimated that 15% of the terrestrial organic matter flux to the oceans originate from wetlands (Hedges et al., 1997; Tranvik and Jansson, 2002).

Wetlands are widely referred to as “the kidneys of the catchment” due to their effectiveness in trapping sediment and nutrient loadings from surface waters (Mitchell, 1994; Mitsch and

Gosselink, 2007). But the fact that wetlands can be net exporters of organic carbon (OC) potentially offsets their purifying benefits. Discharge of carbon from wetlands can result in water quality degradation with the release of dissolved organic carbon (DOC), also known as water color (Worrall et al., 2003). At high concentrations, DOC reacts with chlorine during drinking water treatment to form carcinogenic disinfection byproducts (Chow et al., 2003). Also because of its hydrophobic nature, DOC is shown to be a medium of transport for other pollutants such as nutrients and heavy metals (Canário et al., 2008; Steinberg, 2003).

Because of the great influence of wetlands on global C cycling, and specifically considering the significant impact of greenhouse gas (GHG) emissions from wetlands on global warming, considerable scientific efforts have been invested in quantifying wetland C storage, turnover, and exchanges between wetland soils and atmosphere. Wetland models have provided powerful tools for quantifying these budgets where field studies were not practical or projections for future budgets were called for. Various C cycling models have been developed for wetlands over the past three decades (Mitsch et al., 1988). Although these models varied in scale of application (temporally and spatially), complexity and approach (empirical vs. physically based) they all roughly targeted similar objectives. These objectives were to 1) synthesize our knowledge of complex interactions between wetland soil, hydrology and vegetation; and 2) assess, quantify and predict impacts of climate change or management alternatives on C dynamics in wetlands (Cui et al., 2005; Zhang et al., 2002).

## 1. Objectives of this study

After studying existing wetland C cycling models, we noticed important shortcomings in existing models and gaps that were not properly addressed by current models. For example, many of the existing wetland carbon cycling models focus on a single end product of the carbon cycle that is either CH<sub>4</sub>/CO<sub>2</sub> production or OC deposition (peat accumulation) and do not consider all the processes/interactions of the C cycle on the same framework. Another example is that all existing models ignore the effects of thin oxidized zone at wetlands soil-water interface and the oxidation-reduction reactions taking place within that zone. Moreover, we noticed that hydrologic export of organic C from natural wetlands was missing from previous modeling efforts.

Given the facts above, **the first objective** of this study was to advance the current state of wetland modeling by introducing a computationally simple – yet comprehensive – mechanistic wetland carbon cycling model that reflects various biogeochemical interactions affecting C cycling in flooded wetlands, and is capable of simulating the dynamics of OC retention, OC export and GHG emissions on the same platform. Development, application and validation of such a model, which was later named WetQual-C is explained in Chapter 2.

The second objective aimed to address another important limitation of existing wetland biogeochemical models. Most models are lumped in the horizontal plain, considering uniform concentrations and reaction rates throughout wetland water and soil. This limitation prevents demonstration of spatial variability of concentrations in water and sediment of various biogeochemical zones (active and passive zones) of the wetland. Accordingly, **the second objective** of this study was to improve WetQual's spatial resolution in the horizontal domain (x-

y plain) through compartmentalization, therefore enabling it to capture the spatial variability of hydrology and geochemical reactions along different zones of the wetland. Chapter 3 explains the methodology behind compartmentalization and case study application of the compartmentalized model.

The third objective aimed to expand our model's abilities to simulate dynamics of carbon pools in wetland soil through different hydroperiods. As mentioned earlier, WetQual-C was developed to model dynamics of C cycling in flooded wetlands, meaning that existence of a standing pool of water was a requirement. Accordingly, **the third objective** of this study was to enhance the domain of our model in order to make it applicable to unsaturated wetland soils. The methodology and case study application regarding this objective is presented in Chapter 4.

## **2. Classifications of existing wetland carbon models**

Existing wetland C models can generally be classified into various categories based on the final specific product of the C cycle that they are geared to simulate. These categories can be confined to long term-peat accumulation related models, greenhouse gas (CH<sub>4</sub> and CO<sub>2</sub>) emission models and wetland OC turnover and export models. Models falling into the last category are more or less specific to treatment wetlands (e.g. King et al., 2003; Penha-Lopes et al., 2012 and Stern et al., 2007). Wetland GHG emission models have received the most attention among all categories in recent years. In the sections to follow, we look into GHG emission models in detail and analyze characteristics (required inputs, pools of C, processes, etc.) of such models. In this review, the focus will be on mechanistic (processed based) models only, as the objective of this research is to develop a process based model.

### **3. Greenhouse gas (CH<sub>4</sub> and CO<sub>2</sub>) emission models**

“Greenhouse effect” is a term that is often heard when carbon cycling in wetlands is discussed. In recent years, wetland GHG emission models have received the greatest attention among different categories of wetland C models. As methane is known to have a much higher global warming potential (GWP<sub>M</sub>) compared to CO<sub>2</sub> (25:1 in 100 years; IPCC, 2007), in most models of such type, the main focus is on CH<sub>4</sub> production and emission rather than CO<sub>2</sub>.

In this review, we examine 7 prominent models in this category, and compare how they simulate different important processes related to GHG emissions from wetlands (Table 1.1). These 7 models were selected from a larger pool of GHG related models, and identified prominent based on expert judgment and number of citations. All of these models are process-based to varying extents; however, some level of dependency on empirical parameterizations exists within all of them, and they call for differing amounts of input data (Wania, 2007). As mentioned earlier, CO<sub>2</sub> production is not a priority in these models, and in some cases, there is no specific pool assigned to CO<sub>2</sub> in the model’s structure.

In wetlands, GHG emission to the atmosphere is a balance between GHG production, oxidation and transport within the soil and water (Bradford et al., 2001; 2000; Reddy and DeLaune, 2008; Wania et al., 2010). Therefore, to capture these complicated interactions correctly, the following key processes have to be represented in a proper mechanistic model: 1) Allocation of available carbon substrate to aerobic decomposition and methanogens, 2) production of CO<sub>2</sub> and CH<sub>4</sub>, 3) aerobic and anaerobic methane oxidation, and 4) transport processes governing GHG flux from soil into the water column and to the atmosphere (Wania, 2007, Reddy and Delune, 2004).

### **3.1 Allocation of available carbon substrate to microbial decomposition**

Biotic decomposition of organic matter is a process where microorganisms obtain energy from degradation of organic molecules, resulting in the production of carbon dioxide and methane. To simulate CH<sub>4</sub> and CO<sub>2</sub> production, the common practice among wetland C models is to first determine a potential pool of organic material suitable for microbial decomposition (Wania et al., 2010). This pool mainly consists of root exudates, easily degraded plant material and less recalcitrant soil organic material. Depending on the level of complexity, models account for different classes of organic C substrate that make up the potential pool suitable for microbial decomposition. For instance in Wetland DNDC (Zhang et al, 2002; Cui et al., 2005), available carbon substrate to microbial decomposition is comprised of 7 pools: Very labile litter, labile litter, resistant litter, labile microbes, resistant microbes, labile humads and resistant humads. Having 7 pools to represent available substrate for decomposition can be more problematic than beneficial. First, having too many state variables in a model adds to prediction uncertainty. Second, it is very difficult (if not impossible) to distinguish between these pools through laboratory experiments, thus there is no way to verify model performance on simulation of such pools.

Many models have a layered soil structure (e.g. Wania et al., 2010, Tang et al., 2010). In such models, once this potential pool is allocated, it is distributed over all soil layers, weighted by the root distribution. More carbon is allocated to the top layers where root density is greatest compared to lower layers (Wania et al., 2010).

Table 1.1: Review of prominent wetland GHG emission models

	Cao et al. (1996) WMEM	Walter et al. (1996, 2001)	Potter (1997) CASA	Cui et al. (2005) Wetland DNDC
<b>Input data</b>	Climate data Vegetation distribution Soil characteristics	Precipitation - Soil temperature Soil and rooting depths Quality of plant-mediated transport	Climate data Satellite imagery (for estimating NPP)	Climate data Hydrologic data (inflow-outflow rates) - Soil specifications Vegetation parameters
<b>C pools</b>	Vegetation Soil Decomposed C CH <sub>4</sub>	CH <sub>4</sub> Vegetation	Leaf litter - Root Litter Microbes SOM CH <sub>4</sub> and CO <sub>2</sub>	Labile and resistant litter, microbes & humads passive humus - CH <sub>4</sub> -CO <sub>2</sub>
<b>Layering of soil</b>	Soil column is lumped	Soil column is divided into 1 cm thick parallel layers	Wetland soil profile is layered with depth into a surface ponded layer, a surface organic layer, a surface organic mineral layer, and a subsurface mineral layer	Soil profile is divided into layers of different characteristics (e.g. organic and mineral soils). The soil layers are then grouped into two zones of unsaturated zone above the water table and the saturated zone below it
<b>Water table</b>	Fixed at 0.1 m above the soil surface in inundated areas. Model calculates water table position for non-inundated tundra	Seasonal variations of the water table are simulated using a hydrological sub-model	water table is simulated daily as a function of moisture inputs and field capacity of poorly drained soil	Model explicitly simulates water table dynamics. The soil moisture content is determined for the unsaturated and the saturated zones separately. Water table data can also be used as input directly.
<b>Plant Productivity</b>	Net primary productivity (NPP) imported from TEM (Raich et al., 1991)	NPP imported from BETHY (Knor et al., 2001)	NPP is estimated using Normalized Difference Vegetation Index (NDVI) derived from high Resolution satellite images.	NPP is simulated in the plant growth module of the model (Zhang et al., 2002)
<b>CH<sub>4</sub> production</b>	Depending on temperature and water table position, a fraction of the decomposed carbon pool is turned into methane.	Methane production is simulated based on seasonal availability of OC and temperature	The ratio of carbon dioxide production from decomposition to methanogenesis is governed by location of water table	Methane production occurs in all soil layers if environmental conditions are favorable. CH <sub>4</sub> production is a function of C substrate availability and adjusted for effects of temperature, pH, and redox potential.
<b>CH<sub>4</sub> oxidation</b>	CH <sub>4</sub> oxidation is set to a minimum of 60% and a maximum of 90% depending on growth stage	Only occurs in soil layers above the water table position, with rates adjusted based on temperature and methane availability in soil	Potential oxidation is a function of water table position. There is no methane oxidation if the water table is above the surface.	Methane oxidation is controlled by the CH <sub>4</sub> concentration, redox potential, and temperature
<b>CH<sub>4</sub> transport</b>	Not simulated	Mechanistically simulates methane transport pathways of diffusive flux, ebullition and plant mediated transport	Simulates molecular diffusion, ebullition, and plant vascular transport	The CH <sub>4</sub> diffusion process is estimated with empirical relationships. Ebullition emission is considered when the soil CH <sub>4</sub> concentration exceeded a threshold concentration. Plant-mediated emission is estimated based on the plant aerenchyma factor.

Table 1.1 (Continue): Review of prominent wetland GHG emission models

	Tang et al. (2010) TEM	Li et al. (2010) CH <sub>4</sub> MODwetland	Wania et al. (2010) LPJ-WHyMe
Input data	Climate data Soil temperature Vegetation & soil characteristics Soil characteristics	Daily soil or air temperature Standing water depth Soil properties Plant growth related controls	Climate data Atmospheric CO <sub>2</sub> concentrations
C pools	CH <sub>4</sub> - CO <sub>2</sub> Soil organic matter (SOM)	SOM -CH <sub>4</sub> Root litter and Root exudates C Above ground litter C	Litter C - Fast reacting C pool in soil Slow reacting C pool in soil Potential C for methanogenesis CH <sub>4</sub> and CO <sub>2</sub>
Layering of soil	Soil is separated into anaerobic and aerobic zones by water table position. The soil profile is further divided into 1-cm layers for simulation	Soil is lumped into a single layer	Soil is divided to several layers vertically with varying thicknesses.
Water table	Water table is either simulated within the hydrological module (HM) of TEM at monthly temporal resolution or observed data is used. (Zhuang et al., 2002, 2004)	Model is applicable only to ponded wetlands, and standing water depth is an input to model.	Water table levels are simulated by model using a simple mass balance equation
Plant Productivity	The scaled NPP data are simulated within TEM, driven with monthly climate data	Employs a logistic growth equation, as used in CH <sub>4</sub> MOD (Huang et al., 2004) Both plant growth and senescence are temperature dependent	Uses an updated version of an NPP submodel presented in LPJ model (Sitch et al., 2003)
CH <sub>4</sub> production	Maximum CH <sub>4</sub> production is calculated as function of methanogenesis substrate availability, soil temperature, pH value and redox potential. Methane production is adjusted according to oxygen concentration in soil	CH <sub>4</sub> Production rates are determined by the availability of methanogenic substrates from root exudates, above-and below-ground plant litter as well as soil organic matter. CH <sub>4</sub> production is controlled by PH and temperature	Potential carbon pool for methanogens is created and distributed over all soil layers, weighted by the root distribution. The pool is then split into CO <sub>2</sub> and CH <sub>4</sub> based on oxygen availability
CH <sub>4</sub> oxidation	CH <sub>4</sub> oxidation modeled as a function of soil temperature, soil moisture, redox potential, oxygen availability and CH <sub>4</sub> concentration	Only considers the oxidation through plant transport.	Model assumes that if enough oxygen is available, all of the methane is oxidized. If less oxygen is available than required, then all of the oxygen is used up in oxidizing methane.
CH <sub>4</sub> transport	Revised TEM to consider effects of hydrostacy on ebullition. Also considers methane diffusion and plant-aided transport.	Model considers ebullition and plant mediate transport, however CH <sub>4</sub> diffusion is not considered.	Processes of Ebullition, Transport through aerenchyma and diffusion are modeled mechanistically.

### 3.2 Production of CO<sub>2</sub> and CH<sub>4</sub>

Final step of decomposition is the process where heterotrophic microorganisms assimilate simpler organic substrate, oxidize them and produce CO<sub>2</sub> and methane. In the water column and to the top thin layer of surface soil, where oxygen is present, aerobic microbes dominate decomposition and release CO<sub>2</sub>. In lower sediment layers where oxygen is unavailable, dominant microbial groups are anaerobes. Depending on availability of oxidants (electron acceptors such as  $NO_3^-$ ,  $Mn^{4+}$ ,  $Fe^{3+}$ ,  $SO_4^{2-}$ ) in wetland soil, different groups of anaerobes oxidize organic substrate and release carbon dioxide. Methanogenesis only occurs when all other electron acceptors are exhausted in soil (Mitsch and Gosselink, 2007).

A common method for simulating production of CO<sub>2</sub> and CH<sub>4</sub> is to first define a maximum production rate and then adjust this rate according to different environmental factors. Among these factors, temperature and position of water table have been always present. Temperature is a key regulator influencing biogeochemical processes, as reactions concerning organic substrate decomposition progress at a faster pace as the temperature is increased (Reddy and Delune, 2004). Position of water table controls the break between aerobic soil and anaerobic soil. Presence of water in wetland soil limits the availability of oxygen; therefore, decomposition occurs at a much slower rate in anaerobic soil, with methanogens dominating once all other electron acceptors are exhausted. Soil redox potential acts as a surrogate for soil aeration status and availability of other oxidants. Thus, instead of tracing oxygen and electron acceptors concentrations, models commonly use simulated redox potential as a balancing factor for methane production. For instance in TEM model (Zhuang et al., 2004), methane production is

limited to soils with redox potentials below  $-100$  mV. Redox potential itself is simulated as a function of water table position, root distribution and fraction of water-filled pore space.

pH is another factor employed in some models for limiting methanogenesis rates (Zhuang et al., 2004; Li et al., 2010; Cui et al., 2005). In TEM model, methane production is optimum at pH = 7.5, and methanogenesis is limited to an observed pH range of 5.5 to 9.0.

### **3.3 Aerobic and anaerobic oxidation of CH<sub>4</sub>**

Wetland soils that are aerated to an extent may be hosting aerobic methanotrophs, which consume methane as a carbon energy source, and release CO<sub>2</sub> (Reddy and Delune, 2004). The methanotrophic activity directly depends on oxygen concentration in soil; therefore, aerobic oxidation of methane only occurs in the surface oxic–anoxic boundary or within rhizosphere where oxygen is transported from the plant to its roots. Wetland C models have handled aerobic methane oxidation more or less in a similar fashion. If the oxygen concentration is simulated within model, it is used to quantify how much methane could potentially be oxidized within standing water and soil layers. If not, CH<sub>4</sub> oxidation rate is quantified based on simulated redox potential or water table position, where there would be no methane oxidation if the water table is above the surface (Potter et al., 1997).

Another recently discovered process that acts as a sink for methane is anaerobic oxidation of methane in wetland soil (Raghoebarsing et al., 2006). In this process, which is also referred to as denitrification, methane is oxidized to carbon dioxide via microorganisms that use nitrate as an electron acceptor. None of the reviewed models consider this process.

### **3.4 Transport processes governing CH<sub>4</sub> flux to atmosphere**

Methane is transported to atmosphere via three different pathways of 1) plant aided diffusive exchange 2) molecular diffusion 3) ebullition (Mitch and Gosselink, 2007; Reddy and Delune, 2008).

Methods employed by wetland models concerning CH<sub>4</sub> transport processes have been evolving over time. In simpler models, these processes are not considered; and all the produced methane that isn't oxidized would be released to the atmosphere directly (Cao et al., 1996). However, most models concerning GHG emission from wetlands do consider methane transport processes, but with varying levels of complexities.

Vascular plants adapt to flooded environment by delivering oxygen to their roots via aerenchyma. Plant aerenchyma, consisting of any tissue that contains large, air-filled intercellular space, not only deliver oxygen to the roots, but also establish direct canals for transport of methane and carbon dioxide from the soil to the atmosphere. The flux of gases transported via aerenchyma is a function of internal structure of the plant (openings of the aerenchyma, rooting depth and density) and total gas pressure gradients between soil and atmosphere. In most cases, plant mediated transport is modeled similar to a diffusive flux, forced by gas pressure gradients between soil and air, and mediated by specific conductivity of root system, seasonal root length density in soil and diffusivity of methane.

The most challenging process to model is ebullition of gas bubbles. When methanogenesis rate surpasses diffusion rate, concentration of methane increases to the point that methane bubbles are formed. Ebullition, the process of abrupt elimination of these bubbles, is not instant. Rather, some type of disturbance is required to trigger ebullition. The disturbance can be a simple

alteration in atmospheric or hydrostatic pressure, temperature, or a sudden influx of flow (Bade, 2009). Often times, ebullition is modeled as a threshold phenomenon (Tang et al., 2010), i.e. when methane concentration surpasses some universally prescribed threshold, the amount of methane in excess of that threshold concentration is released to the atmosphere (e.g. Wania et al., 2010; Cao et al., 1995; Kellner et al., 2006; Zhang et al., 2002). The most complex development regarding ebullition modeling is the work of Tang et al. (2010). Tang et al. (2010) state that “the ebullition threshold defined in terms of gas volumes is fuzzy rather than deterministically predictable because of possible re-dissolution and gas entrapping, during the course of ebullition”. To overcome the randomness of re-dissolution and gas entrapping, and to reflect effects of other substances on composition of gas bubbles in wetland soil, Tang et al. (2010) proposed a probabilistic pressure based algorithm in a four substance system (CH<sub>4</sub>, O<sub>2</sub>, CO<sub>2</sub> and N<sub>2</sub>).

#### **4. Dissertation organization**

This dissertation is organized according to the following framework. Chapter 1 delivers an introductory overview motivating this research, presents the research objectives and provides a review of existing prominent wetland GHG emission models. Chapter 2 provides the methodology, case study application and verification of WetQual-C, the process based model for carbon cycling in flooded wetlands which was developed in response to objective 1. This chapter has been accepted for publication in Ecological Modelling journal (Sharifi et al., 2013). Chapter 3 explains the structure, parameterization and validation of the compartmentalized wetland model, developed in response to the second objective of this study. Following objective 3 of this study, chapter 4 presents the development and application of an updated wetland model, capable

of simulating dynamics of carbon pools in wetland soil under unsaturated conditions. Finally, Chapter 5 provides a summary of the entire research, and concludes the major findings through this study.

## **Chapter 2: Carbon dynamics and export from flooded Wetlands: A modeling approach**

### ***Abstract***

Described in this chapter is development and validation of a process based model for carbon cycling in flooded wetlands, called WetQual-C. The model considers various biogeochemical interactions affecting C cycling, greenhouse gas emissions, organic carbon export and retention. WetQual-C couples carbon cycling with other interrelated geochemical cycles in wetlands, i.e. nitrogen and oxygen; and fully reflects the dynamics of the thin oxidized zone at the soil-water interface. Using field collected data from a small restored wetland receiving runoff from an agricultural watershed on the eastern shore of Chesapeake Bay, we assessed model performance and carried out a thorough sensitivity and uncertainty analysis to evaluate the credibility of the model. Overall, the model performed well in capturing TOC export fluctuations and dynamics from the study wetland. Model results revealed that over a period of 2 years, the wetland removed or retained  $47 \pm 12\%$  of the OC carbon intake, mostly via OC decomposition and DOC diffusion to sediment. The study wetland appeared as a carbon sink rather than source and proved its purpose as a relatively effective and low cost means` for improving water quality.

## 1. Introduction

Wetlands only cover a small fraction of the terrestrial land surface (less than 8%); however, they possess qualities that characterize them as the most important influencer of the global C budgets . Wetlands are the greatest single source of methane emission to the atmosphere, they contain one third of the terrestrial soil carbon globally and act as a primary source of humic substances to freshwater aquatic systems (Walter and Heimann, 2000; Stern et al., 2007; Ziegler and Fogel, 2003). On an account of the facts mentioned above, considerable scientific efforts have been devoted to building wetland C models over the past three decades (Mitsch et al., 1988). The biogeochemical processes in wetlands are the most complex of all ecosystems in terms of carbon dynamics and greenhouse gas emissions. This is due to involvement of highly mobile microbial communities and complicated physical processes involving carbon dioxide and methane transport in an often mobile liquid environment (Lloyd, 2013). For the stated reason, biogeochemical models concerning wetlands demand higher levels of sophistication compared to models of other ecosystems. Wetland models have served scientists as powerful apparatuses for quantifying wetland C storage, turnover, hydrologic exports and carbon exchanges between wetland soils and atmosphere. A full review of wetland GHG emission models was provided in chapter 1.

In Chapter 1, we demonstrated the shortcomings of existing wetland C cycling models and pointed to gaps that are not addressed properly in current models. As stated earlier, many of the existing wetland water quality models focus on a single end product of the carbon cycle, i.e. methane production or OC deposition. It was pointed out that hydrologic export of organic C from natural wetlands was the missing chain of previous modeling efforts. Dissolved and

particulate organic matter exported from wetlands react with chlorine during drinking water treatment to form carcinogenic disinfection byproducts (Chow et al., 2003). Also because of its hydrophobic nature, DOC is shown to be a medium of transport for other pollutants such as nutrients and heavy metals (Canário et al., 2008; Steinberg, 2003).

The purpose of this chapter is to develop a physically based model for carbon cycling and methane production in flooded wetlands. In this study, we aim to advance the current state of wetland modeling by introducing a computationally simple – yet comprehensive – mechanistic wetland carbon cycling model. The proposed model in this study reflects various biogeochemical interactions affecting C cycling in wetlands, and is capable of simulating the dynamics of OC retention, OC export and CH<sub>4</sub> emissions. What makes this model special is the fact that it is coupled with other interrelated geochemical cycles (i.e. nitrogen and oxygen) and fully reflects the dynamics of sediment-water interactions in flooded wetlands. Another unique aspect of the developed model is its approach towards modeling the formation of the thin oxidized zone at wetlands soil-water interface and the oxidation-reduction reactions taking place within that zone (Mitsch and Gosselink, 2007; Reddy and DeLaune, 2008; Hantush et al., 2013). We perform a thorough sensitivity and uncertainty analysis on model components to validate its credibility using field collected data from a small restored wetland that receives runoff from an agricultural land. In the following sections of the paper, we describe the structure of the model and the methodology on model assessment. Finally the results are presented and discussed.

## **2. Model description**

WetQual-C model is an extension to WetQual model, a previously developed wetland nutrient cycling model (Hantush et al., 2013). WetQual is a process based model for nitrogen and

phosphorus retention, cycling, and removal in flooded wetlands. The model simulates oxygen dynamics and the impact of oxidizing and reducing conditions on nitrogen transformation and removal as well as phosphorus retention and release. WetQual explicitly accounts for nitrogen loss pathways of volatilization and denitrification. The model separates free floating plant biomass (e.g., phytoplankton) from rooted aquatic plants and uses a simple model for productivity in which daily growth rate is related to daily solar radiation and annual growth rate of plants.

## **2.1 Wetqual-C model**

In developing WetQual-C, we followed the same compartmental structure as WetQual, where a wetland is partitioned into two basic compartments; the water column (free-water) and wetland soil layer. The soil layer is further partitioned into a generalized model of aerobic and anaerobic zones where the boundary between the two zones fluctuates up or down based on competing oxygen supply and removal rates. To reflect the complex cycling of organic matter and methane production in flooded wetlands, it was necessary to posit several organic and inorganic carbon pools within WetQual-C model. As can be viewed in Figure 2.1, two pools for particulate organic carbon (POC) are considered in the model, one representing fast reacting, easily degradable organic material (e.g. non-humic substances, carbohydrates) and the other describing recalcitrant, slow reacting solids (e.g. phenolic and humic substances). The former pool is called labile particulate organic carbon (LPOC) and the latter pool is referred to as refractory particulate organic carbon (RPOC). A third organic pool represents dissolved organic carbon (DOC). The Model allows for allochthonous sources (hydrologic loads) and autochthonous sources to contribute to all three organic pools. If the wetland is hydrologically connected to surface flow,

or is intended as means for treating water, a significant amount of external organic C can be transferred into the system via incoming flow, originating from point sources (e.g. sewage pipes) or diffuse source upland areas (e.g. agricultural fields). An internal source for DOC and POC includes plant matter from emergent macrophytes, algal mats and litter fall from trees in forested wetlands.

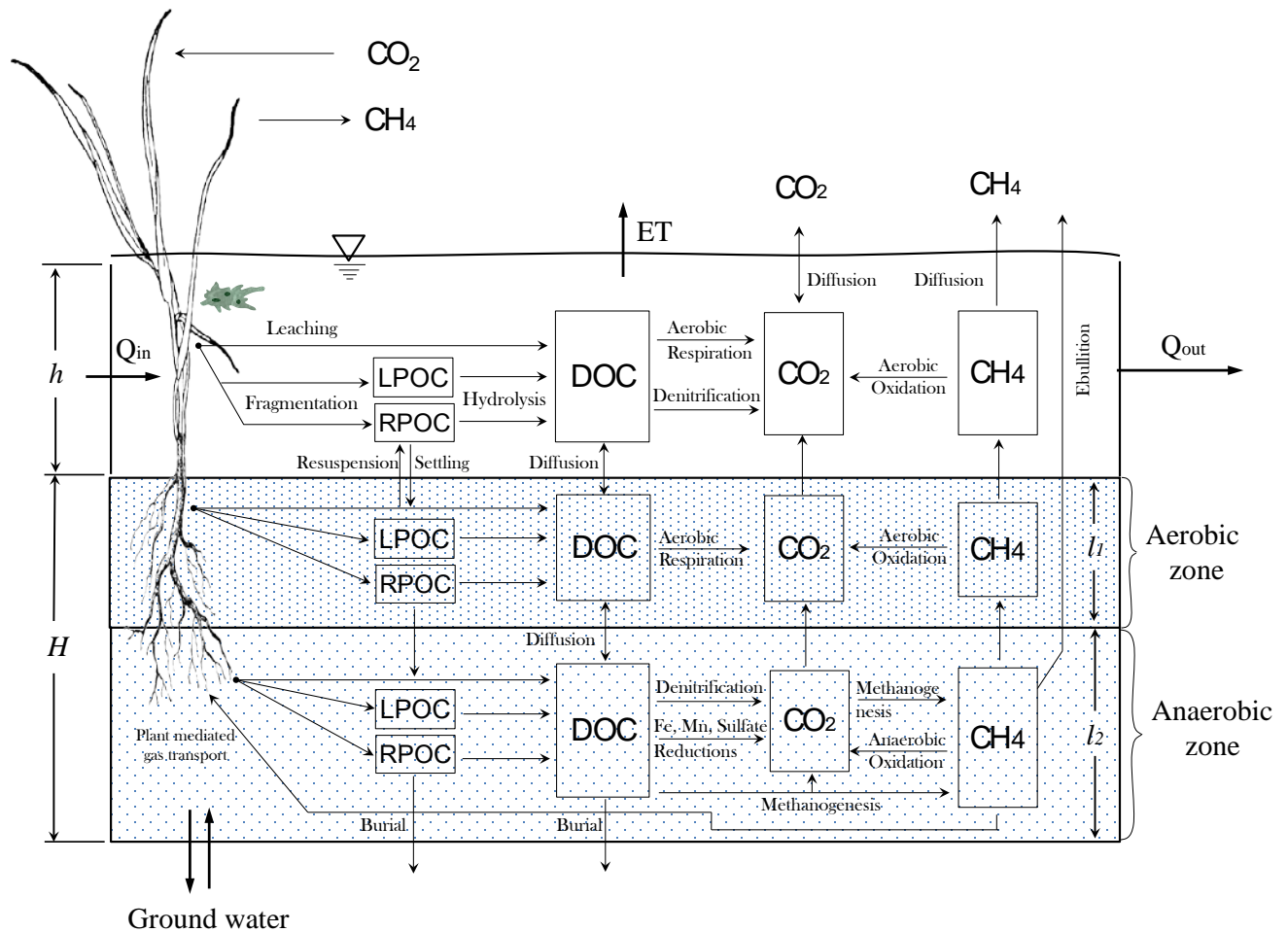


Figure 2.1: Conceptual model for carbon cycling in flooded wetlands.

A stepwise conversion process is considered in the model to portray all stages of plant turnover and OM decomposition. When plants senesce, part of their biomass leaches out physically in form of water soluble – highly labile – organic compounds (Reddy and DeLaune, 2008). Within

each compartment in the model (water and sediment), this portion of the biomass is directly added to the DOC pool. Rest of the biomass (detritus) is fragmented between LPOC and RPOC pools with split ratios depending on type of plant and quality of detritus. Parts of the plants with higher biodegradability and low in lignin content are directed to the LPOC pool, whereas more stable fragments, such as conductive and supportive tissue cells, are allocated to RPOC pool. In a process called hydrolysis, complex high molecular-weight organic matter is broken down into smaller and simpler compounds. This process is mediated by extracellular enzymes released by microorganisms (bacteria and fungi) living in soil and on the surface of plants. In the model, hydrolysis process affects LPOC and RPOC pools, such that they gradually decay and turn into DOC. In the model, LPOC and RPOC hydrolysis rates are temperature dependent, however, on average, LPOC hydrolysis rate is about 10 times faster than RPOC in the model (Cerco and Cole, 1995; Reddy and DeLaune, 2008). This difference makes RPOC in water column more prone to settling and burial whereas LPOC can decompose partly in water. In natural wetlands, burial is a potential loss pathway caused by net sedimentation. This important process might have significant long-term impact on OC mass balance (e.g., at the annual time scale or decades). Burial is considered in WetQual-C by moving the water-soil interface upward. In other words, both particulate and dissolved pore-water constituents are moving downward with a velocity equal to the burial rate relative to an upward moving soil water interface.

At the last step of decomposition, simpler organic compounds are assimilated, oxidized and turned into inorganic molecules, mainly CO<sub>2</sub>, by heterotrophic microorganisms. In the water column and the aerobic sediment layer, where oxygen is abundant, aerobic heterotrophs dominate decomposition and release CO<sub>2</sub>. In the anaerobic sediment layer and in the absence of oxygen, dominant microbial groups are anaerobes. Depending on availability of electron

acceptors (oxidants) in wetland soil (e.g.  $NO_3^-$ ,  $Mn^{4+}$ ,  $Fe^{3+}$ ,  $SO_4^{2-}$ ), different communities of anaerobes oxidize simple organic molecules and release carbon dioxide. Methane is only produced when all other electron acceptors are reduced in wetland soil (Mitsch and Gosselink, 2007). This process is called methanogenesis and is performed by a group of microbes named methanogens, commonly using  $CO_2$  as electron acceptor (Reddy and DeLaune, 2008). WetQual-C considers DOC pool as potential reservoir for oxic and anoxic/anaerobic respiration.

## 2.2 Mass balance equations

The mass balance equations presented below account for the processes, interactions and loss pathways for organic and inorganic carbon in a typical flooded wetland. The equations are in form of ordinary differential equations and solved numerically using an explicit scheme with forward difference approximation. In the following section, mass balance relationships for organic C pools in water and sediment columns are expressed first. Following that, we present relationships employed in WetQual-C model for dynamic simulation of inorganic C pools (methane in water and sediment columns).

### 2.2.1 Organic C

Water Column:

$$\phi_w \frac{d(V_w C_{Lw})}{dt} = Q_{in} C_{Li} + a_{ca} k_{da} f_{aL} a + a_{ca} k_{db} f_{bw} f_{bL} b - \phi_w V_w k_L C_{Lw} - Q_o C_{Lw} - v_s \phi_w A C_{Lw} + v_r \phi_w A C_{L1} \quad (2.1)$$

$$\phi_w \frac{d(V_w C_{Rw})}{dt} = Q_{in} C_{Ri} + a_{ca} k_{da} f_{aR} a + a_{ca} k_{db} f_{bw} f_{bR} b - \phi_w V_w k_R C_{Rw} - Q_o C_{Rw} - v_s \phi_w A C_{Rw} + v_r \phi_w A C_{R1} \quad (2.2)$$

$$\begin{aligned}
\phi_w \frac{d(V_w C_{Dw})}{dt} = & Q_{in} C_{Di} + a_{ca} k_{da} f_{aD} a + a_{ca} k_{db} f_{bw} f_{bD} b + \phi_w V_w k_L C_{Lw} \\
& + \phi_w V_w k_R C_{Rw} - Q_o C_{Dw} + F_{C_{Dg}}^w + \beta_{D1} A (C_{D1} - C_{Dw}) \\
& - \phi_w V_w \frac{O_w}{O_w + K_O} k_D^1 C_{Dw} - \phi_w V_w \frac{K_O^{in}}{O_w + K_O^{in}} \frac{N_{nw}}{N_{nw} + K_N} k_D^2 C_{Dw}
\end{aligned} \tag{2.3}$$

in which

$$F_{C_{Dg}}^w = \begin{cases} Q_g C_{D1}, & Q_g > 0 \\ Q_g C_{Dw}, & Q_g < 0 \end{cases} \tag{2.4}$$

where  $C_{Lw}$ ,  $C_{Rw}$  and  $C_{Dw}$ , respectively, are concentrations of labile (fast reacting) particulate organic C (LPOC), refractory (slow reacting) particulate organic C and dissolved organic C in free water [ $\text{ML}^{-3}$ ];  $a$  is mass of free floating and attached plants [ $\text{M Chl } a$ ];  $b$  is mass of rooted plants [ $\text{M Chl } a$ ];  $C_{Li}$ ,  $C_{Ri}$  and  $C_{Di}$  are respectively concentrations of LPOC, RPOC and DOC in incoming flow [ $\text{ML}^{-3}$ ];  $C_{Ll}$ ,  $C_{Rl}$  and  $C_{Dl}$  are pore water concentrations of LPOC, RPOC and DOC in aerobic sediment layer, respectively [ $\text{ML}^{-3}$ ];  $v_s$  and  $v_r$  are effective settling and resuspension rates for organic material in water [ $\text{LT}^{-1}$ ];  $V_w$  is water volume of wetland surface water [ $\text{L}^3$ ];  $A$  is wetland surface area [ $\text{L}^2$ ];  $Q_i$  is volumetric inflow rate [ $\text{L}^3\text{T}^{-1}$ ];  $Q_o$  is wetland discharge (outflow) rate [ $\text{L}^3\text{T}^{-1}$ ];  $F_{C_{Dg}}^w$  is groundwater source/loss for DOC [ $\text{MT}^{-1}$ ] and  $Q_g$  is groundwater flow [ $\text{LT}^{-3}$ ] that can be either positive (upwards – discharging to the wetland) or negative (downwards – recharging groundwater table).  $O_w$  and  $N_{nw}$  are, respectively, concentration of oxygen and  $\text{NO}_3$  in water column. Since plant biomass occupies part of submerged wetland volume, we defined  $\phi_w$  as effective porosity of wetland surface water to account for such effects. Other related biochemical parameters and reaction rates applied in Wetland-C formulation are defined in Table 2.1. When oxygen is present in water, aerobic

heterotrophs dominate microbial decomposition. Thus, as appears in Eq. (2.3), oxic respiration is the dominant reaction when oxygen is abundant in water column. When oxygen is depleted from water, the model allows for denitrification in water column. In freshwater wetlands, it is safe to assume that redox potential does not drop below 100 mv in water column (Reddy and DeLaune, 2008), thus, the lowest redox reaction allowed in water column is denitrification. Using Michaelis–Menten kinetics, the rate of aerobic DOC oxidation is limited by oxygen levels (concentration) in water.  $K_O$  is half saturation concentration of oxygen for aerobic respiration, equivalent to a concentration of  $O_2$  at which aerobic respiration rate is half of its maximum ( $k_D^1$ ). Similarly, denitrification of DOC (last term on right hand side of Eq. (2.3) is limited by both nitrate and oxygen concentrations. Michaelis–Menten coefficients of  $K_O$ ,  $K_O^{in}$  and  $K_N$  are used as calibration parameters throughout most DOC and  $CH_4$  related equations.

Aerobic Sediment Layer:

$$V_{s1} \frac{dC_{L1}}{dt} = a_{ca} k_{db} f_1 f_{bs} f_{bL} b - V_{s1} k_L C_{L1} + f_1 \phi_w v_s A C_{Lw} - f_1 v_r A C_{L1} - v_b A C_{L1} \quad (2.5)$$

$$V_{s1} \frac{dC_{R1}}{dt} = a_{ca} k_{db} f_1 f_{bs} f_{bR} b - V_{s1} k_R C_{R1} + f_1 \phi_w v_s A C_{Rw} - f_1 v_r A C_{R1} - v_b A C_{R1} \quad (2.6)$$

$$\begin{aligned} \phi V_{s1} \frac{dC_{D1}}{dt} = & a_{ca} k_{db} f_1 f_{bs} F_{bD} b + V_{s1} k_L C_{L1} + V_{s1} k_R C_{R1} - B_{D1} A (C_{D1} - C_{Dw}) \\ & - \beta_{D2} A (C_{D1} - C_{D2}) + F_{C_{Dg}}^1 - \phi V_{s1} \frac{O_{s1}}{O_{s1} + K_O} k_D^1 C_{D1} - \phi v_b A C_{D1} \end{aligned} \quad (2.7)$$

in which

$$F_{C_{Dg}}^1 = \begin{cases} Q_g C_{D2} - Q_g C_{D1}, & Q_g > 0 \\ Q_g C_{D1} - Q_g C_{Dw}, & Q_g < 0 \end{cases} \quad (2.8)$$

where  $V_{s1}$  is volume of aerobic sediment layer ( $V_{s1} = l_1 \times A_w$ ) [ $L^3$ ];  $C_{D2}$  is pore water concentration of DOC in lower anaerobic sediment layer [ $ML^{-3}$ ],  $O_{s1}$  is oxygen concentration in aerobic sediment ( $O_{s1} = O_w/2$ ) and  $F_{CDg}^1$  is groundwater source/loss of DOC from aerobic sediment layer [ $MT^{-1}$ ]. Eq. (2.9) defines the thickness of the top oxic soil layer [L] (Hantush et al., 2013):

$$l_1 = -\phi\tau\delta + \sqrt{(\phi\tau\delta)^2 + 2\phi\tau D_o^* O_w / \Omega} \quad (2.9)$$

where  $O_w$  is oxygen concentration in free water [ $ML^{-3}$ ],  $\delta$  is the thickness of a laminar (diffusive) boundary layer situated on top of the soil-water interface [L] ( $\delta \approx h/2$  for shallow wetland waters);  $\tau$  is the wetland soil tortuosity factor;  $D_o^*$  is free-water oxygen diffusion coefficient [ $L^2T^{-1}$ ] and  $\Omega$  is oxygen removal rate per unit volume of aerobic soil layer [ $ML^{-3}T^{-1}$ ]. Once  $l_1$  is computed, the thickness of the lower anoxic layer would be  $l_2 = H - l_1$  where  $H$  is the thickness for active sediment layer [L]. Refer to Hantush et al. (2013) for more details on oxygen dynamics in WetQual model. Definitions for rest of the parameters are either presented earlier or could be found in Table 2.1.

#### Anaerobic Sediment Layer:

$$V_{s2} \frac{dC_{L2}}{dt} = a_{ca} k_{ab} f_2 f_{bs} f_{bL} b - V_{s2} k_L C_{L2} + f_2 \phi_w v_s A C_{Lw} - f_2 v_r \phi_w A C_{L2} - v_b A (C_{L2} - C_{L1}) \quad (2.10)$$

$$V_{s2} \frac{dC_{R2}}{dt} = a_{ca}k_{db}f_2f_{bs}f_{bR}b - V_{s2}k_R C_{R2} + f_2\phi_w v_s A C_{Rw} - f_2v_r\phi_w A C_{R2} - v_b A (C_{R2} - C_{R1}) \quad (2.11)$$

$$\begin{aligned} \phi V_{s2} \frac{dC_{D2}}{dt} = & a_{ca}k_{db}f_2f_{bs}f_{bD}b + V_{s2}k_L C_{L2} + V_{s2}k_R C_{R2} - \beta_{D2}A(C_{D2} - C_{D1}) \\ & + F_{C_{Dg}}^2 - \phi v_b A (C_{D2} - C_{D1}) - \phi V_{s2} \frac{N_{n2}}{N_{n2} + K_N} k_D^2 C_{D2} \\ & - \phi V_{s2} \frac{K_N^{in}}{N_{n2} + K_N^{in}} k_D^3 C_{D2} \end{aligned} \quad (2.12)$$

in which

$$F_{C_{Dg}}^2 = \begin{cases} Q_g C_g - Q_g C_{s2}, & Q_g > 0 \\ Q_g C_{s2} - Q_g C_{s1}, & Q_g < 0 \end{cases} \quad (2.13)$$

where  $V_{s2}$  is volume of aerobic sediment layer ( $V_{s2} = l_2 \times A_w$ ) [ $L^3$ ];  $C_{L2}$  and  $C_{R2}$  are pore water concentrations of LPOC and RPOC in lower anaerobic sediment layer respectively [ $ML^{-3}$ ];  $F_{C_{Dg}}^2$  is groundwater source/loss of DOC from anaerobic sediment layer [ $MT^{-1}$ ].

Since resuspension is a purely hydrodynamic process and independent of the soil redox condition, we allow resuspension from the entire active soil layer rather than limiting LPOC and RPOC resuspension to the top aerobic soil compartment. Each of the soil compartments contributes an amount proportional to its respective thickness.

Table 2.1: Wetqual-C model parameter definitions

Symbol	Definition	Dimension/unit
$a_{ca}$	ratio of carbon to chlorophyll-a in algae	$MM^{-1}$
$a_{mc}$	the stoichiometric yield of Methane from the anaerobic decomposition of gram of organic carbon during methanogenesis	$MM^{-1}$
$\beta_{D1}, \beta_{M1}$	diffusive mass-transfer rates, respectively, of DOC and $CH_4$ between wetland water and aerobic soil layer (see appendix B for details)	$LT^{-1}$
$\beta_{D2}, \beta_{M2}$	diffusive mass-transfer rates, respectively, of DOC and $CH_4$ between wetland water and lower anaerobic soil layer (see appendix B for details)	$LT^{-1}$
$C^*$	equilibrium concentration of $CH_4$ in atmosphere	$ML^{-3}$
$D^\sigma$	diffusivity of Methane in air	$L^2T^{-1}$
$D_M^*, D_D^*$	diffusivity of methane and DOC in water, respectively	$L^2T^{-1}$
$f_1$	volumetric fraction of the active soil layer that is aerobic $f_1 = l_1/(l_1 + l_2)$	dimensionless
$f_2$	volumetric fraction of the active soil layer that is anaerobic $f_2 = l_2/(l_1 + l_2)$	dimensionless
$f_{aL}, f_{aR}, f_{aD}$	fraction of, respectively, labile particulate, refractory particulate and dissolved organic C produced by death/loss of free floating plants and attached algae ( $f_{aL} + f_{aR} + f_{aD} = 1$ )	dimensionless
$f_{bL}, f_{bR}, f_{bD}$	fraction of, respectively, labile particulate, refractory particulate and dissolved organic C produced by death/loss of rooted and benthic plants ( $f_{bL} + f_{bR} + f_{bD} = 1$ )	dimensionless
$f_{bw}, f_{bs}$	fraction of rooted plant biomass, respectively, above and under soil-water interface	dimensionless
$H$	thickness of active soil layer $H = l_1 + l_2$	L
$h$	average depth of water in wetland	L
$J_M$	methane mass exchange coefficient between water and atmosphere	$LT^{-1}$
$k_D^1, k_D^2, k_D^3$	maximum dissolved organic C utilization rate for, respectively, aerobic respiration, denitrification and methanogenesis	$T^{-1}$
$k_M^1, k_M^2$	maximum methane utilization rate for, respectively, aerobic respiration and denitrification	$T^{-1}$
$k_{da}$	death rate of free floating plants	$T^{-1}$
$k_{db}$	death rate of rooted and benthic plants	$T^{-1}$
$K_O^{in}$	Michaelis–Menten oxygen inhabitation coefficient	$ML^{-3}$
$K_N^{in}$	Michaelis–Menten nitrate-N inhabitation coefficient	$ML^{-3}$
$k_L, k_R$	first order hydrolysis rate of labile particulate organic carbon and refractory particulate organic carbon, respectively	$T^{-1}$

Table 2.1 (Continue): Wetqual-C model parameter definitions

$K_N$	Michaelis–Menten nitrate N half saturation concentration required for denitrification	$ML^{-3}$
$K_O$	Michaelis–Menten half saturation concentration of dissolved oxygen required for oxic respiration	$ML^{-3}$
$l_1, l_2$	thickness of aerobic and anaerobic sediment layers	L
$Sc_M$	Schmidt number of methane	dimensionless
$S_B$	Bunsen solubility coefficient for methane	dimensionless
$v_r$	resuspension/recycling rate of particulate organic C	$LT^{-1}$
$v_s$	settling loss rate of particulate organic C	$LT^{-1}$
$\theta$	Temperature coefficient in Arhenious equation. (see appendix A for parameters that are adjusted with temperature)	dimensionless
$\lambda_r$	specific conductivity of root system	$LL^{-1}$
$\tau$	tortuosity of sediment	dimensionless
$\phi$	porosity of sediment	dimensionless
$\phi_w$	effective porosity of wetland surface water	dimensionless

Table 2.2: Model parameters with fixed values (i.e. constants)

Parameter	Value
$a_{mc}$ (gr $CH_4$ /gr DOC)	0.267
$\lambda_r$ (m root/ m soil)	0.0003

### 2.2.2 Methane-C ( $CH_4$ )

Before being released to the atmosphere, methane produced in reduced wetland soil is subjected to several geochemical and physical transformations. Methane emission to atmosphere is a balance between methane production, oxidation and transport within the soil and water (Bradford et al., 2001; Chan and Parkin, 2000; Reddy and DeLaune, 2008; Wania et al., 2010). Methane is transported to atmosphere via three different pathways of 1) plant aided diffusive exchange via aerenchyma of plants roots and stands 2) diffusive flux through soil and water 3) abrupt elimination in form of bubbles (ebullition). Much of the transferred methane through molecular

diffusion (up to 90%) and plant aided exchange (up to 50%) is oxidized to carbon dioxide by methanotrophic bacteria that consume methane as carbon and energy source (King, 1992; Reddy and Schipper, 1996). This fact reveals the importance of ebullition as major processes that regulate methane emission into the atmosphere. Ebullition may account for 30- 85% of the total methane release from wetlands (Byrnes et al., 1995; Reddy and DeLaune, 2008). To capture the complicated cycle of methane, a robust model shall include proper equations to represent all processes related to methane production, transfer and consumption. Since methane is generally produced in reduced soil and transferred upwards, we present methane mass balance equations in sediment layers first and then move upwards to water layer.

#### Sediment Columns:

Methane in sediment columns are simulated in a two-step process. In step one, processes other than ebullition (diffusion, oxidation, advective transport and plant mediated transport) are considered to define methane concentration. If the methane concentration calculated in step one exceeds a certain partial pressure, the excess is transferred upwards to the atmosphere in form of bubbles (ebullition). This method is similar to approaches suggested by Kellner et al. (2006) and Wania et al. (2010). For anaerobic and aerobic sediment layers, the mass balance equations form as follows:

$$\begin{aligned} \phi V_{s2} \frac{dC_{M2}}{dt} = & a_{mc} \phi V_{s2} \frac{K_N^{in}}{N_{n2} + K_N^{in}} k_D^3 C_{D2} + \beta_{M2} A(C_{M1} - C_{M2}) \\ & - \phi V_{s2} \frac{N_{n2}}{N_{n2} + K_N} k_M^2 C_{M2} + F_{C_{Mg}}^2 + \lambda_r f_2 f_{bs} b R_v D^\sigma (C^* - C_{M2}) \end{aligned} \quad (2.14)$$

$$\begin{aligned} \phi V_{s1} \frac{dC_{M1}}{dt} = & \beta_{M1} A(C_{Mw} - C_{M1}) + \beta_{M2} A(C_{M2} - C_{M1}) - \phi V_{s1} \frac{O_{s1}}{O_{s1} + K_O} k_M^1 C_{M1} \\ & + F_{C_{Mg}}^1 + \lambda_r f_1 f_{bs} b R_v D^{\sigma} (C^* - C_{M1}) \end{aligned} \quad (2.15)$$

$$\text{if } C_{Mi} > C_{Mi}^{eq} \quad (i=1,2) \quad \text{then} \quad \begin{cases} J_{Ebul}^{Mi} = (C_{Mi} - C_{Mi}^{eq}) \phi V_{si} / (\Delta t A) \\ \text{and} \quad C_{Mi} = C_{Mi}^{eq} \end{cases} \quad (2.16)$$

$$\text{in which} \quad F_{C_{Mg}}^2 = \begin{cases} -Q_g C_{M2}, & Q_g > 0 \\ Q_g C_{M2} - Q_g C_{M1}, & Q_g < 0 \end{cases} \quad (2.17)$$

$$F_{C_{Dg}}^1 = \begin{cases} Q_g C_{M2} - Q_g C_{M1}, & Q_g > 0 \\ Q_g C_{M1} - Q_g C_w, & Q_g < 0 \end{cases}$$

where  $C_{M2}$ ,  $C_{M1}$  and  $C_w$  are methane concentration in anaerobic sediment, aerobic sediment layer and water respectively [ $ML^{-3}$ ];  $a_{mc}$  is the stoichiometric yield of Methane from the anaerobic decomposition of gram of organic carbon during methanogenesis [ $MM^{-1}$ ] (see Table 2.2 for constant value),  $\beta_{M2}$  is methane mass exchange coefficient between aerobic and anaerobic sediment [ $LT^{-1}$ ];  $\beta_{M1}$  is methane mass exchange coefficient between aerobic sediment and water [ $LT^{-1}$ ];  $k_D^3$  is first-order reaction rate for DOC consumption by methanogenesis in reduced soil [ $T^{-1}$ ];  $k_M^2$  is first order reaction rate for methane consumption via denitrification [ $T^{-1}$ ];  $k_M^1$  is first order reaction rate for aerobic methane oxidation [ $T^{-1}$ ] and  $F_{C_{Mg}}^1$  and  $F_{C_{Mg}}^2$  are groundwater source/loss for methane [ $MT^{-1}$ ]. Groundwater is more likely to be a sink for methane rather than a source; however some studies indicate that methane in ground water resources can constitute a significant pool of carbon (Barker and Fritz, 1981). The last term on right hand side of Eq. (2.14) and Eq. (2.15) accounts for plant mediated transfer of methane to atmosphere. Plant aided transfer of methane is assumed to be a function of root density and methane concentration

gradient between soil and air (Yu et al., 1997). Following Tang et al. (2010),  $C^*$  is equilibrium concentration of  $\text{CH}_4$  in atmosphere [ $\text{ML}^{-3}$ ],  $\lambda_r$  is specific conductivity of root system [ $\text{LL}^{-1}$ ] (See Table 2.2 for constant value),  $R_v$  is root length density in soil [ $\text{L root/ M chla}$ ];  $D^o$  is diffusivity of methane in air [ $\text{L}^2\text{T}^{-1}$ ] (see appendix A for relationship of  $D^o$  with temperature) and  $C^*$  is equilibrium concentration of  $\text{CH}_4$  in atmosphere [ $\text{ML}^{-3}$ ] (see appendix A for details).  $C_{Mi}^{eq}$  [ $\text{ML}^{-3}$ ] is an upper limit for concentration of dissolved methane for sediment layer  $i$  ( $i=1,2$ ) in which solubility of  $\text{CH}_4$  is maximum. Such concentration for both sediment layers is obtained by combining Bensen solubility coefficient of methane and ideal gas law (Wania et al., 2010):

$$C_{Mi}^{eq} = \frac{p_i}{RT} (S_B) \quad (2.18)$$

where,  $T$  is the ambient water temperature ( $\text{K}^\circ$ ),  $R$  is the universal gas constant ( $8.3145 \text{ m}^3 \text{ Pa K}^{-1} \text{ mol}^{-1}$ ),  $S_B$  is the Bunsen solubility coefficient, defined as maximum volume of gas dissolved per volume of liquid at given temperature and pressure (see A.2 for a temperature dependent relationship of  $S_B$ ).  $P_i$  (unit: Pa) is the sum of atmospheric and hydrostatic pressures for sediment layer  $i$  ( $p_i = p_{atm} + \rho g z$ ) where  $g$  is gravitational acceleration [ $\text{LT}^{-2}$ ],  $\rho$  is density of water [ $\text{ML}^{-3}$ ] and  $z$  is average water height over sediment layer [ $\text{L}$ ]:

$$z = \begin{cases} h + \frac{l_1}{2} & i = 1 \\ h + l_1 + \frac{l_2}{2} & i = 2 \end{cases} \quad (2.19)$$

Excessive methane over maximum solubility is promptly cast out of the sediment layers via ebullition such that concentration of methane never exceeds the maximum limit.  $J_{Ebul}^M$  represents the flux of methane released by bubbling at each time step [ $ML^{-2}T^{-1}$ ].

Water Column:

$$\begin{aligned} \phi_w \frac{d(V_w C_{Mw})}{dt} = & \alpha_M \phi_w A (C^* - C_{Mw}) + \beta_{M1} A (C_{M1} - C_{Mw}) + F_{C_{Mg}}^w - Q_o C_{Mw} \\ & - \phi_w V_w \frac{O_w}{O_w + K_O} k_M^1 C_{Mw} - \phi_w V_w \frac{K_O^{in}}{O_w + K_O^{in}} \frac{N_{nw}}{N_{nw} + K_N} k_M^2 C_{Mw} \end{aligned} \quad (2.20)$$

in which

$$F_{C_{Mg}}^w = \begin{cases} Q_g C_{M1} & Q_g > 0 \\ Q_g C_{Mw} & Q_g < 0 \end{cases} \quad (2.21)$$

where,  $C_{Mw}$  is methane concentration in water [ $ML^{-3}$ ];  $\alpha_M$  is methane gas transfer velocity between water and atmosphere [ $LT^{-1}$ ];  $F_{C_{Dg}}^w$  is groundwater source/loss for methane [ $MT^{-1}$ ].  $\alpha_M$ , also referred to as piston velocity, is empirically derived using inert tracer gases and is usually related to wind speed over water (Wanninkhof et al., 2009). A variety of relationships for gas transfer velocities have been presented by Wanninkhof et al. (2009). The following relationship, valid for wind speeds less than  $3.6 \text{ m s}^{-1}$ , was selected for methane:

$$\alpha_M = 0.17 U_{10} \left( \frac{Sc_M}{600} \right)^{-0.5} \quad (2.22)$$

where  $\alpha_M$  has a unit of  $\text{cm hr}^{-1}$ ,  $Sc_M$  is Schmidt number of methane in a given temperature (see A.2 for details) and  $U_{10}$  is wind speed at 10 meters above water ( $\text{m s}^{-1}$ ) (Riera et al., 1999; Wanninkhof et al., 2009).

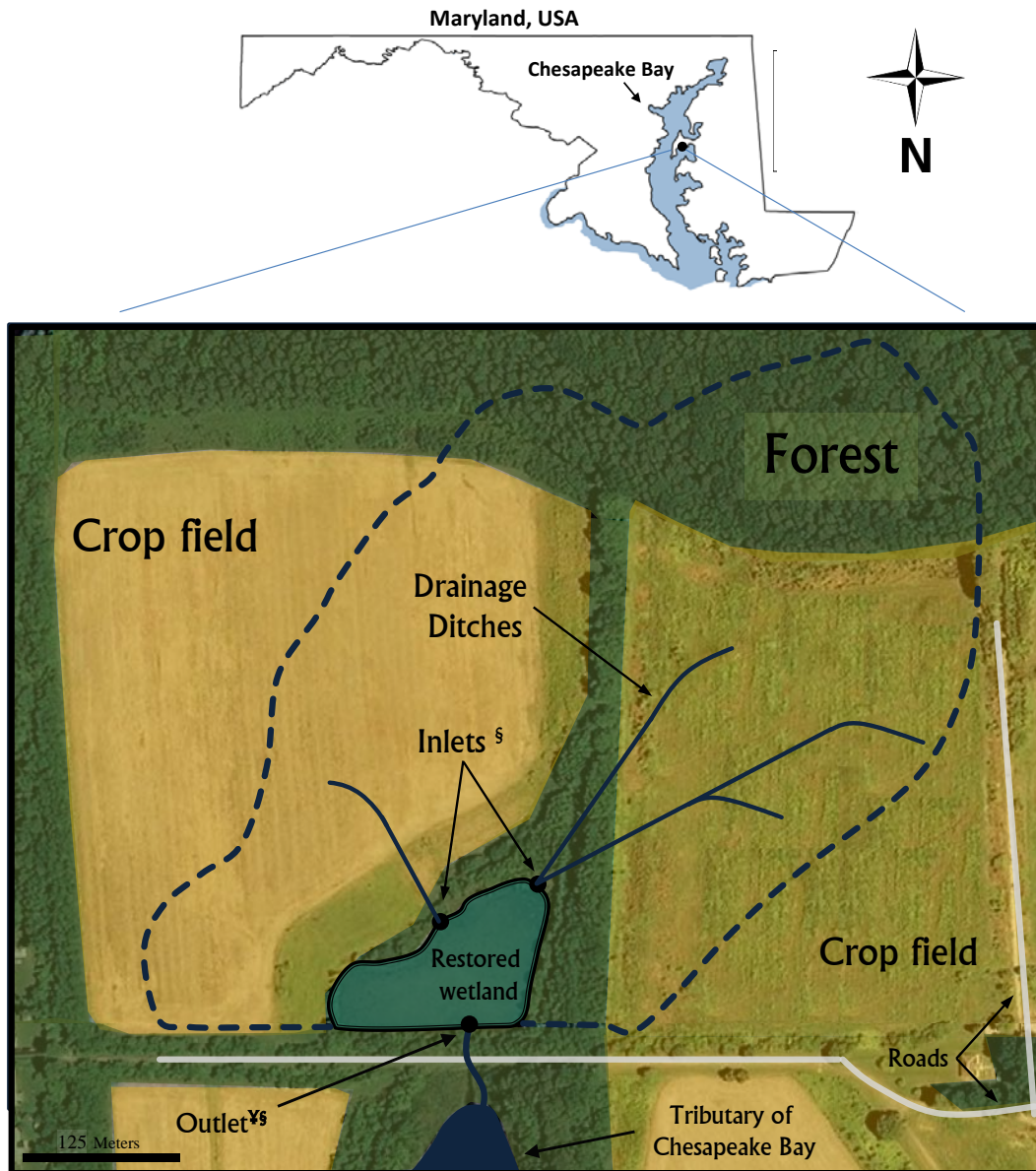
### 3. Model assessment

#### 3.1 Study area and input data

The developed model was applied to a study wetland with approximately two years of monitored flow and water quality data, described thoroughly by Jordan et al. (2003). The study site is a small restored wetland located on Kent Island, Maryland (Figure 2.2). During the two year sampling period, the study wetland had an average area of 1.3 ha and drained a 14 ha watershed that was mainly covered by crop fields (82 %) and forest (18%). The study wetland was restored from an artificially drained cropland by the Chesapeake Wildlife Heritage with the intention to provide wildlife habitat and improve the quality of runoff from surrounding crop fields. A maximum 90% of the wetland surface was covered by emergent vegetation during growing season; this portion dropped to a minimum of 10% during non-growing season. Three most dominant macrophyte species in the wetland were Blunt spikerush [*Eleocharis obtusa* (Willd.) Schult.], Water-purslane [*Ludwigia palustris* (L.) Elliott] and American bulrush [*Schoenoplectus americanus*]. Water entered the wetland through ditches draining surface runoff from surrounding catchment and outflowed via a standpipe connected to a 120° V-notch weir. The entire 1.3-ha area of the wetland was submerged and lacked well-defined flow channels when the water was deep enough to flow out of the weir. An impermeable layer of clay, within 0.5 m of soil surface during wetland restoration blocked groundwater exchanges and infiltration.

Automated instruments were used to measure unregulated water inflows and to sample water entering and leaving the wetland from 8 May 1995 through 12 May 1997. Weekly (typically 5 to 8 days) flow averaged nitrate N, total ammonia N, organic N, inorganic P, and TSS and TOC (total organic carbon) concentrations in runoff were available from Jordan et al. (2003). Details of data collection and analysis can be found in Jordan et al. (2003).

To convert weekly average concentrations reported by Jordan et al. (2003) into daily values, we assumed that concentrations were constant over the given weekly periods. The dataset also contained periods where data were missing. We reconstructed the records during such periods by taking averages of the last available measurement before the gap and the first available measurement at the end of the gap. Sources for other input data (precipitation, temperature, etc.) used in the model could be found in Kalin et al. (2013) who validated the N and P cycles of WetQual model on the same study wetland. Unfortunately the dataset does not include methane emission measurements, so we were not able to validate completely the methane component of the model. Yet, parameter values acquired from literature allowed us to perform a thorough sensitivity analysis on methane production and emission from the study wetland. Figure 2.3 exhibits the hydrology of the study wetland (inflow, outflow and average water depth) in addition to inflow concentrations of TOC to the study wetland from May 1995 to May 1997.



¶ Outflow structure consisted of a standpipe connected to a 120° V-notch weir.

§ Automated samplers were installed to sample water entering and leaving the wetland.

Figure 2.2: Study wetland and its watershed outlined by dashed lines (regenerated from Jordan et al., 2003).

### 3.2 Numerical scheme verification

An explicit scheme with forward-difference approximation of the time derivatives was employed as a stable/efficient method for numerical integration. The named scheme was previously employed and explained by Hantush et al. (2013). The selected numerical integration time step is  $\Delta t = 0.01$  day, however to save memory storage, results are aggregated to daily averages. Hantush et al. (2013) verified the used numerical approach by comparing model results with analytical solutions for simplified cases. However, in this study, we employed a secondary numerical structure to verify solutions provided by the explicit scheme. For the secondary numerical scheme, all equations contained within in the larger WetQual model (equations for nitrogen, phosphorus, carbon and sediment) were solved implicitly as coupled system of ordinary differential equations (ODEs) with central difference approximation.

The secondary solution uses a time step of same length ( $\Delta t = 0.01$  day), yet the model takes about three times as long to run. Solutions provided by both methods were compared for different carbon constituents (DOC, LPOC, RPOC and  $\text{CH}_4$ ). The differences between time series provided by both methods were indistinguishable for carbon pools within water and both oxidized and reduced soil layers. The perfect match between two solutions provided confidence and proof in effectiveness of the used explicit numerical scheme.

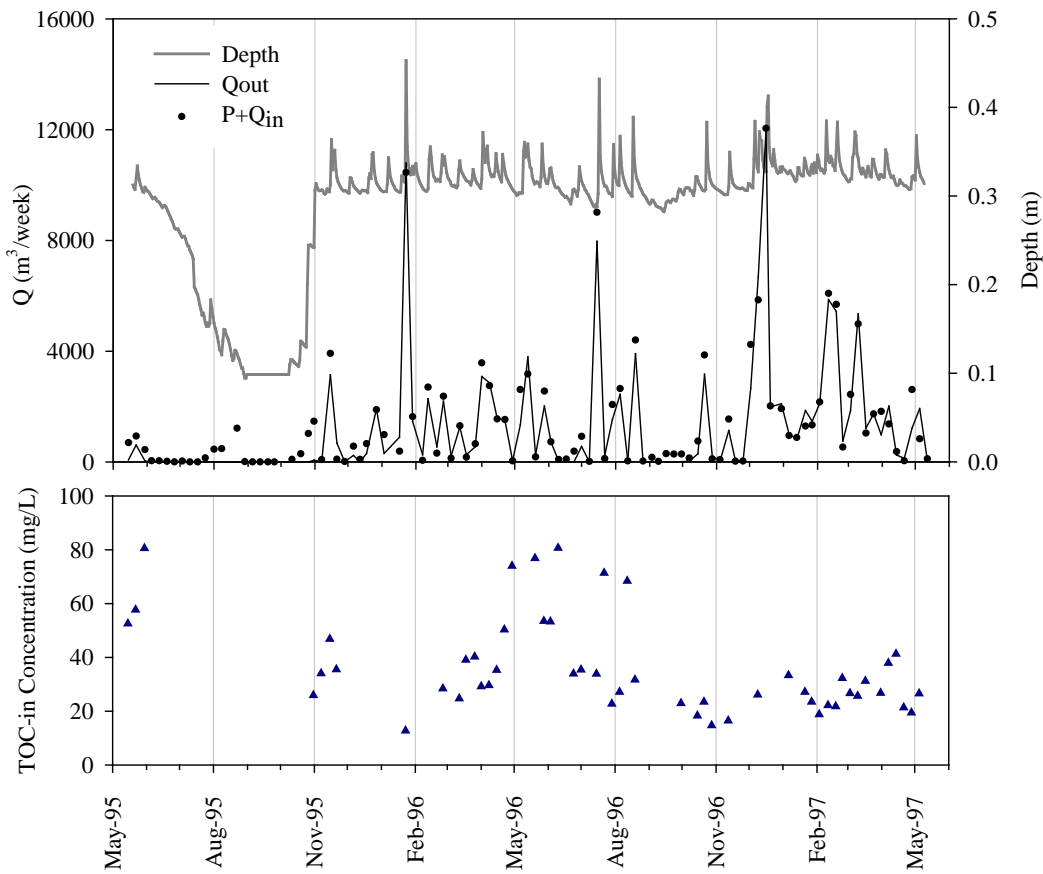


Figure 2.3: Top panel: Hydrology of Barnstable wetland during study period. Bottom panel: Measured concentration of TOC inflow (mg/L) to wetland over the study period.

### 3.3 Uncertainty and Sensitivity assessment

Generalized Likelihood Uncertainty Estimation (GLUE), introduced by Beven and Binley (1992), advocates the idea that there are always several different models and parameter sets for a single model that represent an observed natural process equally well. In other words, as Beven and Freer (2001) put it, “there are many different model structures and many different parameter sets within a chosen model structure that may be behavioral or acceptable in reproducing the observed behavior of a system”. Following this notion referred to as “Equifinality”, model

calibration is not sought in the traditional way (i.e. finding an “optimum” parameter set), and rather, a *group* of parameter sets that generate model results consistent with observations are sought after. GLUE provides a simple uncertainty estimation method easily applicable to non-linear complex models. GLUE methodology is an extension to Generalized Sensitivity Analysis (GSA), first introduced by Spear and Hornberger (1980). Both GSA and GLUE are based upon Monte Carlo (MC) simulations. In this study, we employed a combination of both GLUE and GSA methods to simultaneously assess model prediction uncertainty and quantitative sensitivity to input parameters. A brief portrayal of the GSA/GLUE methodology applied in this study is presented in Figure 2.4. To apply GSA/GLUE method, we generated 100,000 statistically independent parameter sets, sampled randomly from previously defined distributions. The parameter distribution and their respective upper and lower bounds (quantities) are listed in Table 2.3. Such information was extracted from literature values/tabulations (e.g. Schnoor, 1996; Chapra, 1997; Di Toro, 2001; Reddy and Delaune, 2008; Cerco and Cole, 1995 and Ji, 2008) and authors’ judgment. To perform MC simulations, the model was run 100,000 times, each time with one set of parameters to yield an ensemble of 100,000 time series for constituent concentrations. Two performance criteria were used to construct a likelihood function that evaluates the goodness of fit between model-predicted concentrations and observed data for each MC simulation. The likelihood function uses a combination of Mass Balance Error (*MBE*) and Nash-Sutcliffe efficiency ( $E_{ns}$ ) (Kalin and Hantush, 2006) such that:

$$L_k = 0.5 \times (E_{ns} + \exp(\frac{-|MBE|}{100})) \quad (2.23)$$

The likelihood function  $L$  can theoretically range between  $-\infty$  to 1. Such a measure enables us capture goodness of fit for both average constituent concentrations and its variation over time. Following the methodology presented in Figure 2.4, model parameter sets were sorted from largest to smallest respective likelihoods and the top 1000 datasets (top 1%) with the highest likelihoods were separated as behavioral dataset (**B**) from the rest of the parameter sets (non-behavioral datasets, **B'**). Special attention was given in selecting the cutoff limit for behavioral datasets. After special consideration, 1% limit was recognized as effectual cutoff limit, yet for the parameters to be selected as behavioral dataset, the respective model performance needed to yield a Nash-Sutcliffe efficiency larger than 0.7 ( $E_{ns} > 0.7$ ) and a mass balance error smaller than 5% ( $|MBE| < 5\%$ ).

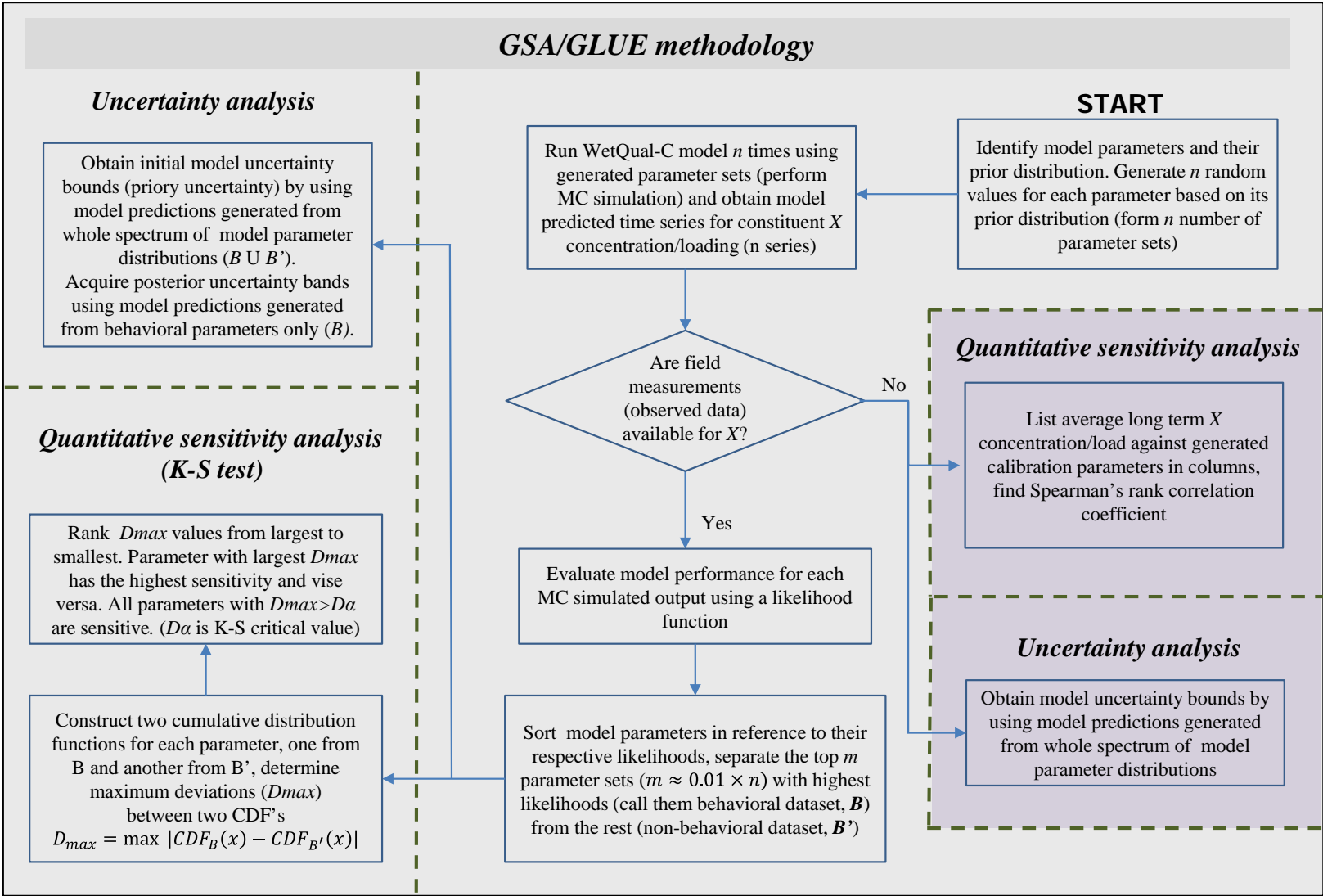


Figure 2.4: Stepwise flowchart to GSA/GLUE methodology applied in this study.

Table 2.3: Model parameters considered random and their best estimates based on TOC export

Parameters	Distribution (literature) <sup>†</sup>	Min(a) (literature) <sup>†</sup>	Max(a) (literature) <sup>†</sup>	Best estimates for TOC model	Best estimates for ON model <sup>^</sup>
$H$ [cm]	$U$ <sup>‡</sup>	5.00	50.00	23.94	21.20
$\theta$	$U$	1.15	1.35	1.307	1.10
$k_{ga}$ [d <sup>-1</sup> ]	$\log-N$ <sup>§</sup>	0.01	0.2	0.00143	0.0014
$k_{gb}$ [d <sup>-1</sup> ]	$\log-N$	0.01	0.2	0.00142	0.0014
$\rho_s$ [g/cm <sup>3</sup> ]	$U$	1.5	2.2	2.01	2.01
$v_s$ [cm/d]	$\log-N$	0.025	25	1.779	2.34
$v_b$ [cm/d]	$U$	0.000274	0.006575	0.0034	0.0035
$\phi$	$U$	0.5	0.9	0.668	0.684
$\phi_w$	$U$	0.65	0.95	0.8768	0.865
$v_r$ [mm/yr]	$\log-N$	0.0146	8.74	0.029	0.024
$a_{ca}$ [gC/gChl]	$U$	15	160	86.174	
$f_{aL}$	$U$	0.01	0.99	0.423	
$f_{aR}$	$U$	0.01	0.99	0.421	
$f_{aD}$	$U$	0.01	0.33	0.156	
$f_{bL}$	$U$	0.01	0.99	0.430	
$f_{bR}$	$U$	0.04	0.99	0.412	
$f_{bD}$	$U$	0.01	0.33	0.158	
$k_L$ [d <sup>-1</sup> ]	$\log-N$	0.000001	0.0001	0.0000135	
$k_R$ [d <sup>-1</sup> ]	$\log-N$	0.0000001	0.00001	0.00000127	
$K_O$ [mg/lit]	$U$	0.2	1.00	0.5453	
$K_O^{in}$ [mg/lit]	$U$	0	0.51	0.2732	
$K_N$ [mg/lit]	$\log-N$	0.004	0.36	0.0519	
$K_N^{in}$ [mg/lit]	$\log-N$	0.002	0.18	0.0271	
$k_D^1$ [d <sup>-1</sup> ]	$U$	0.0015	0.4	0.2174	
$k_D^2$ [d <sup>-1</sup> ]	$U$	0.001	0.16	0.1086	
$k_D^3$ [d <sup>-1</sup> ]	$U$	0.0005	0.08	0.0276	
$\beta_{D1}$ [cm/d]	- <sup>^</sup>	0.85	109.02	27.87	
$k_M^1$ [d <sup>-1</sup> ]	$U$	0.001	0.25	---	
$k_M^2$ [d <sup>-1</sup> ]	$U$	0.001	0.08	---	
$f_{bw}$	$U$	0.4	0.7	0.547	
$R_v$	$\log-N$	0.001	10.00	---	
$\beta_{M1}$ [cm/d]	-	0.92	131.57	---	

<sup>†</sup> The selected ranges (Min, Max) and distributions for the listed parameters/coefficients are extracted from literature and expert knowledge (e.g. Schnoor, 1996; Chapra, 1997; Di Toro, 2001; Reddy and Delaune, 2008; Cerco and Cole, 1995 and Ji, 2008). Also see Hantush et al. (2013) and Kalin et al. (2013)

for list of other parameters (regarding N+P cycles) in WetQual model; <sup>¥</sup> Uniform distribution; <sup>§</sup> log-normal distribution; <sup>^</sup> no specific distribution assigned. Lower and upper bounds in log-N distributions refer to values corresponding to probabilities of 0.1% and 99.9%. Grey lines mark parameters that are shared with N cycling in WetQual model. <sup>^</sup> Values in last column (Best estimates for ON model) are from Kalin et al., (2013).

Given that the used measures have unequal domains, implementing such limits gives both measures more or less equal weights in the likelihood function. A simple weighing average method was used to yield best estimations for WetQual-C model parameters. Behavioral parameter values were given a weight proportional to their respective likelihood and averaged as follows:

$$x' = \frac{\sum_{i=1}^n (e^{L_k-1} x_i)}{\sum_{i=1}^n e^{L_k-1}} \quad (2.24)$$

where  $x'$  is best estimate for parameter  $x$ ,  $L_k$  is the corresponding likelihood from the  $i^{\text{th}}$  model run of the MC simulation,  $n$  is the total number of MC simulations, and  $x_i$  is the generated value of parameter  $x$  in  $i^{\text{th}}$  parameter set.

Subsequently, quantitative sensitivity analysis was performed using Kolmogorov-Smirnov test (Massey Jr, 1951) to reveal the most sensitive parameters. Kolmogorov-Smirnov test is a nonparametric test that is used to quantify a distance between the reference cumulative distribution function (CDF) – generated from non-behavioral parameter values or  $B'$ – and posterior CDF of a parameter generated from behavioral datasets (or  $B$ ). If such distance – referred to as  $D_{max}$  – is significant at 5% confidence level, the parameter is declared sensitive. Prior and posterior prediction uncertainty were next obtained by using model predictions

generated respectively from the whole spectrum of model parameter distributions ( $\mathbf{B} \mathbf{U} \mathbf{B}'$ ), and from behavioral parameters only ( $\mathbf{B}$ ).

For simulated constituents that do not have equivalent field measurements (like methane in this study), a simple method for determining most sensitive parameters quantitatively is to use Spearman's rank correlation coefficient (Saltelli and Sobol, 1995). In this method the strength of monotonic relationship (linear correlation) between the ranks of each input (parameter values) and output (simulated constituent concentration) is measured. Spearman's correlation coefficient ranges from -1 to 1, and a negative correlation between a parameters and constituent concentration imposes an inverse relationship between the two.

#### **4. Results and discussion**

As stated before, the measured observed data are limited to flow and weekly averaged incoming and outflowing TOC concentration measurements.  $\text{CO}_2$  and  $\text{CH}_4$  emissions were not monitored on the study wetland. Thus, in the following sections, we will demonstrate model performance, uncertainty and parameter sensitivity on TOC export. The  $\text{CH}_4$  component of the model was examined thoroughly by performing rank correlation sensitivity analysis. At the end, carbon budgets for the study wetland are presented. Many of the equations presented earlier require the concentration of  $\text{NO}_3$  in water and sediment layers as input. Kalin et al. (2013) validated the nitrate component of the WetQual model, therefore model simulated concentrations of  $\text{NO}_3$  were used when required.

## 4.1 TOC export

Simulated TOC concentrations are obtained by lumping model generated concentrations of DOC, LPOC and RPOC at each time step. Although model required separate inflow concentrations for LPOC, RPOC and DOC, such information was not available for the case study wetland; instead, the lumped amount of the three pools (TOC) was measured at wetland inlets. We disaggregated the sum into three separate pools by relying on model fine tuning and information provided by Jordan et al. (1999). Model fine tuning exposed that best fits to observed data are achieved when roughly 89% of the inflowing TOC is considered as DOC. The study by Jordan et al. (1999), which performed an experimental study on the same study wetland between 1994 and 1995, supports this finding by stating that DOC constituted over 75% of TOC entering the study wetland between 1994 and 1995. Model performance showed small sensitivity to how the remaining 11% of TOC inflow was distributed between LPOC and RPOC pools, thus the remainder was split equally between the two pools.

### 4.1.1 Quantitative Sensitivity analysis (K-S test)

Figure 2.5 presents results of the K-S test performed on model parameters. Ten model parameters were identified as sensitive using the test (top panel), in which all had small p-values ( $p < 0.0003$ ). Bottom panel of Figure 2.5 shows the maximum gap ( $D_{\max}$ ) between cumulative distribution functions of behavioral and non-behavioral data sets for the three top sensitive parameters. Most sensitive parameter was identified as  $\theta$ , imposing the notion that temperature plays a significant role in regulating TOC export. Knowing that TOC pool is mostly comprised of DOC (~ 90%), and considering the repeated effects of temperature related to DOC transfer (diffusion), origination (LPOC, RPOC hydrolysis) and conversion (aerobic/anaerobic

decomposition), it is not unexpected to see  $\theta$  as a sensitive parameter. Four other parameters in order of sensitivity were  $\beta_{D1}$ ,  $k_D^1$ ,  $\phi_w$  and  $k_D^2$ . Given the fact that  $D_{max}$  of first five parameters are considerably close to each other ( $0.4 < D_{max} < 0.47$ ), we can state that the most equally important processes governing TOC export in this studied wetland system are diffusion of DOC, aerobic decomposition and denitrification of DOC. Similar to  $\theta$ ,  $\phi_w$  (fourth in order of sensitivity) does not present a specific process, rather it accounts for plant biomass and other debris obstructing flow and flow-accessibility in wetland water pool. The second half of sensitive parameters (last five) include  $k_D^3$ ,  $v_s$ ,  $H$ ,  $K_O$  and  $K_O^{in}$ , conveying secondary importance of methanogenesis, settling, thickness of active sediment layer and oxygen concentration on TOC export.

#### **4.1.2 Parameter estimation**

Based on the averaging method explained earlier (section 3.3), best estimates for parameters involved in TOC export modeling were calculated (Table 2.3). Presenting a single value for a parameter might promote the concept of calibration and seem against the notion of equifinality, yet our intention of presenting such values is rather to give the reader estimates of mean parameter values. This practice also allows us to compare best estimates obtained in this study to those obtained in Kalin et al. (2013) for organic nitrogen (ON). These shared parameters are marked in grey in Table 2.3. As no observed data were available for methane emission, best estimates for some methane related parameters could not be obtained. In general, calculated best estimates for shared parameters are reasonably close to estimations obtained from ON simulations. As explained previously, best estimate for  $\theta$  obtained for carbon export is 16%

larger than the value estimated for ON, expressing higher sensitivity of C cycling to temperature variation.

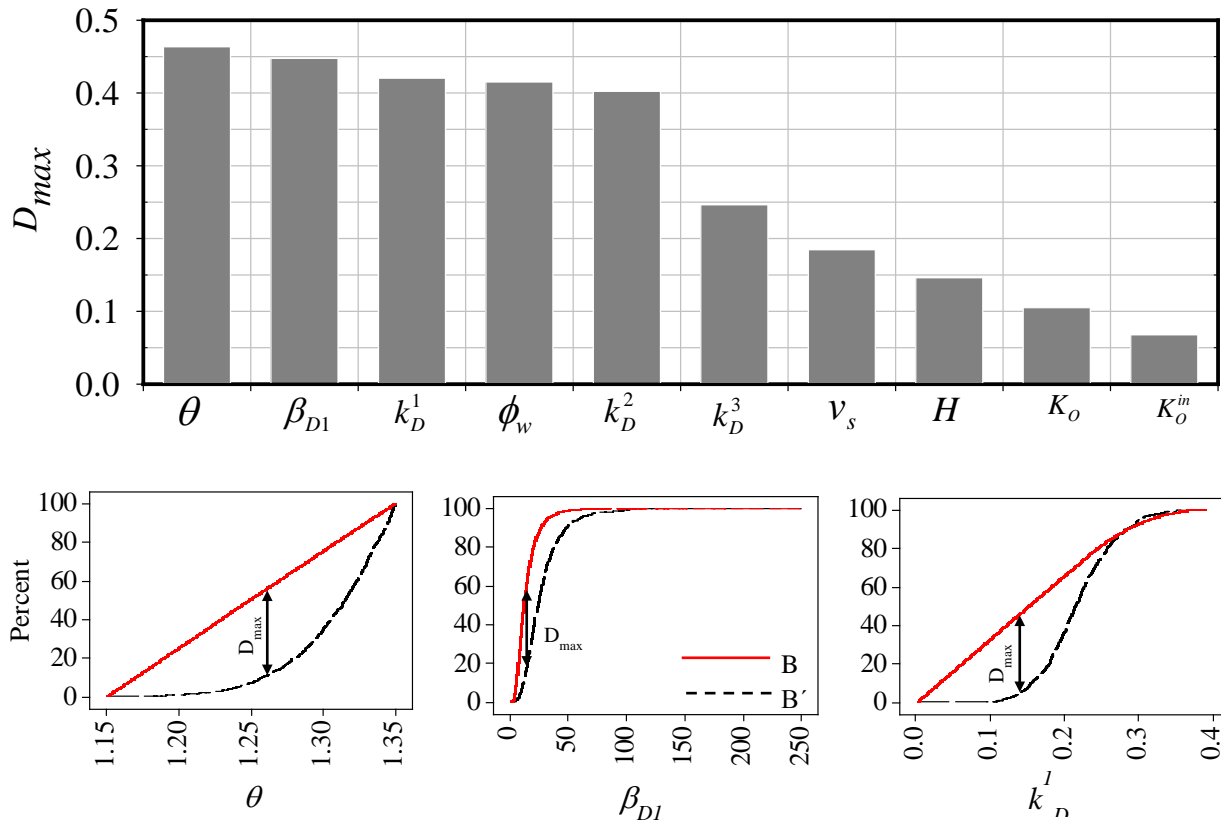


Figure 2.5: Top: Summary of the K-S test and order of sensitivities based on TOC export for the whole study period.

#### 4.1.3 Model performance and uncertainty analysis

Figure 2.6 demonstrates the comparison between field measured TOC export (top) and outflow concentrations (bottom) with model results, generated from the behavioral and non-behavioral MC simulations. As declared earlier, there are periods with no observed data (no field measurements). For purpose of presentation, we discarded those absent weeks in order not to leave any breaks, thus the horizontal axes in the figures do not reflect consecutive weeks. As

appears in Figure 2.6, the model performs decently in predicting TOC export from case study wetland with relatively small uncertainty. Average  $L_k$ ,  $E_{ns}$  and MBE for behavioral simulations concerning TOC export are respectively equal to 0.93, 0.87 and 0.81%.

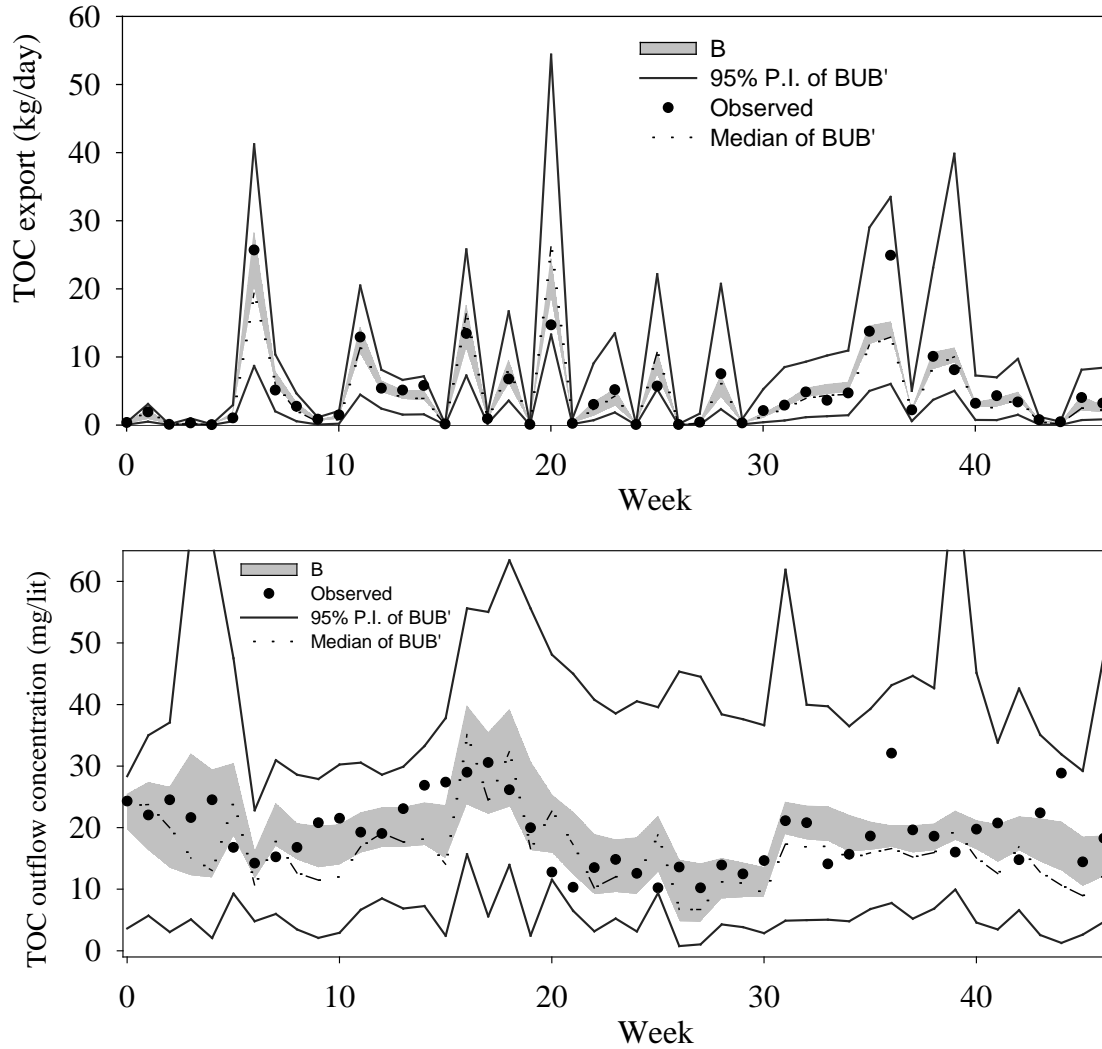


Figure 2.6 :Model generated 95% prediction interval (P.I.) from 100,000 MC simulations versus field observations.

95% prediction intervals at the top panel of Figure 2.6 disclose that uncertainty is highest when TOC export is at a local peak. These peaks happen to coincide with peaks in outflow (not shown), suggesting that highest model uncertainty can be expected when flow is high. At low flows, when TOC export is minimal, model has a very narrow uncertainty band (both prior and posterior). The uncertainty for behavioral simulations is relatively small. The bottom panel reveals that behavioral model uncertainty is wider when concentration is simulated. The median time series for MC simulations performed in this study are shown in Figure 2.6 with dashed lines. As can be seen, the median time series on both panels have close agreements with observations.

The defined likelihood measure used in this study benefits from two discrete goodness of fit criteria, namely Mass Balance Error (MBE) and Nash-Sutcliff Efficiency ( $E_{ns}$ ). Both measures offer valuable information on how well model can mimic the dynamics of carbon cycling in flooded wetlands.  $E_{ns}$  measures model goodness of fit by comparing both shape and volume of simulated OC export profile versus field observations, whereas MBE evaluates model fitness based on relative percentage difference between the average of two profiles (simulated and observed) over simulation period (Arabi et al., 2007; Dongquan et al., 2012). Indeed, combining fitness measures only becomes rewarding when each measure offers independent information, in other words fitness measures ought to be independent from one another. We checked the correlation between MBE and  $E_{ns}$  values obtained from comparing model simulations of TOC export with field observations. The dot plot in Figure 2.7 has  $E_{ns}$  on vertical axis and MBE on horizontal axis for simulations which yielded  $E_{ns} > 0.7$  and  $|\text{MBE}| < 5\%$ . Dots scatter all around the plot suggest a non-existent, or rather a weak correlation ( $R^2 = 0.05$ ,  $p \cong 0$ ) between the two

measures, confirming their independence, thus supporting the use of both fitness measures to distinguish behavioral from non-behavioral parameter sets.

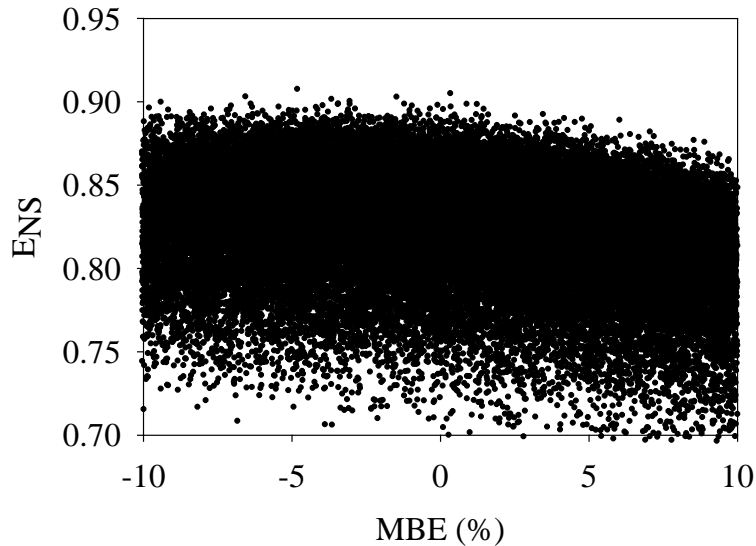


Figure 2.7: Dotty plot exhibiting ENS vs. MBE. The relative scatterings of dots over the graph reveal non-independence of the two performance criteria.

## 4.2 Methane emission

Methane and carbon dioxide emissions were not monitored at the study wetland. This prohibits verifying the methane component of the model against observed data. However, as pointed out earlier, we scrutinized the methane module via testing its sensitivity to model parameters.

Spearman's rank correlation test (Table 2.4) revealed that thickness of active sediment (H) has a high positive correlation ( $R=0.76$ ) with amount of modeled methane emission. Methanogenesis rate in anaerobic soil ( $k^3_D$ ) also appeared sensitive ( $R=0.33$ ) and positively correlated with methane emission. Third sensitive parameter with strong positive correlation ( $R=0.29$ ) appeared as nitrate inhibition factor ( $K_N^{in}$ ). This means that model allows for more methane production

when  $K_N^{in}$  is set to higher concentrations. Methane component of the model did not show strong sensitivity to other model parameters.

Table 2.4: Rank correlation coefficients (%) of model outputs versus model parameters for methane emission

Parameter	rank correlation
$H$	0.76
$k_D^3$	0.33
$K_N^{in}$	0.29
$\beta_{M1}$	-0.10
$\phi$	-0.08
$\theta$	0.07
$\phi_w$	-0.05
$K_O$	0.05
$K_O^{in}$	0.03
$k_M^1$	-0.01
$k_M^2$	-0.01
$\rho_s$	-0.01

### 4.3 Carbon mass exchanges and exports

Figure 2.8 presents the carbon mass exchanges and exports for the study wetland, averaged over behavioral model outputs in year 1, year 2 and the whole simulation period (year 1 + year 2). Note that in Figure 2.8, biomass accumulation is equivalent to net primary productivity multiplied by average area of the wetland. Over the two year study period, 3849 kg of allochthonous organic carbon was washed into the wetland through inflow. In addition,  $176 \pm 88$  kg of atmospheric C was fixed by plants over the simulation period. Over the two year period,  $1350 \pm 269$  kg of OC (equivalent to  $35.1 \pm 7.0\%$  of OC loading) was removed via microbial

decomposition processes and emitted to the atmosphere (Gaseous loss in Figure 2.8). It should be noted that at current state, WetQual-C does not trace CO<sub>2</sub> transport and consumption. For that reason, the reported gaseous loss averages were obtained by adding masses of CO<sub>2</sub> and CH<sub>4</sub> produced from aerobic and anaerobic microbial oxidation of DOC. Diffusion of DOC to soil layers retained  $269 \pm 122$  kg ( $7.0 \pm 3.2\%$  of OC loading) and a relatively small amount ( $172 \pm 79$  kg, equivalent to  $4.5 \pm 2.1\%$  of OC load) was retained in the soil as a result of settling. In the second year, wetland received around 66% (1000 kg) more OC than year 1. This could be traced back to a long dry period at the beginning of year 1 (see Figure 2.3) where hydrologic import to the wetland was limited. Reduced inflow discharge and loading in year 1 allowed for higher percentage of OC retention/removal compared to second year. According to Figure 2.8, in year 1, equivalent to  $42.8 \pm 4.7\%$  of the OC loading was removed by the study wetland whereas for year 2, this ratio was  $33.2 \pm 4.0\%$ . By comparison Jordan et al. (2003) measured 41% and 30% removal of TOC for years 1 and 2, respectively.

## **5. Summary and conclusion**

In this paper, we described development and validation of WetQual-C, a process based mathematical model for carbon cycling in flooded wetlands. The model is an extension to WetQual model (Hantush et al., 2013), a previously developed wetland nitrogen and phosphorus cycling model. WetQual-C reflects various biogeochemical interactions affecting C cycling in wetlands, and is capable of simulating the dynamics of OC retention, OC export and GHG emissions all at once. WetQual-C is coupled with other interrelated geochemical cycles (i.e. nitrogen and oxygen) and fully reflects the dynamics of the thin oxidized zone at wetlands soil-water interface, and the oxidation-reduction reactions taking place within that zone.

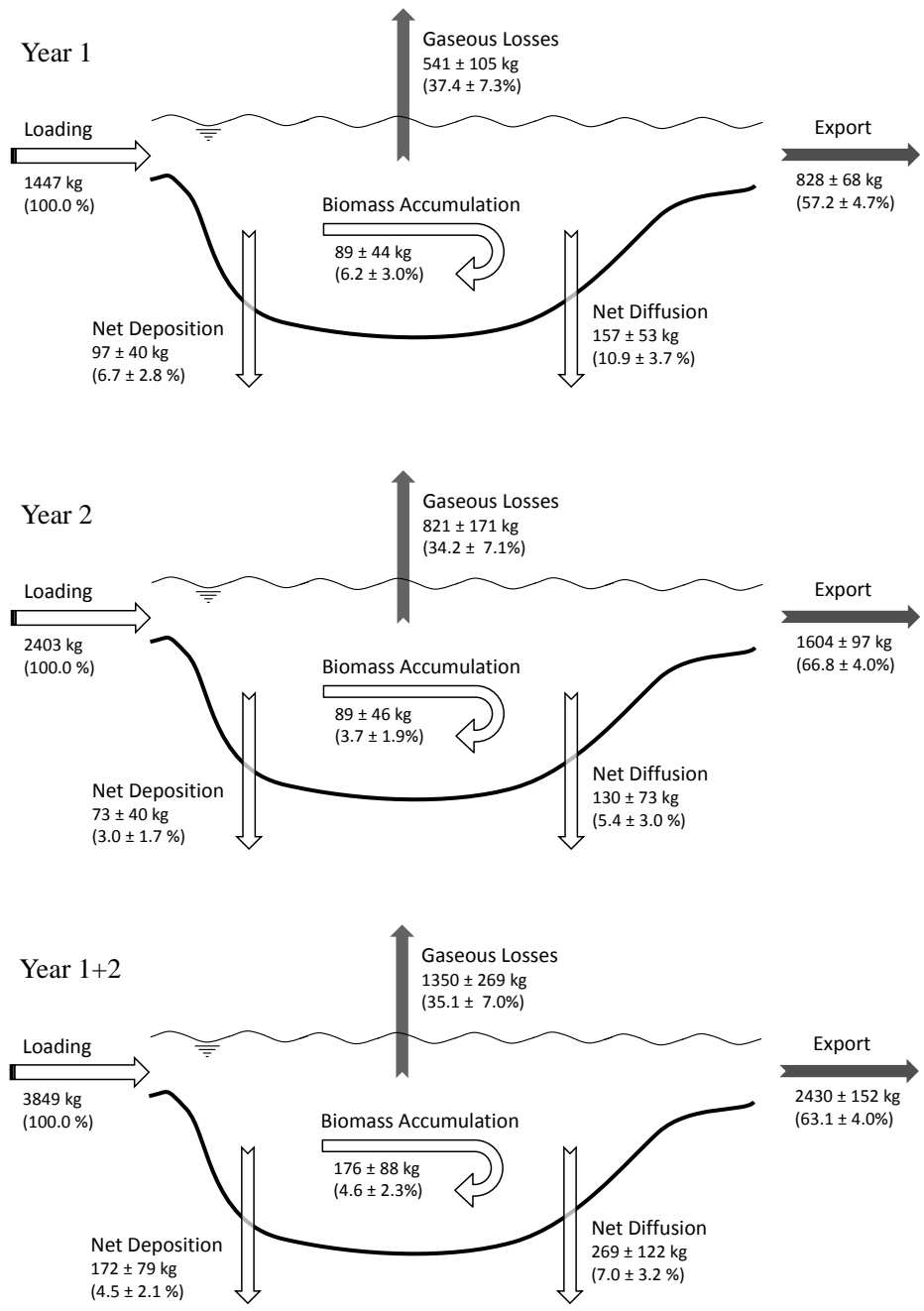


Figure 2.8: Carbon net mass exchanges and export in study wetland over year 1, year 2 and the whole simulation period.

A thorough sensitivity and uncertainty analysis was performed on model components to evaluate its credibility using field collected data from a small wetland. The model showed a narrow behavioral uncertainty predicting TOC export, however, overall model uncertainty peaked substantially when outflow was high. Overall, model performed well in capturing TOC export fluctuations and dynamics from the study wetland. Model appears to be more reliable and less uncertain when it's predictions on TOC export is used; nevertheless, model performance on concentration simulations was shown to be relatively acceptable too.

The presented model in this study is a process based model, i.e. most parameters and constants have physical meanings. Through lab and in-situ experiments, most variables could potentially be estimated. Although the number of parameters used in WetQual-C might appear disproportionate, if water quality is monitored (even for a short period of time), least sensitive parameters could easily be identified via sensitivity analysis, and fixed at their average values. In case observed data are not available for the study wetland, model users can still benefit from the median results of the MC simulation time series.

Over the period of 2 years, the study wetland removed equivalent to  $35.1 \pm 7.0\%$  of the OC carbon intake via OC decomposition, and retained equivalent to  $11.5 \pm 5.3\%$  mainly through DOC diffusion to sediment. Thus, the study wetland appeared as a carbon sink rather than source and proved its purpose as a relatively effective and low cost mean for improving water quality. As WetQual-C was intended for fresh water wetlands, it does not account for methane removal by anaerobic oxidation processes other than denitrification. This can be a limitation if WetQual-C is applied to salt water wetlands where sulfate and other minerals are abundant.

Since hydrology was an input to the model, we did not consider uncertainties related to flow measurements. Uncertainty in field measurements (input uncertainty) was not assessed either, assuming that field measurements are accurate and not too deviant. Such additional uncertainties were ignored due to lack of information on measurement deviations; however, if they were counted for, the marks representing observed data (black dots on Figure 2.6) would have appeared with uncertainty bands, enabling us to compare model uncertainty with input uncertainty.

The process of parting behavioral parameter sets from non-behavioral ones is indeed exceedingly delicate and one should pay particular attention to selecting right likelihood measures for such purposes. Faulty, imprecise uncertainty and sensitivity analysis is a very probable consequence of relying on improper likelihood measures for testing model fitness. In this study, we defined a new likelihood measure that combines two discrete goodness of fit criteria, namely Mass Balance Error and Nash-Sutcliff Efficiency. By means of a dotty plot (Figure 2.7), it was revealed that there was a weak correlation between the two goodness of fit measures, confirming their independence. This independence promises that each measure offers unique information, thus supporting the use of both fitness measures for distinguishing behavioral from non-behavioral parameter sets.

The primary productivity rate that the model reported was roughly  $8.6 \pm 4.0 \text{ gC m}^2 \text{ year}^{-1}$ . This productivity rate is considerably less than that of reported rates for freshwater marshes (155-6180  $\text{gC m}^2 \text{ year}^{-1}$ , Reddy and Delaune, 2008). This fact indicates that plant growth module of WetQual model needs to be re-evaluated and enhanced.

## 6. Appendix

### Temperature dependence of reaction rates and coefficients

- Arrhenius equation (Chapra, 1997; Schnoor, 1996) is used to describe dependence of several reaction rates and model variables to temperature variation:

$$k_T = k_{20} \theta^{T-20} \quad (2.25)$$

where,  $T$  is temperature expressed in  $^{\circ}\text{C}$ ;  $\theta$  is a constant temperature coefficient; and  $k_{20}$  is the rate constant at the reference temperature  $20^{\circ}\text{C}$ .  $\theta$  is usually greater than 1 and can be considered as a calibration coefficient.  $k_{da}$ ,  $k_{db}$ ,  $k_L$ ,  $k_R$ ,  $k_D^1$ ,  $k_D^2$ ,  $k_D^3$ ,  $K_N^{in}$ ,  $K_O^{in}$ ,  $K_N$ ,  $K_O$ ,  $k_M^1$ ,  $k_M^2$  are among the variables and rates adjusted for temperature.

- Diffusivity of DOC in open water,  $D_D^*$  (unit:  $\text{cm}^2 \text{d}^{-1}$ ) is adjusted for temperature using an average form suggested by Boudreau (1997)

$$D_D^* = 0.0864(9.5 + 0.3319T) \quad (2.26)$$

where  $T$  is water temperature in  $^{\circ}\text{C}$ .

$D^{\sigma}$ , defined as diffusivity of  $\text{CH}_4$  in air ( $\text{m}^2 \text{s}^{-1}$ ), is adjusted for temperature following Tang et al. (2010):

$$D^{\sigma} = 1.9 \times 10^{-5} \times \left( \frac{T}{298} \right)^{1.82} \quad (2.27)$$

where  $T$  is ambient air temperature in  $^{\circ}\text{K}$ .

- Equation for methane free water diffusion coefficient,  $D_M^*$  (unit:  $\text{cm}^2 \text{d}^{-1}$ ) is given by (Arah and Stephen, 1998; Tang et al., 2010):

$$D_M^* = 1.5 \times 10^{-9} \times \left( \frac{T}{298} \right) \quad (2.28)$$

- Wania et al. (2010) provided a temperature dependent relationship for methane Bunsen solubility coefficient ( $S_B$ ) by fitting a second order polynomial to observations provided by Yamamoto et al. (1976):

$$S_B = 0.05708 - 0.001545T + 0.00002069T^2 \quad (2.29)$$

where T is water temperature in  $^{\circ}\text{K}$ .

- Equilibrium concentration of  $\text{CH}_4$  in atmosphere,  $C^*$  [ $\text{ML}^{-3}$ ] can be obtained from Henry's law. Following equation describes  $C^*$  when dependency of Henry's coefficient to temperature is considered (Sander, 1999):

$$C^* = 1.4 \times 10^{-3} \exp \left[ -1700 \left( \frac{1}{T} - \frac{1}{298} \right) \right] \times p_{\text{CH}_4} \quad (2.30)$$

where  $C^*$  has a unit of  $\text{mol L}^{-1}$  and T is ambient air temperature in  $^{\circ}\text{K}$ .  $p_{\text{CH}_4}$  is atmospheric partial pressure of methane, assigned a constant value of  $1.7 \times 10^{-6}$  atm (Wania et al., 2010).

- Following Rietta et al (1999) and Wania et al. (2010), a third order polynomial, fitted to observations obtained by Jähne et al. (1987), was used to describe temperature dependency of methane Schmidt number:

$$Sc_M = 1898 - 110.1T + 2.834T^2 - 0.02791T^3 \quad (2.31)$$

where T is water temperature in  $^{\circ}\text{C}$ .

### **Diffusive mass transfer coefficients**

Diffusive mass transfer coefficients of  $\beta_D$  and  $\beta_M$  are calculated using a two-layer approach similar to Hantush et al. (2013). Assuming linear variation of concentration between layers, for

substance  $x$ , effective mass transfer coefficient between water and aerobic sediment,  $\beta_{x1}$  is given by

$$\beta_{x1} = \frac{2\phi_w\phi\tau D_x^*}{\phi\tau h + \phi_w l_1}, \quad x = D, M \quad (2.32)$$

Similarly,  $\beta_{x2}$  (effective mass transfer coefficient between aerobic and anaerobic sediment layers) is

$$\beta_{x2} = \frac{2\phi\tau D_x^*}{l_1 + l_2}, \quad x = D, M \quad (2.33)$$

where,  $D_x^*$  is free-water diffusion coefficient for substance  $x$  [ $L^2T^{-1}$ ]; and  $\tau$  is tortuosity of sediment (Refer to Table 2.1 for definition of other parameters).

### **Chapter 3: Capturing spatial variability of concentrations and reaction rates in wetland water and soil through model compartmentalization**

#### ***Abstract***

An important limitation of most existing wetland geochemical models is their assumption of uniformity along the horizontal plain. Such models are lumped in the horizontal domain, considering average reaction rates throughout the whole wetland soil and water, and thus not able to capture the dynamics of geochemical exchanges within (and between) active and passive areas of the wetland. In this chapter, we aimed to expand WetQual model's spatial resolution through compartmentalization of the model, in order to capture the spatial variability of constituent concentrations in water and sediment of various zones in the wetland. The compartmental model was applied to data collected from a restored wetland in California's Central Valley during growing season of 2007. The study wetland has a formation of a large stagnant zone at the southern end which constitutes more than 50% of the wetland area. Mass balance analysis revealed that over the course of study period, about  $23.4 \pm 3.9\%$  of the incoming TN load and  $21.1 \pm 4.4\%$  of the TOC load was removed or retained by the study wetland. It was observed that mass of all exchanges (physical and biogeochemical) regarding nitrogen and carbon cycling decreased along the activity gradient from active to passive zones of the wetland. More deposition of OC occurred in active and transient zones compared to passive zone. It was also revealed that anaerobic processes become more significant along activity gradient toward passive areas. Despite less availability of  $\text{NO}_3$  in passive areas, there was a more favorable environment for denitrification in passive regions of the wetland.

## 1. Introduction

Wetlands have been widely recognized as effective means for water quality improvement and alleviation of nonpoint-source pollution associated with agricultural runoff (Mitsch and Gosselink, 2007). A common phenomenon that is observed in natural and constructed wetlands is short circuiting of flow and formation of stagnant zones that are only indirectly available to the incoming water (Min and Wise, 2009). Such formations offset treatment effectiveness of wetlands by reducing active volume and consequently shortening the hydraulic retention time (Kadlec and Wallace, 2008).

Wetland models are useful tools for understanding complex interactions between wetland soil, hydrology and vegetation. Biogeochemistry of passive areas are potentially different than that of active zones (Reddy and Delaune, 2008), making it difficult for many existing wetland models to capture the dynamics of geochemical exchanges within (and between) active and passive areas of the wetland. An important limitation of most existing wetland geochemical models, including the ones reviewed in chapter 1, is their assumption of uniformity along the horizontal plain. Such models are lumped in the horizontal domain, considering uniform concentrations and reaction rates throughout water and soil columns of the whole wetland, and thus not able to capture the full spectrum of geochemical interactions in different zones of the wetland. When there is non-uniformity in flow and geochemical reactions throughout the wetland, a more sophisticated wetland model is called for to overcome the limitations of lumped models.

Consider the wetland presented in Figure 3.1, a generic (hypothetical) wetland characterized by a deeper open channel in the middle and shallower stagnant zones with emergent vegetation on the sides. Most probably, soil characteristics and thus dominant processes of the main channel are

very different from those of stagnant zones on the side. The main channel conveys a large amount of flow, thus not supporting emergent macrophytes, whereas the stagnant zones are ideal for emergent vegetation. A study by Anderson et al. (2006) on two constructed wetlands detected higher mean sediment accumulation in the deeper open water zones than in the emergent vegetation zones. On the contrary, authors reported higher organic C concentrations in the sediment of stagnant zones. Another finding of Anderson et al. (2006) was gradual decrease in accumulation of sedimentation from inflow to outflow in deeper zones. In this chapter, we aim to upgrade WetQual model to a quasi-3D state in terms of spatial resolution. This upgrade will allow us to consider different soil characteristics, depth and reaction rates for various zones of the wetland, enabling us to capture the spatial variability of constituent concentrations in water and sediment of various zones in the wetland.

In previous chapters, it was indicated that WetQual is comprised of three compartments in the vertical domain ( $z$ ), including standing water and two soil compartments (aerobic and anaerobic) and lumped in the horizontal domain ( $x$ - $y$  plain). Thus WetQual qualified as a quasi-1D model. This chapter aims to expand model resolution in the horizontal domain by discretizing the spatial domain (wetland area) into compartments, and connecting neighboring compartments through advective and dispersive/diffusive exchange. In general terms, a compartment is defined as a volume of medium within which the chemical concentrations do not vary spatially and thus system parameters are constant (Little, 2012). In the compartmental scheme, the spatial domain of the wetland is abstracted as a set of compartments, with the total number of compartments reflecting the desired spatial resolution. In our case, the numbers and sizes of compartments are specified by user. The new compartmentalization scheme allows us to consider different depths, shapes and reaction rates for different compartments along the wetland.

The compartmental model is applied to data collected from a restored wetland located on the west side of the San Joaquin River in California's Central Valley during growing season of 2007. Due to close vicinity of inflow and outflows in the northern side of the wetland, the study site has a formation of a large stagnant zone at the southern end of the wetland which constitutes more than 50% of the wetland area. The study wetland was divided to 4 compartments along the activity gradient from north to south (most active to most passive). Through a detailed sensitivity and mass balance analysis, we aim to identify the most important processes engaging nitrogen and carbon constituents along the activity gradient line.

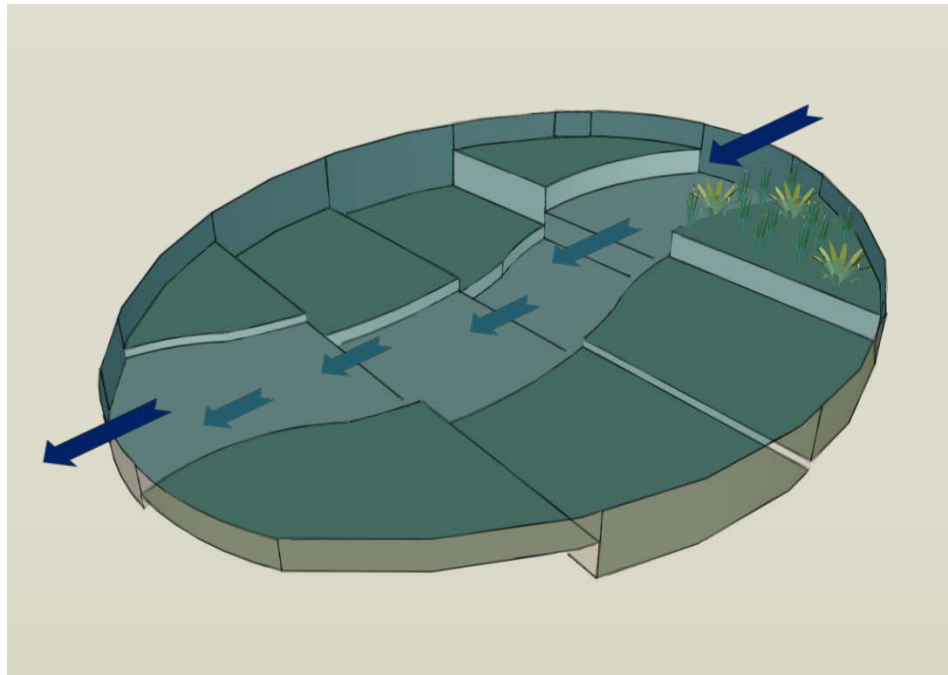


Figure 3.1: A hypothetical wetland, catalogued to a number of compartments with varying depths

## 2. Compartmentalization approach

As discussed earlier, in the horizontally lumped model, the wetland was partitioned into three columns in the vertical (z) direction: water, aerobic sediment and anaerobic sediment columns. For each constituent, a set of three ordinary differential equations were coupled to explain the variation of concentration in the water and sediment columns. It was assumed that concentrations are spatially uniform throughout the whole wetland, in other words, model was lumped in the x-y (horizontal) domain.

For a generic constituent in water column (such as DOC), we had

$$\phi_w \frac{dV_w C_w}{dt} = Q_{in} C_{in} - Q_{out} C_w - k \phi_w V_w C_w + \beta_1 A (C_s - C_w) \quad (3.1)$$

where the left hand side of the equation explains variation of concentration ( $C_w$ ) over time in water column; and the four terms on the right hand side, respectively, explain direct loading gain through inflow, loss through outflow, loss through internal decay, and exchanges between water and sediment columns through diffusive transport.

In the compartmental approach, we divide the wetland further into compartments or volumes in the horizontal domain, and write the set of three coupled differential equations` for each compartment. Concentrations and parameters (coefficients) are assumed to be spatially uniform within each compartment (as opposed to the whole wetland). Figure 3.2 shows a 2-D schematic plan of the hypothetical compartmentalized wetland previously depicted in Figure 3.1.

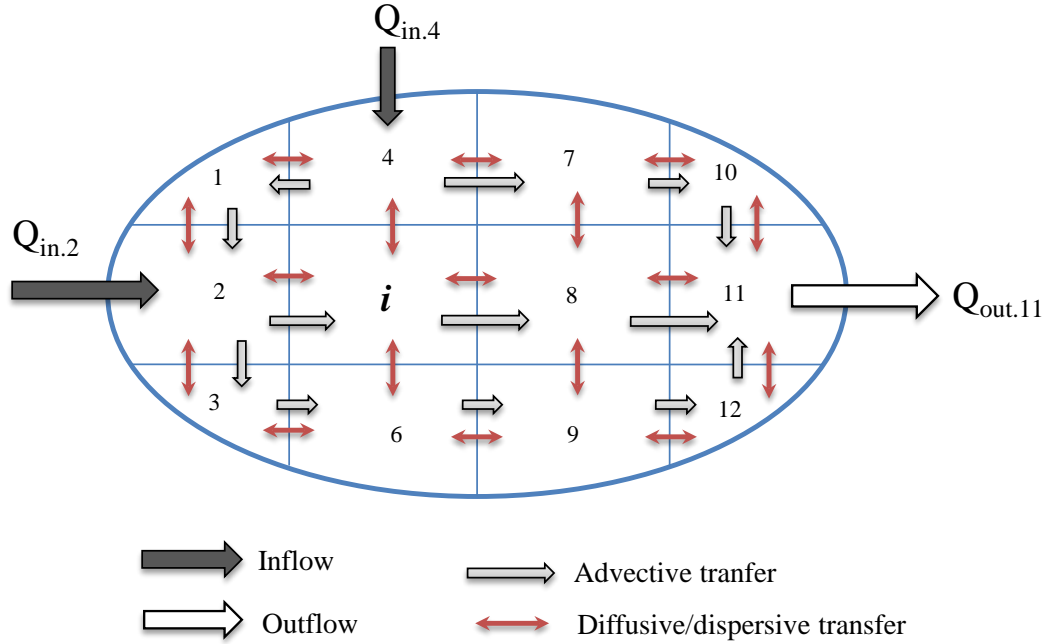


Figure 3.2: A schematic plan of a compartmentalized wetland

Under this compartment modeling approach, equation (3.1) is re-written for each compartment as:

$$\begin{aligned}
 \phi_{w,i} \frac{dV_i C_{w,i}}{dt} = & Q_{in,i} C_{in,i} - Q_{out,i} C_{w,i} \\
 & + \sum_{j=1,n} (Q_{j,i} C_{w,j} - Q_{i,j} C_{w,i}) + \sum_{j=1,n} \beta_{i,j} A_{i,j} (C_{w,j} - C_{w,i}) \\
 & - k_i \phi_{w,i} V_{w,i} C_{w,i} + \beta_1 A_i (C_{s,i} - C_{w,i})
 \end{aligned} \quad (3.2)$$

Where  $i$  is the index for compartment  $i$ , thus  $C_{w,i}$  becomes the constituent concentration at the center of compartment  $i$  and  $V_{w,i}$  is the volume of compartment  $i$ , and so on. There are two additional terms that appear on equation (3.2) (third and fourth term on the right hand side) which explain the advective and diffusive/dispersive mass exchanges between compartments. Within the new terms,  $Q_{i,j}$  is the advective flow rate across interface from compartment  $i$  to  $j$

( $L^3T^{-1}$ );  $\beta_{i,j}$  is the dispersive/diffusive mass transfer rate across  $i,j$  boundary ( $LT^{-1}$ ) and  $A_{i,j}$  is the area of the interface between compartments  $i$  and  $j$ .

### 2.1.1 Advective exchange

As appears in Figure 3.2, the new compartmental scheme allows for external inflows and outflows to/from any compartment within the wetland. The inflow/outflow rates, in addition to inflowing constituent concentrations have to be provided by the user in separate text files.

Estimation of advective flow rates across interface between compartments ( $Q_{i,j}$  in Equation (3.2)) is a complicated matter. Since our wetland model is not capable of estimating these interchanges directly, ideally, it would be best if the model is paired with a hydrodynamic model. In other words, the advective interchanges between compartments need to be provided by user, and a hydrodynamic wetland model would be the best tool for estimating these discharges, specifically in wetlands with complicated geometry. Nevertheless, there are approximations that could be used in wetlands with simpler geometries. To give an example, consider the wetland presented in Figure 3.3, a simple wetland divided to 5 compartments, with the main inlet placed on compartment 2 and the outlet placed on compartment 4. There are two stagnant zones within the wetland, compartments 1 and 5, which are not directly connected to the main flow path. For the sake of simplicity, it could be assumed that water level in all five compartments rise or fall simultaneously. In other words, at any given time step, when (*inflows* – *outflows*) > 0, then all compartments will have an increase in volume of standing water; and when (*inflows* – *outflows*) < 0, water level in all compartments drop simultaneously. Increase or decrease of the volume of standing water in compartments will be proportional to their area, since it is assumed that depth of increase/decrease is same all over the wetland.

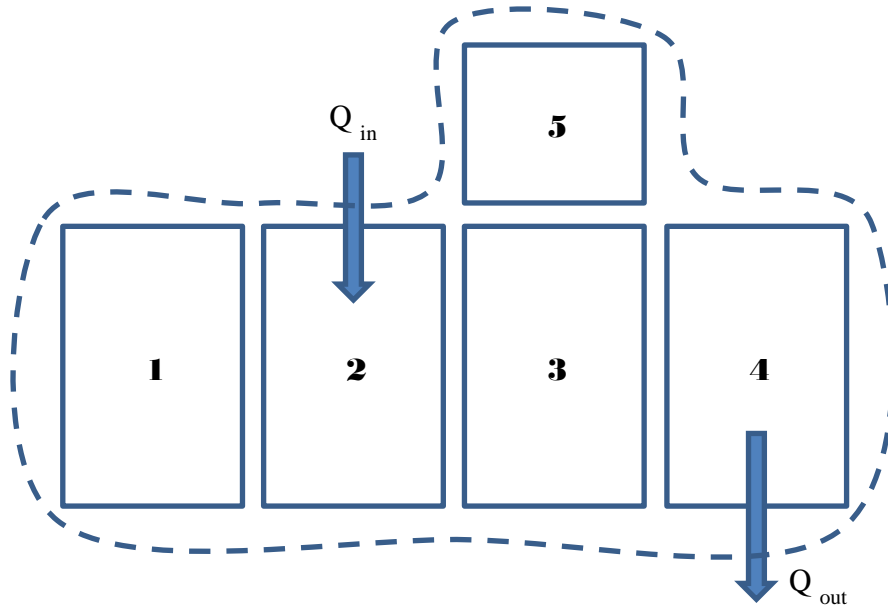


Figure 3.3: A schematic representation of a simple wetland with 4 compartments

At each time step, model forms a matrix called  $[Q_{\text{advect}}]$  which contains the internal advective discharges passed between elements.  $[Q_{\text{advect}}]$  is a square matrix of order  $n$ , where  $n$  is the total number of compartments in wetland, and zeros on the main diagonal. For the wetland in Figure 3.3,  $[Q_{\text{advect}}]$  will have the following form:

$$[Q_{\text{advect}}]_{5 \times 5} = \begin{matrix} & \begin{matrix} 1 & 2 & 3 & 4 & 5 \end{matrix} \\ \begin{matrix} 1 \\ 2 \\ 3 \\ 4 \\ 5 \end{matrix} & \begin{bmatrix} 0 & Q_{1,2} & 0 & 0 & 0 \\ Q_{2,1} & 0 & Q_{2,3} & 0 & 0 \\ 0 & Q_{3,2} & 0 & Q_{3,4} & Q_{3,5} \\ 0 & 0 & Q_{4,3} & 0 & 0 \\ 0 & 0 & Q_{5,3} & 0 & 0 \end{bmatrix} \end{matrix}$$

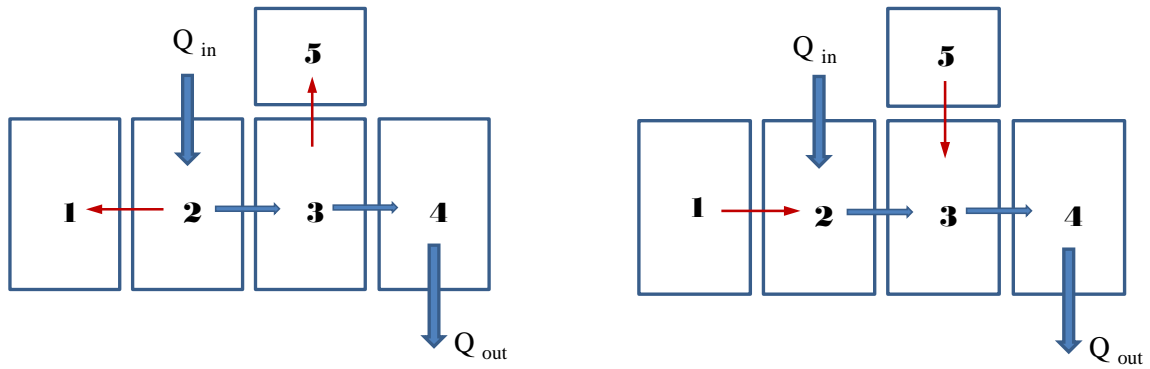


Figure 3.4: direction of interval advective exchanges between compartments when the water level is rising (left pannel) and falling (right pannel)

Note that at time step  $t$ , the internal advective exchange between compartments  $i$  and  $j$  is unidirectional, meaning that flow is either from  $i$  to  $j$  ( $Q_{i,j}$ ), or from  $j$  to  $i$  ( $Q_{j,i}$ ). In other words,  $Q_{i,j}$  and  $Q_{j,i}$  will not appear on  $[Q_{advect}]$  at the same time step.

For the case when there is a rise in water level throughout the wetland ( $Q_{in} > Q_{out}$ , left panel of, Figure 3.4),  $[Q_{advect}]$  is formulated as:

$$[Q_{advect}]_{5 \times 5} = \begin{matrix} & \begin{matrix} 1 & 2 & 3 & 4 & 5 \end{matrix} \\ \begin{matrix} 1 \\ 2 \\ 3 \\ 4 \\ 5 \end{matrix} & \begin{bmatrix} 0 & 0 & 0 & 0 & 0 \\ Q_{2,1} & 0 & Q_{2,3} & 0 & 0 \\ 0 & 0 & 0 & Q_{3,4} & Q_{3,5} \\ 0 & 0 & 0 & 0 & 0 \\ 0 & 0 & 0 & 0 & 0 \end{bmatrix} \end{matrix}$$

where

$$\begin{aligned}
Q_{2,1} &= \frac{|V_{w,1}^{t+\Delta t} - V_{w,1}^t|}{\Delta t} & Q_{3,5} &= \frac{|V_{w,5}^{t+\Delta t} - V_{w,5}^t|}{\Delta t} \\
Q_{2,3} &= Q_{in} - Q_{2,1} & Q_{3,4} &= Q_{2,3} - Q_{3,5}
\end{aligned} \tag{3.3}$$

And for the case when water level falls throughout the wetland ( $Q_{in} < Q_{out}$ , right panel of, Figure 3.4)  $[Q_{advect}]$  is formulated as:

$$[Q_{advect}]_{5 \times 5} = \begin{matrix} & \begin{matrix} 1 & 2 & 3 & 4 & 5 \end{matrix} \\ \begin{matrix} 1 \\ 2 \\ 3 \\ 4 \\ 5 \end{matrix} & \begin{bmatrix} 0 & Q_{1,2} & 0 & 0 & 0 \\ 0 & 0 & Q_{2,3} & 0 & 0 \\ 0 & 0 & 0 & Q_{3,4} & 0 \\ 0 & 0 & 0 & 0 & 0 \\ 0 & 0 & Q_{5,3} & 0 & 0 \end{bmatrix} \end{matrix}$$

where

$$\begin{aligned}
Q_{1,2} &= \frac{|V_{w,1}^{t+\Delta t} - V_{w,1}^t|}{\Delta t} & Q_{5,3} &= \frac{|V_{w,5}^{t+\Delta t} - V_{w,5}^t|}{\Delta t} \\
Q_{2,3} &= Q_{in} + Q_{1,2} & Q_{3,4} &= Q_{2,3} + Q_{5,3}
\end{aligned} \tag{3.4}$$

Terms  $V_{w,i}^t$  and  $V_{w,i}^{t+\Delta t}$  which represent volume of standing water of compartment  $i$  at beginning and end of the time step should be provided by user. Ideally, such information comes from field measurements; however, in case such data is not available, it can be easily calculated through flow routing (given that wetland bathymetry is available). Defining components of the  $[Q_{advect}]$  matrix is the biggest challenge that confronts model users. There is no general formulation that could be applied for forming  $[Q_{advect}]$  matrix, as the size and composition of  $[Q_{advect}]$  varies with depending on labeling, connectivity and positioning of compartments.

### 2.1.2 Diffusive/dispersive exchange

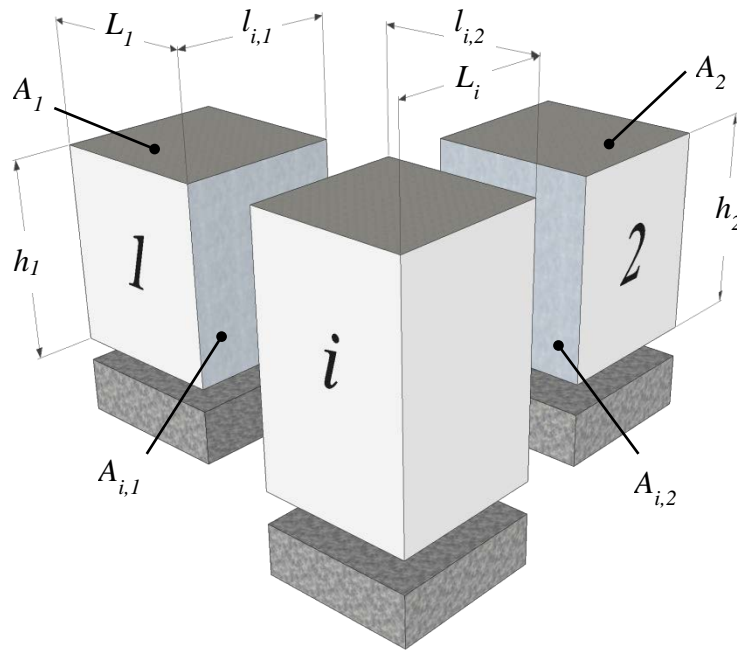


Figure 3.5: Schematic illustration of three adjacent compartments and concept of effective diffusion/dispersion parameter

Diffusion and dispersion are two distinct processes that take place in very different scales; diffusion acts at the molecular level whereas dispersion is a macro process caused by non-uniform flow patterns. Molecular diffusion happens with a rate of  $10^{-8}$  to  $10^{-4}$   $\text{cm}^2/\text{sec}$  whereas longitudinal dispersion has a rate of  $10^4$  to  $10^7$   $\text{cm}^2/\text{sec}$  (Chapra, 1997); thus dispersion typically overshadows molecular diffusion in aquatic environments. However, diffusion and dispersion are modeled identically, thus we will consider their effects collectively in a mass transport term as dispersion/diffusion.

Similar to Hantush et al. (2013), for the dispersive/diffusive mass transfer rate across  $i,j$  boundary,  $\beta_{i,j}$  can be obtained by conserving mass flow in the schematic compartmental system

depicted in Figure 3.5. Between two adjacent compartments (like  $i$  and  $l$  in Figure 3.5), assuming linear drop in concentration from the center of the compartment  $i$  to the interface separating the two compartments, the expression for the effective diffusive/dispersive mass transfer coefficient ( $\beta_{i,j}$ ) could be obtained as:

$$\beta_{i,1} = \frac{2\phi_1\phi_i\tau_1\tau_i(D^* + D_d)}{\phi_i L_1 + \phi_1 L_i} \quad (3.5)$$

where  $\tau_i$  is tortuosity of compartment  $i$ ,  $D^*$  is free-water molecular diffusion coefficient [ $L^2T^{-1}$ ] and  $D_d$  is dispersion coefficient between compartments  $i$  and 1.  $L_l$  and  $L_i$  are non-shared lengths of the two compartments, computed by dividing area of each compartment over the shared length between two compartments ( $L_i = A_i / l_{i,1}$  and  $L_1 = A_1 / l_{i,1}$ ). Initial area of each compartment, as well as the length shared with adjacent compartments need to be provided by user; however, these two variables shrink and expand dynamically as the total area of the wetland shrink and expands over time, and are updated routinely at the beginning of the time step.

Several formulas have been suggested for estimation of dispersion coefficient in streams and rivers (Chapra, 1997), where longitudinal dispersion is computed as a function of shear velocity/discharge. Fischer et al. (1979) have suggested the following relationship for rivers:

$$D_d = 0.011 \frac{U^2 B^2}{H U^*} \quad (3.6)$$

where  $D_d$  is dispersion coefficient ( $m^2s^{-1}$ ),  $U$  is flow velocity ( $ms^{-1}$ ),  $B$  is channel width (m),  $H$  is mean depth (m) and  $U^*$  is shear velocity ( $ms^{-1}$ ). Shear velocity could be defined as:

$$U^* = \sqrt{gHS} \quad (3.7)$$

where  $g$  is gravitational acceleration ( $\text{ms}^{-2}$ ) and  $S$  is channel slope (dimensionless). For wetland applications, channel slope ( $S$ ) should be replaced with wetland bed slope, attainable from wetland bathymetry.

In case of hydrodynamic wetland modeling, dispersion coefficient is generally calculated as a function of flow and grid size, multiplied by a calibration factor. The following formulation, suggested by DHI (2004), is one out of several empirical methods for estimation of dispersion coefficients:

$$D_x = a_x \cdot \Delta x \cdot v_x \quad (3.8)$$

where  $D_x$  the dispersion coefficient in  $x$  direction ( $\text{m}^2 \text{s}^{-1}$ ),  $\Delta x$  is the constant grid spacing,  $v_x$  is the local current velocity in  $x$  direction ( $\text{ms}^{-1}$ ), and  $a_x$  is the calibration factor.

To estimate the dispersion coefficient in this study, we used a combination of the two methods. At the beginning of each time step, model computes a rough estimate of the dispersion coefficient through Equation (3.6), and then multiplies it by a calibration constant called  $Ef_{act}$ . This calibration factor is required as an input for each MC simulation, and thus sensitivity of the model to  $Ef_{act}$  can be quantified through K-S test and interpreted as a surrogate of model sensitivity to dispersion/diffusion.

### 2.1.3 Numerical Integration

Similar to earlier versions of WetQual model, numerical integration is performed using an explicit numerical scheme with forward-difference approximation of the time derivatives. In the compartmental model, however, the solution is repeated for each compartment, with an order

following compartment indices. For the lumped model, the first-order ordinary differential equation (ODE) presented in Equation (3.1) has a solution as following:

$$C_w^{t+\Delta t} = \frac{\Delta t(Q_{in}C_{in} + \beta_1AC_s^t) + V_w^tC_w^t\phi_w}{\Delta t(Q_{out} + \beta_1A + k\phi_wV_w^t) + V_w^{t+\Delta t}\phi_w} \quad (3.9)$$

where  $t$  and  $t + \Delta t$ , respectively, denote time at the beginning and the end of one time step. For the compartmental approach, however, the solution is not as straight forward. The terms with summation signs in Equation (3.2), addressing advective and dispersive interchanges between adjacent compartments make the numerical solution more complicated. The solution requires an inner loop (iteration) to take care of the summation terms. Previously, it was mentioned that the user defines the internal advective relationships between elements. At beginning of each time step, we use this information to form two new parameters,  $\mathbf{X}$  and  $\mathbf{Y}$  to help with the numerical integration.

For  $C_{w,i}$  (concentration of a generic constituent within compartment  $i$ ), at the beginning of the time step,  $\mathbf{X}$  and  $\mathbf{Y}$  are calculated as:

$$\mathbf{X} = \sum_{j=1}^n A_{i,j} [\beta]_{i,j} C_{w,j}^t + \sum_{j=1}^n [Q]_{j,i} C_{w,j}^t \quad (3.10)$$

$$\mathbf{Y} = \sum_{j=1}^n A_{i,j} [\beta]_{j,i} + \sum_{j=1}^n [Q]_{i,j} \quad (3.11)$$

and the final solution is formed as:

$$C_{w,i}^{t+\Delta t} = \frac{\Delta t(Q_{in,i}C_{in,i} + \beta_1 A_i C_{s,i}^t + \mathbf{X}) + V_{w,i}^t C_w^t \phi_{w,i}}{\Delta t(Q_{out,i} + \beta_1 A_i + k_i \phi_{w,i} V_{w,i}^t + \mathbf{Y}) + V_{w,i}^{t+\Delta t} \phi_{w,i}} \quad (3.12)$$

which needs to be solved for each compartment separately.

## 2.2 Updated compartmental model equations

Based on the presented methodology, model equations for nitrogen, phosphorus, oxygen, sediment (Hantush et al., 2013), and carbon compounds were re-written as Equations (3.13) to (3.39). Note that model parameters/variables followed by subscript  $i$  ( $j$ ) represent reaction rates/concentrations specific to  $i^{th}$  ( $j^{th}$ ) compartment. Similarly,  $Q_{i,j}$  is the advective flow rate across interface between compartments  $i$  and  $j$  ( $L^3T^{-1}$ ) and  $A_{i,j}$  is the area of the interface between compartments  $i$  and  $j$ . Please refer to Appendix for definitions of the rest of the parameters presented through Equations (3.13) to (3.39).

### 2.2.1 Organic N

$$\begin{aligned} \phi_{w,i} \frac{d(V_{w,i}N_{ow,i})}{dt} &= Q_{in,i}N_{ow,in,i} + a_{na}k_{da}a_i + a_{na}k_{db}f_{bw}b_i - \phi_w V_{w,i}k_{mw,i}N_{ow,i} - v_{s,i}\phi_{w,i}A_iN_{ow,i} \\ &+ v_{r,i}\phi_{w,i}A_i(N_{or,i} + N_{os,i}) - Q_{o,i}N_{ow,i} + A_i f_{sw}S_i \\ &+ \sum_{j=1,n} (Q_{j,i}N_{ow,j} - Q_{i,j}N_{ow,i}) + \sum_{j=1,n} \beta_{o,i,j}A_{i,j}(N_{ow,j} - N_{ow,i}) \end{aligned} \quad (3.13)$$

$$\begin{aligned} V_{s,i} \frac{dN_{or,i}}{dt} &= f_r a_{na}k_{db}f_{bs}b_i + f_r v_{s,i}\phi_{w,i}A_iN_{ow,i} - v_{r,i}\phi_{w,i}A_iN_{or,i} - V_{s,i}k_{mr,i}N_{or,i} - v_{b,i}A_iN_{or,i} \\ &+ f_r(1 - f_{sw})A_iS_i \end{aligned} \quad (3.14)$$

$$\begin{aligned} V_{s,i} \frac{dN_{os,i}}{dt} &= f_s a_{na}k_{db}f_{bs}b_i + f_s v_{s,i}\phi_{w,i}A_iN_{ow,i} - v_{r,i}\phi_{w,i}A_iN_{os,i} - V_{s,i}k_{ms,i}N_{os,i} - v_{b,i}A_iN_{os,i} \\ &+ f_s(1 - f_{sw})A_iS_i \end{aligned} \quad (3.15)$$

### 2.2.2 Ammonia-N

$$\begin{aligned}
\phi_{w,i} \frac{d(V_{w,i} N_{aw,i})}{dt} &= Q_{in,i} N_{aw\ in,i} + i_p A_i N_{ap} - \phi_{w,i} V_{w,i} f_N k_{nw,i} N_{aw,i} + \beta_{a1} A_i (N_{a1,i} - N_{aw,i}) \\
&+ F_{N_{ag},i}^w - k_v \phi_{w,i} A_i (1 - f_N) N_{aw,i} + \phi_{w,i} V_{w,i} k_{mw,i} N_{ow,i} - Q_{o,i} N_{aw,i} \\
&- f_{aw} a_{na} k_{ga} a_i + A_i q_a \\
&+ \sum_{j=1,n} (Q_{j,i} N_{aw,j} - Q_{i,j} N_{aw,i}) + \sum_{j=1,n} \beta_{a,i,j} A_{i,j} (N_{aw,j} - N_{aw,i})
\end{aligned} \tag{3.16}$$

$$\begin{aligned}
\phi_i V_{1,i} R_{s,i} \frac{dN_{a1,i}}{dt} &= -A_i \beta_{a1,i} (N_{a1,i} - N_{aw,i}) + F_{N_{ag},i}^1 - f_{a1} a_{na} k_{gb} f_1 b_i - \phi_i A_i v_{b,i} N_{a1,i} \\
&- \phi_i V_{1,i} f_N k_{ns,i} N_{a1,i} + A_i \beta_{a2,i} (N_{a2,i} - N_{a1,i}) + V_{1,i} k_{mr,i} N_{or,i} + V_{1,i} k_{ms,i} N_{os,i}
\end{aligned} \tag{3.17}$$

$$\begin{aligned}
\phi_i V_{2,i} R_{s,i} \frac{dN_{a2,i}}{dt} &= -A_i \beta_{a2,i} (N_{a2,i} - N_{a1,i}) - \phi_i A_i v_{b,i} (N_{a2,i} - N_{a1,i}) + F_{N_{ag},i}^2 + V_{2,i} k_{mr,i} N_{or,i} \\
&+ V_{2,i} k_{ms,i} N_{os,i} - f_{a2} a_{na} k_{gb} f_2 b_i
\end{aligned} \tag{3.18}$$

### 2.2.3 NO<sub>3</sub>-N

$$\begin{aligned}
\phi_{w,i} \frac{d(V_{w,i} N_{nw,i})}{dt} &= Q_{in,i} N_{nw\ in,i} + i_p A_i N_{np} + \phi_{w,i} V_{w,i} f_N k_{nw,i} N_{aw,i} + \beta_{n1} A_i (N_{n1,i} - N_{nw,i}) \\
&+ F_{N_{ng},i}^w - f_{nw} a_{na} k_{ga} a_i - Q_{o,i} N_{nw,i} + A_i q_n \\
&+ \sum_{j=1,n} (Q_{j,i} N_{nw,j} - Q_{i,j} N_{nw,i}) + \sum_{j=1,n} \beta_{n,i,j} A_{i,j} (N_{nw,j} - N_{nw,i})
\end{aligned} \tag{3.19}$$

$$\begin{aligned}
\phi_i V_{1,i} \frac{dN_{n1,i}}{dt} &= -A_i \beta_{n1,i} (N_{n1,i} - N_{nw,i}) + F_{N_{ng},i}^1 + \phi_i V_{1,i} f_N k_{ns,i} N_{a1,i} - A_i \beta_{n2,i} (N_{n1,i} - N_{n2,i}) \\
&- f_{n1} a_{na} k_{gb} f_1 b_i - v_{b,i} \phi_i A_i N_{n1,i}
\end{aligned} \tag{3.20}$$

$$\begin{aligned}
\phi_i V_{2,i} \frac{dN_{n2,i}}{dt} &= A_i \beta_{n2,i} (N_{n1,i} - N_{n2,i}) - \phi_i V_{2,i} k_{dn,i} N_{n2,i} - \phi_i A_i v_{b,i} (N_{n2,i} - N_{n1,i}) + F_{N_{ng},i}^2 \\
&- f_{n2} a_{na} k_{gb} f_2 b_i
\end{aligned} \tag{3.21}$$

## 2.2.4 Sediment

$$\begin{aligned} \phi_{w,i} \frac{d(V_{w,i}m_{w,i})}{dt} &= Q_{in,i}m_{w,in,i} - v_{s,i}\phi_{w,i}A_i m_{w,i} + v_{r,i}\phi_{w,i}A_i m_{s,i} - Q_{o,i}m_{w,i} \\ &+ \sum_{j=1,n} (Q_{j,i}m_{w,j} - Q_{i,j}m_{w,i}) + \sum_{j=1,n} \beta_{m,i,j}A_{i,j}(m_{w,j} - m_{w,i}) \end{aligned} \quad (3.22)$$

$$V_{s,i} \frac{dm_{s,i}}{dt} = v_{s,i}\phi_{w,i}A_i m_{w,i} - v_{r,i}\phi_{w,i}A_i m_{s,i} - v_{b,i}A_i m_{s,i} \quad (3.23)$$

## 2.2.5 Oxygen

$$\begin{aligned} \phi_{w,i} \frac{d(V_{w,i}O_{w,i})}{dt} &= Q_{in,i}O_{w,in,i} + i_p A_i O_p + K_o \phi_{w,i} A_i (O^* - O_{w,i}) - r_{on,m} \phi_{w,i} V_{w,i} k_{mw,i} N_{ow,i} \\ &- r_{on,n} \phi_{w,i} V_{w,i} f_N k_{nw,i} N_{aw,i} + a_{oc} r_{c,chl} \{ (k_{gb} - k_{db}) f_{bw} b_i + (k_{ga} - k_{da}) a_i \} \\ &- Q_{o,i} O_{w,i} - A_i S_{o,i} - \phi_{w,i} V_{w,i} S_{w,i} - E_T A_i O_{w,i} \\ &+ \sum_{j=1,n} (Q_{j,i} O_{w,j} - Q_{i,j} O_{w,i}) + \sum_{j=1,n} \beta_{o,i,j} A_{i,j} (O_{w,j} - O_{w,i}) \end{aligned} \quad (3.24)$$

## 2.2.6 Phosphorus

$$\begin{aligned} \frac{d(V_{w,i}P_{w,i})}{dt} &= Q_{in,i}P_{w,in,i} - v_{s,i}F_{sw}m_{w,i}\phi_{w,i}A_iP_{w,i} + f_1v_{r,i}\phi_{w,i}A_iF_{ss}m_{s,i}P_{1,i} + f_2v_{r,i}\phi_{w,i}A_i f_{ss}m_{s,i}P_{2,i} \\ &- a_{pa}k_{ga}a_i + V_{w,i}a_{pn}k_{mw,i}N_{ow,i} + \beta_{p1}A_i(F_{ds}P_{1,i} - F_{dw}P_{w,i}) + F_{Pg,i}^w - Q_{o,i}P_{w,i} \\ &+ \sum_{j=1,n} (Q_{j,i}P_{w,j} - Q_{i,j}P_{w,i}) + \sum_{j=1,n} \beta_{p,i,j}A_{i,j}(P_{w,j} - P_{w,i}) \end{aligned} \quad (3.25)$$

$$\begin{aligned} V_{1,i} \frac{dP_{1,i}}{dt} &= f_1\phi_{w,i}A_i v_{s,i}m_{w,i}F_{sw}P_{w,i} - f_1\phi_{w,i}A_i v_{r,i}m_{s,i}F_{ss}P_{1,i} - \beta_{p1}A_i(F_{ds}P_{1,i} - F_{dw}P_{w,i}) \\ &- v_{b,i}A_iP_{1,i} + \beta_{p2}A_i(f_{ds}P_{2,i} - F_{ds}P_{1,i}) + F_{Pg,i}^1 - a_{pa}k_{gb}f_1b_i + V_{1,i}a_{pn}k_{mr,i}N_{or,i} \\ &+ V_{1,i}a_{pn}k_{ms,i}N_{os,i} \end{aligned} \quad (3.26)$$

$$V_{2,i} \frac{dP_{2,i}}{dt} = f_2 \phi_{w,i} A_i v_{s,i} m_{w,i} F_{sw} P_{w,i} - f_2 \phi_{w,i} A_i v_{r,i} m_{s,i} f_{ss} P_{2,i} + V_{2,i} a_{pn} k_{mr,i} N_{or,i} + V_{2,i} a_{pn} k_{ms,i} N_{os,i} \quad (3.27)$$

### 2.2.7 LPOC

$$\begin{aligned} \phi_{w,i} \frac{d(V_{w,i} C_{Lw,i})}{dt} &= Q_{in,i} C_{L in,i} + a_{ca} k_{da} f_{aL} a_i + a_{ca} k_{db} f_{bw} f_{bL} b_i - \phi_{w,i} V_{w,i} k_{L,i} C_{Lw,i} - Q_{o,i} C_{Lw,i} \\ &\quad - v_{s,i} \phi_{w,i} A_i C_{Lw,i} + v_{r,i} \phi_{w,i} A_i C_{L1,i} \\ &\quad + \sum_{j=1,n} (Q_{j,i} C_{Lw,j} - Q_{i,j} C_{Lw,i}) + \sum_{j=1,n} \beta_{L,i,j} A_{i,j} (C_{Lw,j} - C_{Lw,i}) \end{aligned} \quad (3.28)$$

$$V_{s1,i} \frac{dC_{L1,i}}{dt} = a_{ca} k_{db} f_1 f_{bs} f_{bL} b_i - V_{s1,i} k_{L,i} C_{L1,i} + f_1 \phi_{w,i} v_{s,i} A_i C_{Lw,i} - f_1 v_{r,i} A_i C_{L1,i} - v_{b,i} A_i C_{L1,i} \quad (3.29)$$

$$\begin{aligned} V_{s2,i} \frac{dC_{L2,i}}{dt} &= a_{ca} k_{db} f_2 f_{bs} f_{bL} b_i - V_{s2,i} k_{L,i} C_{L2,i} + f_2 \phi_{w,i} v_{s,i} A_i C_{Lw,i} - f_2 v_{r,i} \phi_{w,i} A_i C_{L2,i} - v_{b,i} A_i (C_{L2,i} \\ &\quad - C_{L1,i}) \end{aligned} \quad (3.30)$$

### 2.2.8 RPOC

$$\begin{aligned} \phi_{w,i} \frac{d(V_{w,i} C_{Rw,i})}{dt} &= Q_{in,i} C_{R in,i} + a_{ca} k_{da} f_{aR} a_i + a_{ca} k_{db} f_{bw} f_{bR} b_i - \phi_{w,i} V_{w,i} k_{R,i} C_{Rw,i} - Q_{o,i} C_{Rw,i} \\ &\quad - v_{s,i} \phi_{w,i} A_i C_{Rw,i} + v_{r,i} \phi_{w,i} A_i C_{R1,i} \\ &\quad + \sum_{j=1,n} (Q_{j,i} C_{Rw,j} - Q_{i,j} C_{Rw,i}) + \sum_{j=1,n} \beta_{R,i,j} A_{i,j} (C_{Rw,j} - C_{Rw,i}) \end{aligned} \quad (3.31)$$

$$V_{s1,i} \frac{dC_{R1,i}}{dt} = a_{ca} k_{db} f_1 f_{bs} f_{bR} b_i - V_{s1,i} k_{R,i} C_{R1,i} + f_1 \phi_{w,i} v_{s,i} A_i C_{Rw,i} - f_1 v_{r,i} A_i C_{R1,i} - v_{b,i} A_i C_{R1,i} \quad (3.32)$$

$$\begin{aligned} V_{s2,i} \frac{dC_{R2,i}}{dt} &= a_{ca} k_{db} f_2 f_{bs} f_{bR} b_i - V_{s2,i} k_{R,i} C_{R2,i} + f_2 \phi_{w,i} v_{s,i} A_i C_{Rw,i} - f_2 v_{r,i} \phi_{w,i} A_i C_{R2,i} - v_{b,i} A_i (C_{R2,i} \\ &\quad - C_{R1,i}) \end{aligned} \quad (3.33)$$

## 2.2.9 DOC

$$\begin{aligned}
\phi_{w.i} \frac{d(V_{w.i} C_{Dw.i})}{dt} &= Q_{in.i} C_{D in.i} + a_{ca} k_{da} f_{ad} a_i + a_{ca.i} k_{ab} f_{bw} f_{bD} b_i + \phi_{w.i} V_{w.i} k_{L.i} C_{Lw.i} \\
&+ \phi_{w.i} V_{w.i} k_{R.i} C_{Rw.i} - Q_{o.i} C_{Dw.i} + F_{C_{Dg}.i}^w + \beta_{D1} A_i (C_{D1.i} - C_{Dw.i}) \\
&- \phi_{w.i} V_{w.i} \frac{O_{w.i}}{O_{w.i} + K_O} k_{D.i}^1 C_{Dw.i} - \phi_{w.i} V_{w.i} \frac{K_O^{in}}{O_{w.i} + K_O^{in}} \frac{N_{nw.i}}{N_{nw.i} + K_N} k_{D.i}^2 C_{Dw.i} \\
&+ \sum_{j=1,n} (Q_{j,i} C_{Dw.j} - Q_{i,j} C_{Dw.i}) + \sum_{j=1,n} \beta_{D.i,j} A_{i,j} (C_{Dw.j} - C_{Dw.i})
\end{aligned} \tag{3.34}$$

$$\begin{aligned}
\phi V_{s1.i} \frac{dC_{D1.i}}{dt} &= a_{ca} k_{ab} f_1 f_{bs} F_{bD} b_i + V_{s1.i} k_{L.i} C_{L1.i} + V_{s1.i} k_{R.i} C_{R1.i} - B_{D1} A_i (C_{D1.i} - C_{Dw.i}) \\
&- \beta_{D2} A_i (C_{D1.i} - C_{D2.i}) + F_{C_{Dg}.i}^1 - \phi_i V_{s1.i} \frac{O_{s1.i}}{O_{s1.i} + K_O} k_{D.i}^1 C_{D1.i} - \phi_i v_{b.i} A_i C_{D1.i}
\end{aligned} \tag{3.35}$$

$$\begin{aligned}
\phi V_{s2} \frac{dC_{D2}}{dt} &= a_{ca} k_{ab} f_2 f_{bs} f_{bD} b + V_{s2} k_L C_{L2} + V_{s2} k_R C_{R2} - \beta_{D2} A (C_{D2} - C_{D1}) + F_{C_{Dg}}^2 - \phi v_b A (C_{D2} \\
&- C_{D1.i}) - \phi_i V_{s2.i} \frac{N_{n2.i}}{N_{n2.i} + K_N} k_{D.i}^2 C_{D2.i} - \phi_i V_{s2.i} \frac{K_N^{in}}{N_{n2.i} + K_N^{in}} k_{D.i}^3 C_{D2.i}
\end{aligned} \tag{3.36}$$

## 2.2.10 CH4

$$\begin{aligned}
\phi_{w.i} \frac{d(V_{w.i} C_{Mw.i})}{dt} &= \alpha_M \phi_{w.i} A_i (C^* - C_{Mw.i}) + \beta_{M1} A_i (C_{M1.i} - C_{Mw.i}) + F_{C_{Mg}.i}^w - Q_{o.i} C_{Mw.i} \\
&- \phi_{w.i} V_{w.i} \frac{O_{w.i}}{O_{w.i} + K_O} k_{M.i}^1 C_{Mw.i} - \phi_{w.i} V_{w.i} \frac{K_O^{in}}{O_{w.i} + K_O^{in}} \frac{N_{nw.i}}{N_{nw.i} + K_N} k_{M.i}^2 C_{Mw.i} \\
&+ \sum_{j=1,n} (Q_{j,i} C_{Mw.j} - Q_{i,j} C_{Mw.i}) + \sum_{j=1,n} \beta_{M.i,j} A_{i,j} (C_{Mw.j} - C_{Mw.i})
\end{aligned} \tag{3.37}$$

$$\begin{aligned}
\phi_i V_{s1.i} \frac{dC_{M1.i}}{dt} &= \beta_{M1} A_i (C_{Mw.i} - C_{M1.i}) + \beta_{M2} A_i (C_{M2.i} - C_{M1.i}) - \phi_i V_{s1.i} \frac{O_{s1.i}}{O_{s1.i} + K_O} k_{M.i}^1 C_{M1.i} \\
&+ F_{C_{Mg}.i}^1 + \lambda_r f_1 f_{bs} b_i R_v D^\sigma (C^* - C_{M1.i})
\end{aligned} \tag{3.38}$$

$$\begin{aligned} \phi_i V_{s2} \frac{dC_{M2}}{dt} = & a_{mc} \phi_i V_{s2.i} \frac{K_N^{in}}{N_{n2.i} + K_N^{in}} k_{D.i}^3 C_{D2.i} + \beta_{M2} A_i (C_{M1.i} - C_{M2.i}) \\ & - \phi_i V_{s2.i} \frac{N_{n2.i}}{N_{n2.i} + K_N} k_{M.i}^2 C_{M2.i} + F_{C_{Mg.i}}^2 + \lambda_r f_2 f_{bs} b R_v D^\sigma (C^* - C_{M2.i}) \end{aligned} \quad (3.39)$$

### 2.3 Site description

The proposed compartmental model was applied to a restored wetland located on the west side of the San Joaquin River in California's Central Valley (Figure 3.6). The materials presented in this section are adopted from Maynard (2009) and Maynard et al. (2011), who conducted research concerning biogeochemical cycling and retention of carbon and nutrients on this wetland from 2004 to 2008.

The 4.4 ha study wetland was restored in 1993 from an agricultural field with the intent to provide wildlife habitat and to improve water quality of agricultural runoff. During growing season (May–September), the study wetland receives irrigation tail-water from about 2300 ha of upstream farmlands; whereas in winter and spring, flow is maintained by episodes of rain and flood events. Accordingly, the study wetland is seasonally inundated for 9 to 11 months each year. San Joaquin valley has a Mediterranean climate with hot, arid summers ( $\bar{T} = 24$  °C) and cool, humid winters ( $\bar{T} = 8$  °C). The mean annual precipitation is 28 cm with most of the rainfall occurring between November and April. In the restoration process in 1993, the wetland surface was covered with local soil (i.e., antecedent soil layer) which had a loamy sand soil texture.

Flow monitoring and water quality sampling were conducted during growing season of 2007 by a group of scientists from University of California at Davis (Maynard, 2009). During the

irrigation season (May–September), the water column was maintained at a relatively constant depth via a water control structure at the outflow.

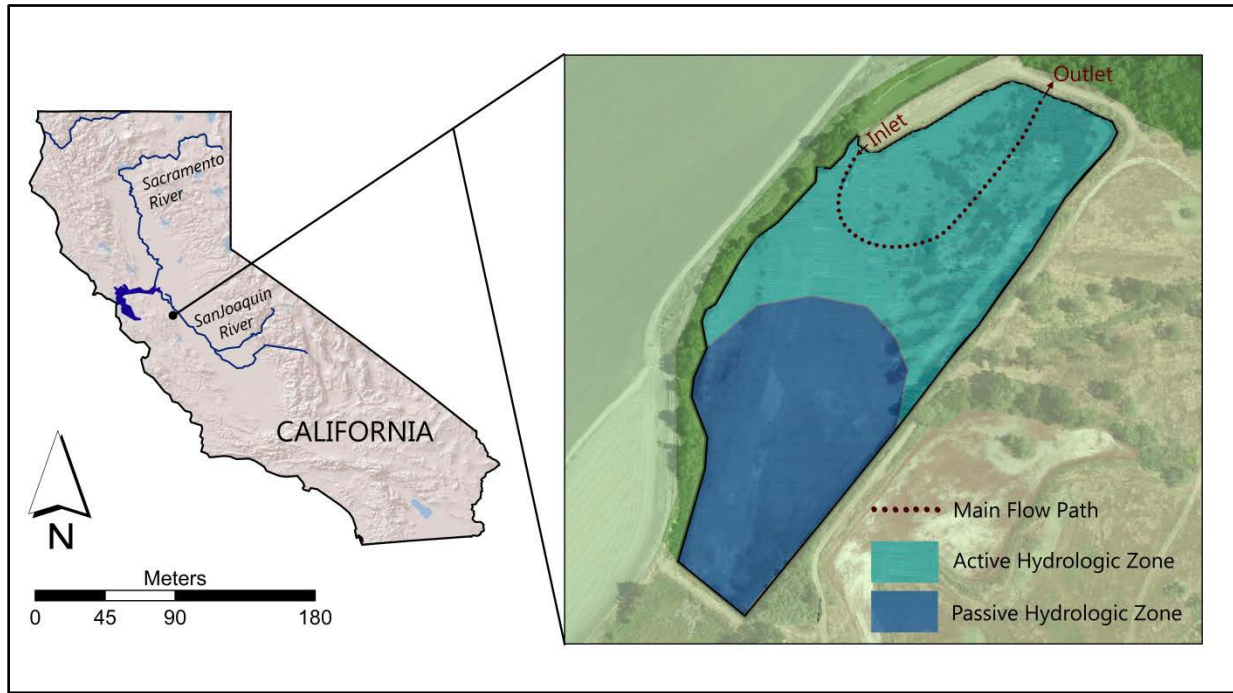


Figure 3.6: Study wetland located on west side of the San Joaquin River in California's Central Valley.

Redrawn from Maynard et al. (2011)

With an average depth of 0.40 meters ( $0.25 < \text{depth} < 0.7\text{m}$ ), the restored wetland had a water holding capacity of  $17684 \text{ m}^3$ . Early spring flooding in 2007 prevented the germination of emergent macrophytes; consequently there were no emergent vegetation within the wetland during the course of this study. What made this study site favorable for application of the proposed compartmental model is the formation of a large stagnant zone at the southern end of the wetland. The close vicinity of inflow and outflows in the northern side of the wetland has led to hydrologic short-circuiting and disconnection of the southern portion which constitutes more than 50% of the wetland area (Figure 3.6). Throughout this chapter, the study wetland will be referred to as SJRW (for San Joaquin Restored Wetland).

### 2.3.1 Hydrologic monitoring

ISCO (ISCO, Lincoln, NE, USA) area-velocity meters were installed in inlet and outlet pipes to measure water inflow and outflow rates every 15 minutes. A mass transfer evaporation equation given by Dunne and Leopold (1978) was employed to calculate daily evaporation rates. Note that due to the absence of plant cover in the wetland during the study period, it was assumed that transpiration was minimal and open water evaporation rate was calculated instead of evapotranspiration. In the employed relationship, evaporation is calculated as a function of wind speed and pressure difference between water surface and atmosphere. The required data for estimating open water evaporation came from a nearby weather station at Patterson, CA, maintained by the California Irrigation Management Information System (CIMIS, 2007). No precipitation was recorded during the study period. Seepage was calculated daily using a simple mass balance equation as the difference between inflow and outflows (outflow = discharge + evaporation) to/from the system. Figure 3.7 presents time series of volume and inflow/outflow discharges to/from the study wetland during the irrigation season of 2007. On average, SJRW received  $10460 \text{ m}^3\text{day}^{-1}$  of inflow during the irrigation season (May-September) of 2007. The average daily volume of inflow is equivalent to 59% of SJRW's effective water holding capacity. Subsequently, this high ratio has resulted in a relatively small residence time of 1.46 day. Moreover, the effective residence time is smaller than 1.46 days due to short circuiting and small flow path in SJRW. A Bromide tracer experiment (conducted on 6 Aug. 2007) demonstrated that the RW has an effective residence time of 0.90 d (variance:  $\pm 18.65 \text{ d}^2$ ) (Maynard, 2009). The large variance of estimated residence time might be a consequence of considerable hourly variation of inflow, observed during the course of experiment on Aug. 6<sup>th</sup>.

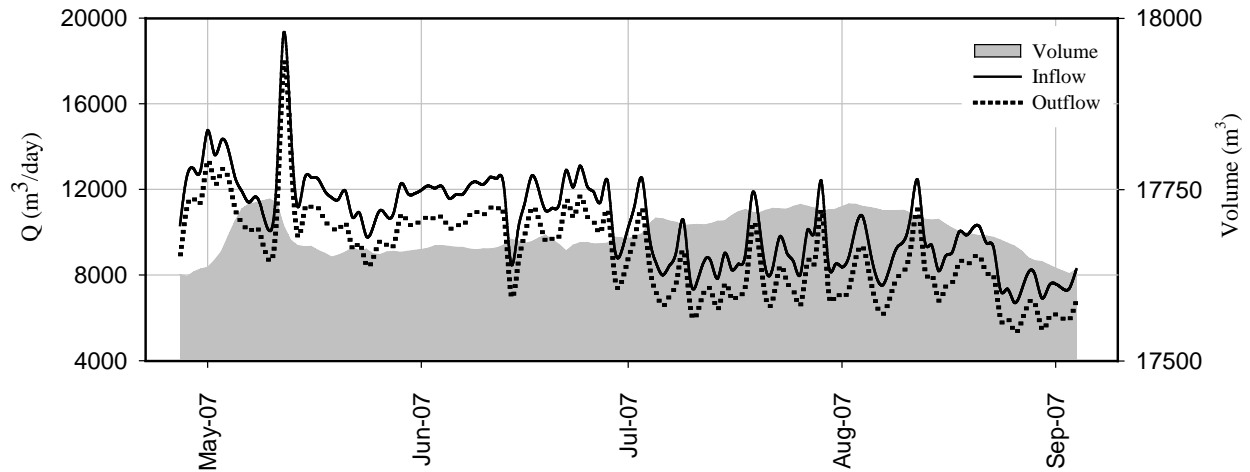


Figure 3.7: Graphical demonstration of the hydrologic regime (inflow/outflow) and volume of SJRW during growing season of 2007

### 2.3.2 Water Quality monitoring

Grab samples were collected on a weekly basis during the 2007 irrigation season from inflow and outflow locations. The samples were tested for various water quality constituents, including concentrations of total suspended solids (TSS), total nitrogen (TN), nitrate ( $\text{NO}_3\text{-N}$ ), ammonia+ammonium ( $\text{NH}_4\text{-N}$ ), total phosphorus (TP), phosphate ( $\text{PO}_4\text{-P}$ ), dissolved organic carbon (DOC) and particulate organic carbon (POC). In addition to the constituents mentioned above, a multi-parameter sonde simultaneously recorded data for dissolved oxygen (DO), electric conductivity, temperature and turbidity. More details on sample analysis could be found in Maynard (2009). Figure 3.8 presents grab sample concentrations of inflowing constituents to SJRW during the study period ( $n=19$ ). Note that concentrations of organic nitrogen (Organic N) and organic phosphorus (Organic P) were not directly measured, rather calculated by subtracting inorganic components out of total N and P concentrations.

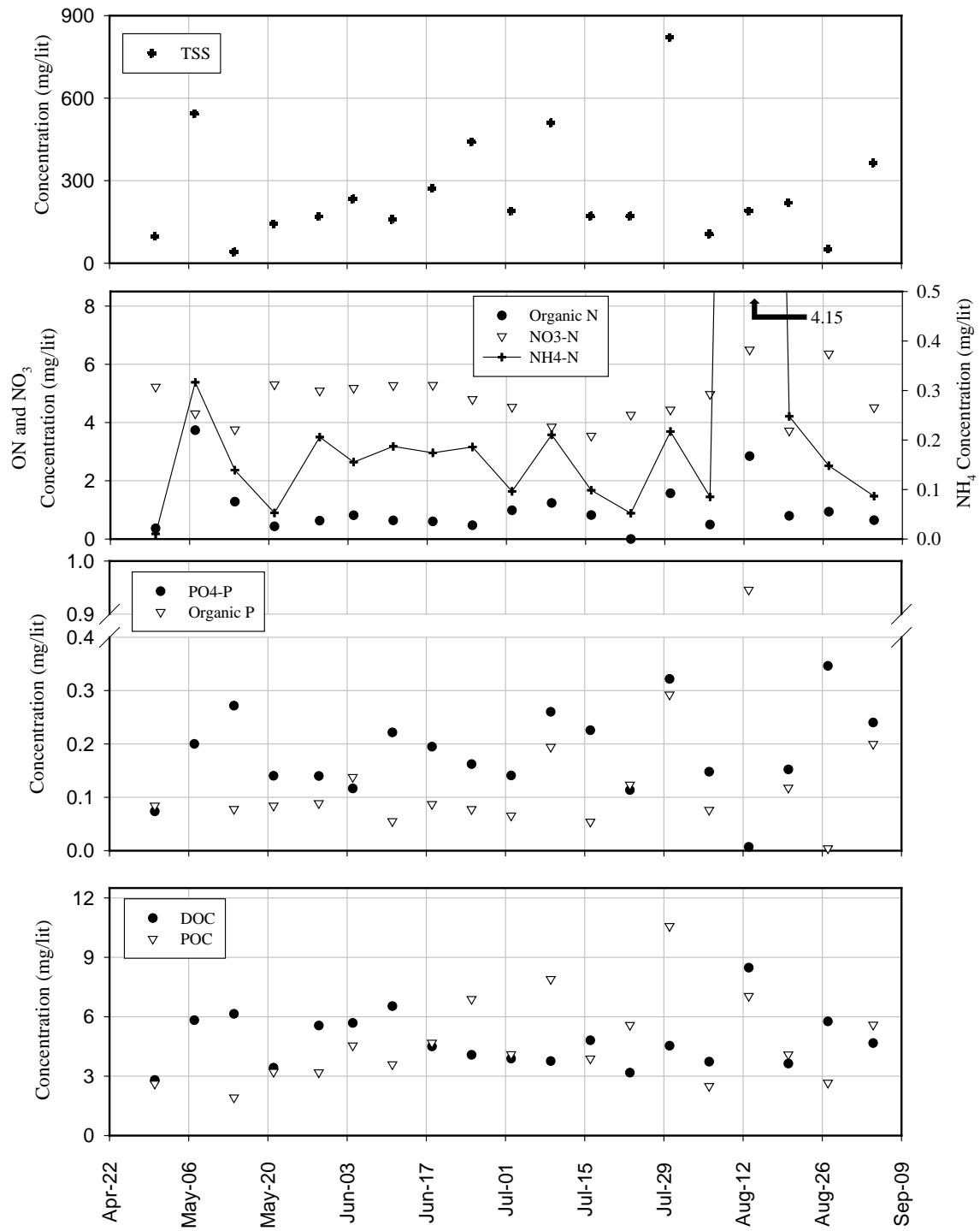


Figure 3.8: Grab sample concentrations of inflowing constituents to SJRW during the study period (n=19).

## **2.4 Regression relationships for collected water quality data at the inlet**

As mentioned earlier, WetQual is a continuous model and requires continuous input data (flow, water quality) to run in a continuous mode. Much of the monitored water quality data from SJRW was collected based on weekly grab sampling, i.e. only snapshots of the inflowing pollutograph was measured at a time. To convert these data points that are scattered over time into a continuous time series, some additional analysis had to be performed. The USGS LOAD ESTimator (LOADEST, Runkel et al., 2004) was employed to extrapolate the weekly grab sample concentration measurements to daily concentrations. The following paragraph describing LOADEST is mainly adopted from Runkel et al. (2004).

LOADEST is a FORTRAN based program which has been used in many studies for estimating constituent loads in rivers and streams. By means of LOADEST, the user is able to develop a regression model for estimation of constituent load, based on given time series of discharge, constituent concentrations and additional data variables (like temperature). Once the regression model is constructed, it is used to estimate loads over a user-specified time interval. There are several predefined models included in LOADEST that are used to identify the form of the regression equation. User has the freedom to select the appropriate model based on prior familiarity of the hydrologic regime. An alternative is to use an automated model selection option provided by LOADEST that selects the “best” model based on the Akaike Information Criterion (AIC) (Akaike, 1974). The predefined model with the lowest value of the AIC statistic then is selected for use in load estimation.

In the case of this study, LOADEST was provided with constituent concentrations collected weekly (n=19) and the equivalent discharge at the time of sampling, and the regression relationship with lowest value of the AIC statistic was used to make continuous (daily) time series of inflowing constituent concentrations.

For all of the constituents of interest, the same form of regression equation was introduced as the best fit with lowest AIC. The regression has the following form:

$$\ln(\text{load}) = a_0 + a_1 \ln Q + a_2 \ln Q^2 \quad (3.40)$$

where  $\text{load}$  = constituent load ( $\text{kg}\cdot\text{d}^{-1}$ ) and  $\ln Q = \ln(\text{streamflow}) - \text{center of } \ln(\text{streamflow})$ .

Table 3.1 presents the regression statistics and coefficient values for constituents of interest, generated by LOADEST. As shown in Table 3.1, the regression relationships have  $R^2$  ranging from 60% to 89%. Although LOADEST does not provide F-test statistics for the regression relationships, judging from the P-values of the coefficients, it could be stated that all regression relationships are significant at the 5% significance level.

Table 3.1: Regression statistics and coefficient values generated by LOADEST for constituents inflowing to SJRW

		<i>Coef.</i>	<i>St. dev.</i>	<i>t-ratio</i>	<i>P-value</i>			<i>Coef.</i>	<i>St. dev.</i>	<i>t-ratio</i>	<i>P-value</i>
TSS	$a_0$	7.38	0.25	29.18	6E-17	TP	$a_0$	1.02	0.12	8.48	3E-08
	$a_1$	1.62	0.37	4.41	1E-04		$a_1$	0.88	0.17	5.08	2E-05
	$a_2$	-1.39	1.04	-1.33	2E-01		$a_2$	-1.62	0.50	-3.26	2E-03
	<i>Regression R<sup>2</sup></i>						60.29%	<i>Regression R<sup>2</sup></i>			
TN	$a_0$	3.61	0.07	49.91	8E-22	PO4-P	$a_0$	0.56	0.14	3.90	4E-04
	$a_1$	1.10	0.10	10.74	4E-10		$a_1$	0.94	0.20	4.62	7E-05
	$a_2$	0.31	0.30	1.05	3E-01		$a_2$	-1.42	0.60	-2.38	2E-02
	<i>Regression R<sup>2</sup></i>						88.59%	<i>Regression R<sup>2</sup></i>			
NH4-N	$a_0$	-0.17	0.18	-0.93	3E-01	DOC	$a_0$	3.54	0.12	29.26	3E-18
	$a_1$	1.80	0.26	6.88	7E-07		$a_1$	1.12	0.19	6.04	2E-06
	$a_2$	0.12	0.77	0.15	9E-01		$a_2$	-0.43	0.51	-0.83	4E-01
	<i>Regression R<sup>2</sup></i>						78.45%	<i>Regression R<sup>2</sup></i>			
NO3-N	$a_0$	3.44	0.07	48.01	2E-22	POC	$a_0$	3.63	0.16	22.55	4E-15
	$a_1$	1.00	0.11	9.08	4E-09		$a_1$	1.03	0.24	4.35	1E-04
	$a_2$	0.39	0.30	1.29	2E-01		$a_2$	-1.56	0.67	-2.32	2E-02
	<i>Regression R<sup>2</sup></i>						84.02%	<i>Regression R<sup>2</sup></i>			

#### 2.4.1 Prediction intervals for regression relationships

Prediction intervals of the regression relationships were calculated to account for the uncertainties associated with regression relationships given by LOADEST. Prediction interval is a range that is likely to contain the mean response with a certain probability. The methodology for estimation of prediction intervals is adopted from Kutner et al. (2005). For a given regression

relationship, the  $(1 - \alpha)$  prediction limit for a new observation  $Y_h$  corresponding to  $X_h$  is estimated as:

$$\hat{Y}_h \pm t\left(1 - \frac{\alpha}{2}; n - p\right) s\{pred\} \quad (3.41)$$

where

$$s^2\{pred\} = MSE + s^2\{\hat{Y}_h\} \quad (3.42)$$

and MSE being the mean square error of the formed regression model. The estimated variance  $s^2\{\hat{Y}_h\}$  is given by:

$$s^2\{\hat{Y}_h\} = X_h s^2\{b\} X_h \quad (3.43)$$

where  $s^2\{b\}$  represents the regression variance-covariance matrix.

Following the given theory, prediction intervals for all the regression relationships were calculated. Figure 3.9 presents two examples (for  $\text{NO}_3$  and TSS) of regression models and their prediction intervals established at 95% confidence level.

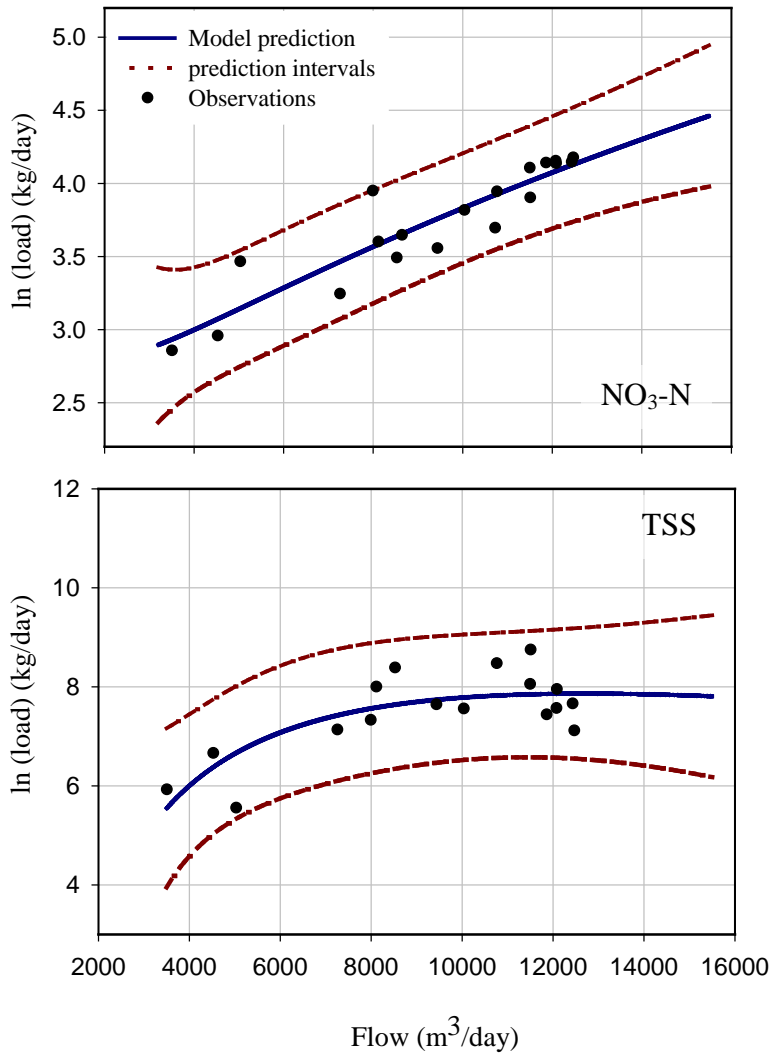


Figure 3.9: Prediction intervals of regression models established for NO<sub>3</sub>-N (top) and TSS (bottom) at 95% confidence level

### 3. Model application

Following the compartmentalization approach, SJRW was divided into 4 compartments. As shown in Figure 3.10, compartment 1 represents a small stagnant zone formed at the north end of the wetland. Compartment 2 represents the most active zone in SJRW, containing the inlet, outlet

and main flow path. Compartments 3 and 4, respectively, represent the transient and stagnant zones formed at the southern end of the wetland.

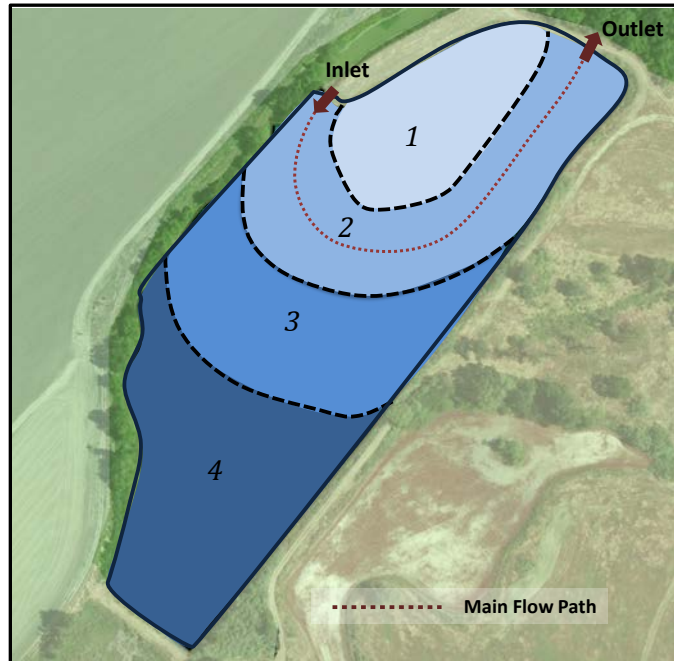


Figure 3.10: Compartmentalized study wetland.

SJRW deepens gradually from north east to south west, thus compartment 4 is the deepest and has the largest volume among compartments. Average area, effective volume and depth of these compartments are presented in Table 3.2.

Table 3.2: Average area, volume and depth of compartments C.1 to C.4 of SJRW

	<b>C.1</b>	<b>C.2</b>	<b>C.3</b>	<b>C.4</b>	<b>Total</b>
<i>Area (m<sup>2</sup>)</i>	2,395	13,791	15,511	12,135	43,832
<i>Volume (m<sup>3</sup>)</i>	700	3484	5035	8464	17683
<i>Depth<sup>‡</sup> (m)</i>	0.29	0.25	0.32	0.70	0.40

<sup>‡</sup> Depth=Volume/Area

The presented compartmentalization was founded based on personal communication with Dr. Jonathan Maynard (field scientist who performed research on study wetland) and with help of some test runs that were performed with different number of compartments. In general, with a given number of observed data points (limited observations), adding more compartments increases parameter uncertainty and adds to computational expenses. Finding the optimal number and positioning of compartments is another challenge that faces model users.

#### **4. Model Assessment**

Model assessment performed in this chapter is similar to the process applied in chapter 2. A combination of both GLUE and GSA methods (Beven and Binley, 1992; Spear and Hornberger, 1980) were employed to assess model prediction uncertainty and quantitative sensitivity to model parameters. Please see Figure 2.4 for a brief portrayal of the GSA/GLUE methodology applied in this chapter. In brief, we generated 100,000 statistically independent parameter sets for each compartment, sampled randomly from previously defined distributions which were extracted from literature values/tabulations. Model parameter distribution and their respective upper and lower bounds (quantities) for carbon cycle could be found in Table 2.3. For N, P and sediment cycles, reader is referred to Kalin et al. (2013). To perform Monte Carlo (MC) simulations, the model was run 100,000 times, each time with one set of parameters to yield an ensemble of 100,000 time series for constituent concentrations. At the beginning of each run, a module within the model generates inflowing concentrations of TSS, TN, NH<sub>4</sub>, NO<sub>3</sub>, TP, PO<sub>4</sub>, DOC and POC to SJRW for the dates with no observed data. These time series will be different from one model run to another, since inflow concentrations are generated randomly within the

95% prediction intervals of developed regression models. In this manner, uncertainty in the input inflow concentrations is accounted for in the GLUE and GSA methods

Two performance criteria ( $MBE$  and  $E_{ns}$ ) were used to construct a likelihood function that evaluates the goodness of fit between model-predicted concentrations and observed data for each MC simulation (Equation (2.23)). For each compartment, parameter sets were sorted based on their likelihoods and the top 1% datasets with the highest likelihoods were separated as behavioral dataset ( $B$ ) from the rest of the parameter sets (non-behavioral datasets,  $B'$ ). Subsequently, quantitative sensitivity analysis was performed using Kolmogorov-Smirnov test (Massey Jr, 1951) to reveal the most sensitive parameters. Kolmogorov-Smirnov test is a nonparametric test that is used to quantify a distance between the reference cumulative distribution function (CDF) – generated from non-behavioral parameter values or  $B'$ – and posterior CDF of a parameter generated from behavioral datasets (or  $B$ ). If such distance – referred to as  $D_{max}$  – is significant at a certain confidence level ( $\alpha$ ), the parameter is declared sensitive. Prior and posterior prediction uncertainty were next obtained by using model predictions generated respectively from the whole spectrum of model parameter distributions ( $B \cup B'$ ), and from behavioral parameters only ( $B$ ).

## 5. Results and discussion

Model fitness was gauged by comparing simulated concentrations of TSS, TN,  $NO_3$ , ON,  $NH_4$ , TOC and  $PO_4$  with observed data collected at the SJRW outlet ( $n = 19$ ) using two performance criteria of Mass Balance Error ( $MBE$ ) and Nash-Sutcliffe efficiency ( $E_{ns}$ ).

Table 3.3 exhibits average model performances ( $E_{ns}$  and  $MBE$ ) for behavioral simulations. Judging from data presented in Table 3.3, model performed decently well capturing dynamics of TOC, with an average  $E_{ns}$  of 0.62 and a mass balance error of less than 1%. In general mass balance error was very small (<1%) for all predicted constituents. Model performed fairly well in predicting N dynamics of the study wetland, with TN having an average  $E_{ns}$  of 0.41. Within the N cycle, best performance was associated with  $\text{NO}_3$  ( $E_{ns}=0.58$ ). Unfortunately, model performance for  $\text{PO}_4$  and TSS were not acceptable, as their  $E_{ns}$  appeared negative. Thus for the rest of the results section, we will focus our attention to model outcomes of carbon and nitrogen related constituents.

Table 3.3: Average model performances (MBE and  $E_{ns}$ ) for behavioral simulations based on observed and simulated concentrations

	$\text{PO}_4$	TN	ON	$\text{NH}_4$	$\text{NO}_3$	TSS	TOC
$E_{ns}$	-0.03	0.41	0.22	0.14	0.58	-0.22	0.62
$MBE$	-0.41%	0.29%	0.15%	-0.07%	0.52%	-0.33%	0.57%

## 5.1 Uncertainty analysis

Figure 3.11 to 3.13, respectively, compare the observed flow-averaged concentrations of  $\text{NO}_3$ , TN and TOC with the model results generated from the behavioral dataset and the 95% prediction interval (the band where 95% of simulated values fall within) of the MC simulations. What is commonly observed in all three figures is that compartment 2 has the lowest posterior uncertainty among all compartments. This observation has a fairly obvious reason behind it. It was earlier mentioned that observed constituent concentrations (shown with black dots in Figure

3.11 to 3.13) were sampled from the wetland outlet which is placed on compartment 2, consequently model validation was performed using model outcomes from compartment 2. In other words, compartment 2 is the most important compartment influencing model fitness, and consequently, it has the smallest uncertainty among all compartments.

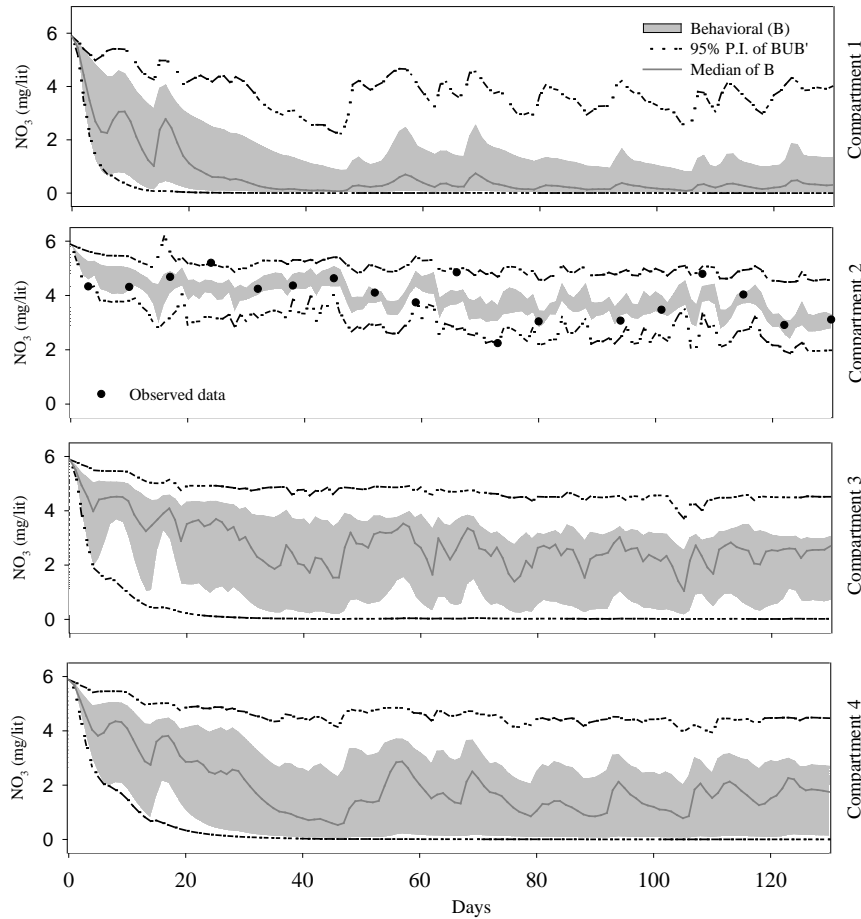


Figure 3.11: Model generated 95% prediction intervals (P.I) from 100,000 MC simulations versus observed concentrations of  $\text{NO}_3$  for compartments C.1 to C.4.

In Figure 3.11, concentration of  $\text{NO}_3$  in compartments 1, 3 and 4 decline initially and stabilize around day 50. It could be interpreted that the initial concentrations set for these compartments

(6 mg/lit) was originally high and better results could have been gained if initial concentration uncertainty was considered. Same phenomenon is observed for TN in Figure 3.12 as well. Except for a few unexpected (and un-explainable) peaks, uncertainty bands of TOC are generally narrower compared to TN and  $\text{NO}_3$ , indicating less uncertainty in TOC predictions.

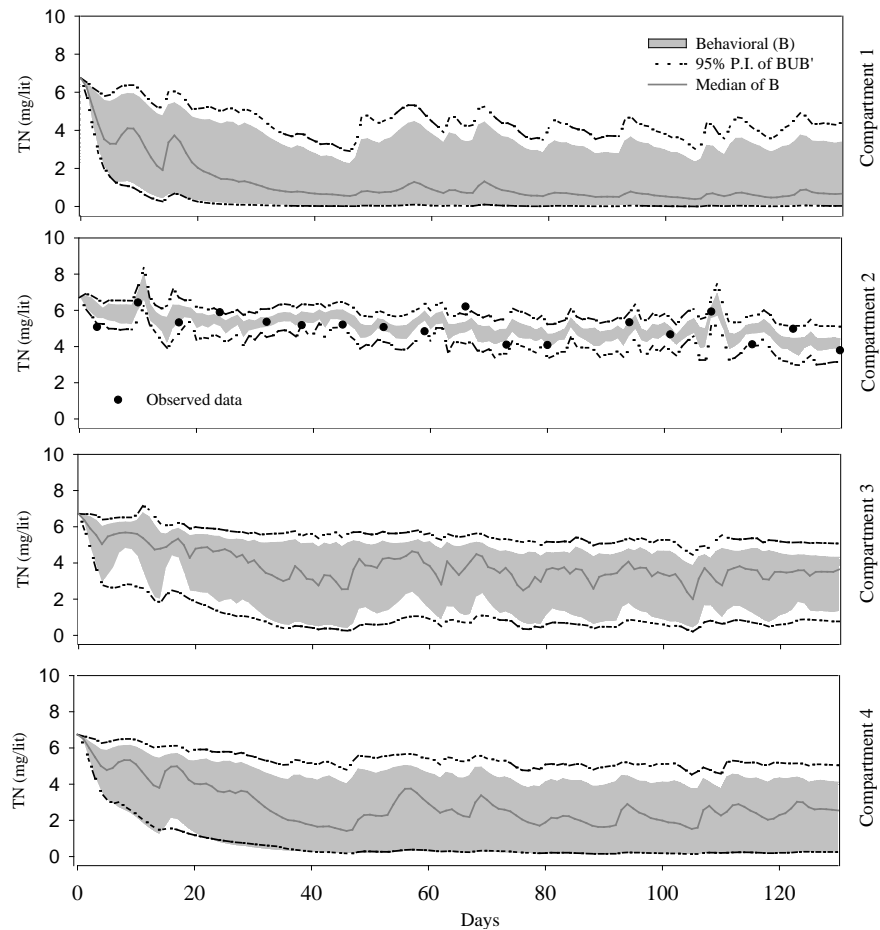


Figure 3.12: Model generated 95% prediction intervals (P.I) from 100,000 MC simulations versus observed concentrations of TN for compartments 1 to 4.

Another observation from Figure 3.13 is that concentration of TOC increases over time and uncertainty bands in all compartments grow wider along with it. In other words, model exhibits

higher prediction uncertainty with higher concentrations of TOC. However, this is not the case with  $\text{NO}_3$  and TN predictions, as uncertainty remains more or less constant, even as concentrations drop over time.

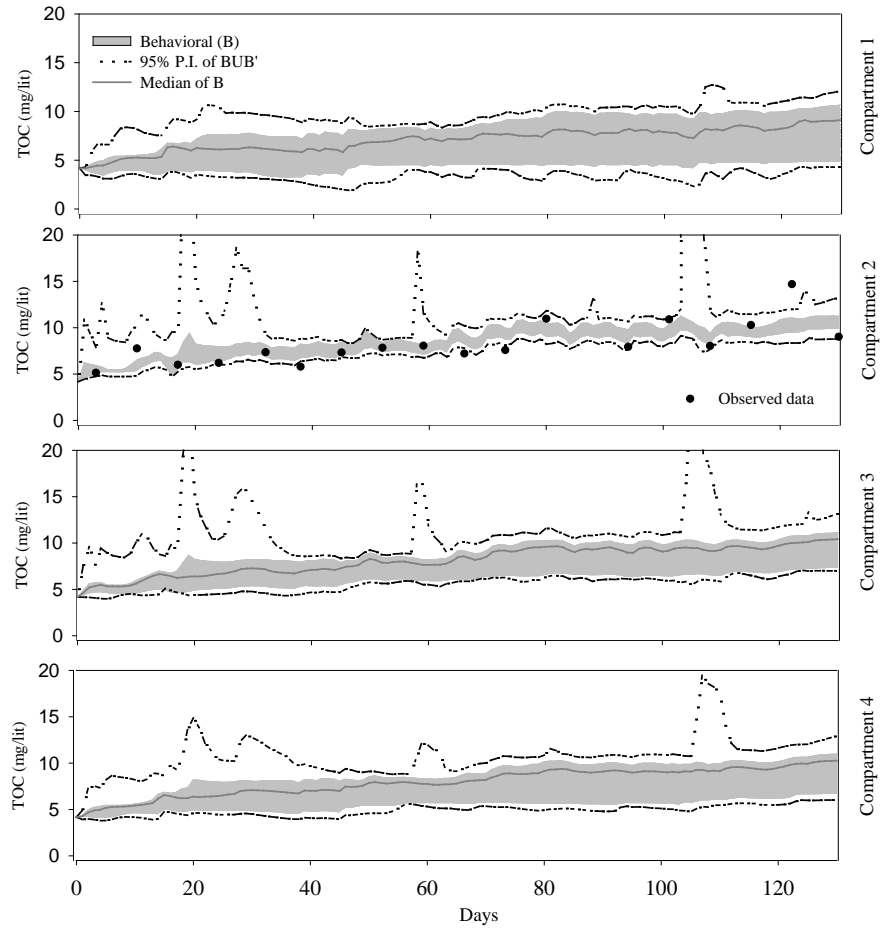


Figure 3.13: Model generated 95% prediction intervals (P.I) from 100,000 MC simulations versus observed concentrations of TOC for compartments 1 to 4.

## 5.2 Sensitivity Analysis

The Kolmogorov-Smirnov (K-S) test was applied to the behavioral ( $B$ ) and non-behavioral ( $B'$ ) datasets of each compartment, to statistically quantify the sensitive and insensitive parameters. Figure 3.14 and Figure 3.15 summarize the most sensitive parameters for all compartments of the study wetland in order of sensitivity based on TN and TOC export respectively. On the vertical axes of the presented graphs is  $D_{\max}$  resulted from K-S test, and sensitive parameters are listed on horizontal axis in order of sensitivity. We gaged the sensitivity at 10% confidence level this time (as opposed to 5% in the last chapter) because not too many parameters were sensitive at the 5% confidence level. The reason behind this observation could stem from limited observation data points for validation, and large pool of model parameters (since we propagated model parameters to each compartment). Compared to the lumped model (single compartment model), we have 4 times more parameters, but the same number of observation points (concentrations measured at the outflow,  $n = 19$ ). Through the figures presented in this section, we can make a judgment on which processes are important in the whole wetland, and which processes gain importance along the activity gradient line, from active to passive zones, regarding N and C constituents within the study wetland.

### 5.2.1 Dispersive/diffusive exchange

According to DHI (2004), it is common knowledge that dispersion coefficient is one of the most important parameters in advection–dispersion simulations of hydrodynamic models. This statement is true for our compartmental model too. K-S test performed based on model performance on TOC and TN export revealed that the most sensitive parameter for all compartments in the wetland is  $Ef_{act}$  (magnification parameter for the processes of horizontal

diffusion and dispersion between compartments). As mentioned earlier, at the beginning of each time step, model computes a rough estimate of the dispersion coefficient through Equation (3.6), and then multiplies it by  $Ef_{act}$ . In other words,  $Ef_{act}$  is a magnification parameter for the processes of horizontal diffusion and dispersion between compartments.  $Ef_{act}$  had a large  $D_{max}$  (ranging from 0.25 to 0.65) and a very small P value (in cases close to  $1 \times 10^{-41}$ ) for every K-S test performed throughout this study. Since the  $D_{max}$  associated with  $Ef_{act}$  dwarfed other parameters bars, it is eliminated from all Figures of this section.

### 5.2.2 TN

Figure 3.14 presents summary of the K-S test and order of sensitivities for all compartments of the study wetland based on TN export. Parameter  $k_{dn}$ , representing denitrification rate, repeatedly shows up as an important parameter for C.2, C.3, and C.4. Accordingly, it could be said that denitrification is an important loss pathway of nitrogen in the whole study wetland. Parameters  $L$  and  $\phi_w$  also repeatedly show up as sensitive parameters, indicating that having an accurate estimation of active sediment depth and effective porosity of wetland surface water is very important for a successful model application.

Parameters  $v_s$  and  $v_r$ , which reflect settling and resuspension velocities, appear higher in sensitivity order at the active zone (C.2) compared to transition and stagnant zones (C.3 and C.4). An explanation for this could be that since both inlet and outlet of the wetland are placed in compartment 2, a large portion of particles entering the wetland settle in compartment 2 before being transferred to other compartments, or exiting the wetland. Also because of the high turbulence within active zone due to large inflow/outflow rates, resuspension will be of more importance compared to stagnant zones.

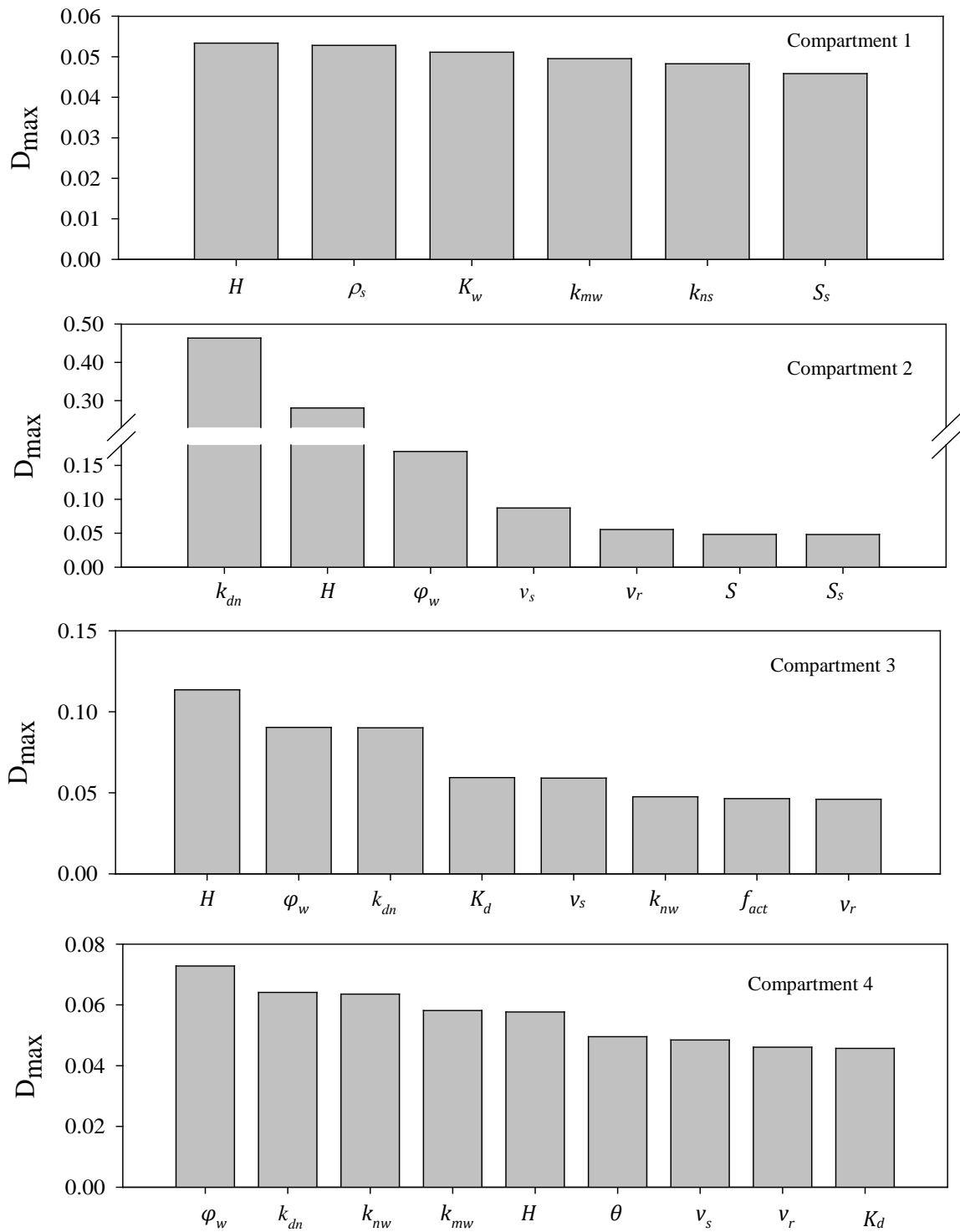


Figure 3.14: Summary of the K-S test and order of sensitivities based on TN export for compartments C.1 to C.4

### 5.2.3 TOC

Figure 3.15 presents Summary of the K-S test and order of sensitivities based on TOC export for all compartments of the study wetland. As appears in Figure 3.15, decomposition of DOC appears to be the dominant process within the whole study wetland, as parameters  $k^1_D$ ,  $k^2_D$  and  $k^3_D$  appear at the top of sensitivity list of all compartments. This finding is expected as 45% of the TOC pool is comprised of DOC. Parameters  $v_s$  and  $\phi_w$ , respectively representing velocity of settling and effective porosity of wetland surface water appear as important parameters for all compartments.  $\phi_w$  was employed in the model to represent the effect of plant biomass occupying part of submerged wetland volume. The fact that  $\phi_w$  is signified as an important parameter, despite knowing that there were no plants present during the study period, can point us to one conclusion. It could be concluded and that there are inaccuracies involved in active volume estimations and that model is taking advantage of  $\phi_w$  to adjust wetland's volume which was given as input. In other words, having an accurate estimate of wetland active volume was shown to be essential for a successful modeling practice.

There is no indication of one specific parameter/process being more important for TOC export along active/passive zones. In other words, K-S test was not able to reveal the information that we were after, i.e. discovering important processes regarding C cycling that are specific to active or passive zones. One reason behind this case might be due to lack of observed data availability for all the compartments of the study wetland. Currently, the fitness of model is gauged based on observed concentrations available for compartment 2. Thus there is a possibility that if observed concentrations of all compartments were taken into account for assessing model fitness, different parameters would have shown up for different compartments of Figure 3.15. Another

explanation can be that in case of TOC export, the system is more or less uniform. In other words, important processes regarding TOC export are similar in all compartments.

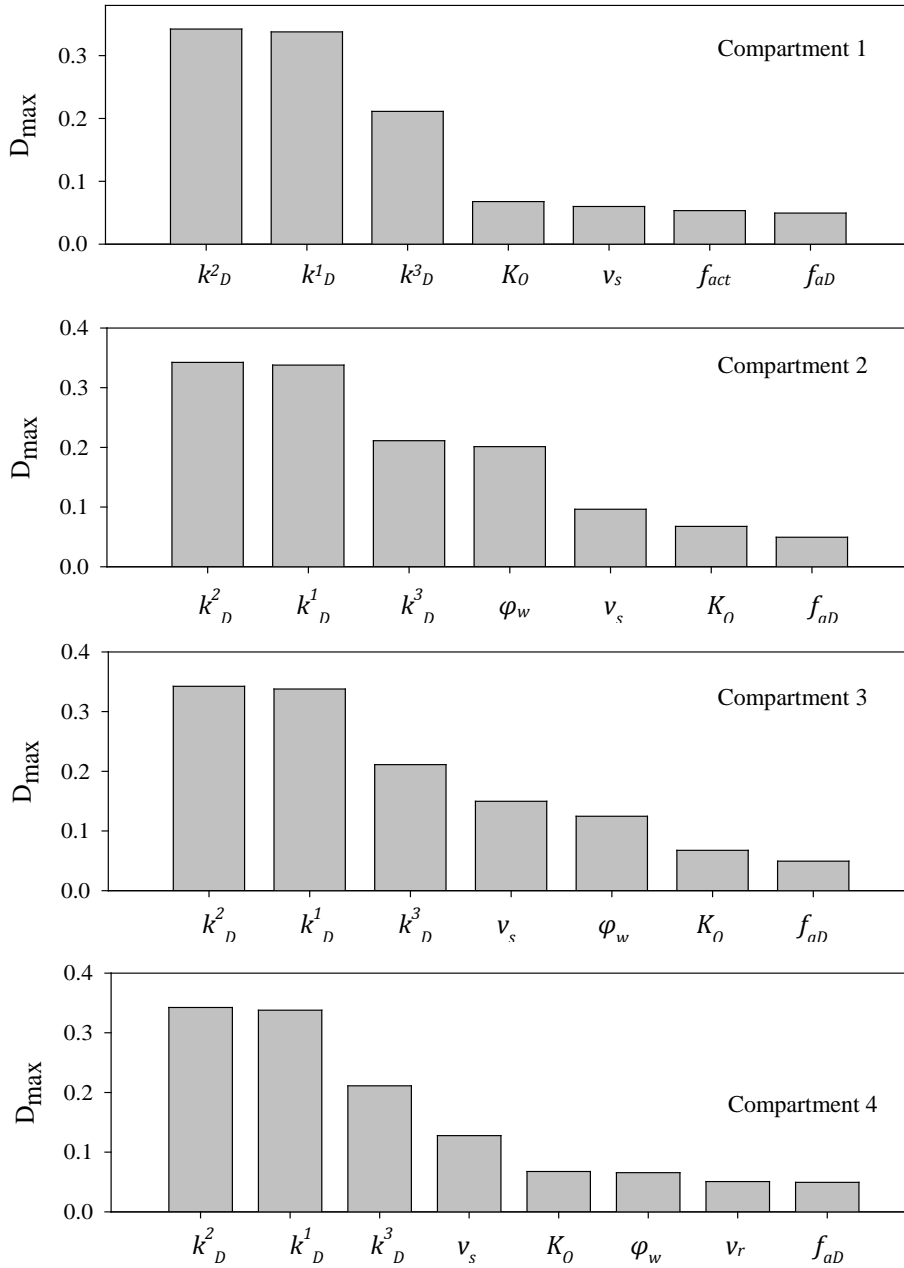


Figure 3.15: Summary of the K-S test and order of sensitivities based on TOC export for compartments C.1 to C.4

### 5.3 Mass balance Analysis

Table 3.4 and Table 3.5 summarize the N and C budgets and the major retention and removal pathways for compartments 1 to 4 and for the whole wetland during the study period. For the last column of both tables, all the numbers are normalized with the incoming load (shown in parentheses) to demonstrate a better picture of all the sources and sinks relative to loading. Values shown are the means +/- one standard deviation obtained from the behavioral set simulations.

Table 3.4: Nitrogen budget in the study wetland. <sup>γ</sup>

	<b>C.1</b>	<b>C.2</b>	<b>C.3</b>	<b>C.4</b>	<b>Total</b>
<i>Run off</i>	0	7921.3 ± 120.1	0	0	7921.3 ± 120.1 (100 ± 1.5%) <sup>‡</sup>
<i>Outflow</i>	0	6069.5 ± 188.6	0	0	6069.5 ± 188.6 (76.6 ± 2.3%)
<i>Net Deposition</i>	0.7 ± 0.4	14.4 ± 22.1	11.9 ± 10.7	7.7 ± 6.1	34.7 ± 38.3 (0.4 ± 0.5%)
<i>Volatilization</i>	0.1 ± 0.1	1.3 ± 2.2	1.1 ± 1.8	0.7 ± 1.1	3.2 ± 5.2 (0.0 ± 0.1%)
<i>Denitrification</i>	37.6 ± 21.9	1342.8 ± 396.3	871.6 ± 359.4	419.4 ± 213.6	2671.4 ± 991.2 (33.7 ± 12.5%)
<i>NH<sub>4</sub> diffusion</i>	-0.2 ± 0.1	0.2 ± 0.9	0.1 ± 0.7	-0.1 ± 0.4	0.0 ± 2.0 (0.0 ± 0.0%)
<i>NO<sub>3</sub> diffusion</i>	9.5 ± 5.5	773.1 ± 139.9	396.0 ± 108.2	144.6 ± 56.4	1322.7 ± 310.0 (16.7 ± 3.9%)
<i>Seepage (GW loss)</i>	7.0 ± 2.7	216.1 ± 4.6	170.4 ± 25.4	95.0 ± 23.7	488.5 ± 56.4 (6.2 ± 0.7%)

<sup>‡</sup> Numbers in parentheses are values normalized with runoff TN loading

<sup>γ</sup> All Units are in kg

Over the course of study period, about 23.4 ± 3.9% (1852 ± 309 kg) of the incoming TN load was removed or retained by SJRW, mainly via processes of denitrification and diffusion of nitrate into wetland soil. Among the removal/retention processes, denitrification stands high by removing 2671.4 ± 991.2 kg (33.7 ± 12.5%) of the nitrate pool. Next of importance is diffusion

of  $\text{NO}_3$  from water to soil layers which retained  $1322.7 \pm 310.0$  kg ( $16.7 \pm 3.9\%$ ) of the nitrate pool. Surprisingly, net deposition of ON plays a very small role in removal of N with  $34.7 \pm 38.3$  kg ( $0.4 \pm 0.5\%$ ). For comparison, Barnstable wetland (case study wetland presented in last chapter) removed  $18.4 \pm 8.9\%$  of its total nitrogen loading via net deposition during 1995-1997 (Kalin et al., 2013). These stated facts point towards importance of Nitrate in the N cycle of SJRW which is not unexpected since 70% of SJRW TN pool was comprised of  $\text{NO}_3$  during the study period. Note that the summarized N budget in Table 3.4 is not a closed budget and there is mass balance error observed in the Table. In other words, difference of inflowing and outflowing mass of N (net reduction = inflow - outflow) is much smaller than mass of N removed/retained by deposition, diffusion, denitrification, volatilization and seepage (GW loss). This error partly stems from high uncertainty involved in estimation of inflowing concentrations (inflow uncertainty) and model parameters (parameter uncertainty). Another source of error in mass balance calculations is the double counting of  $\text{NO}_3$  retained by diffusion and removed by denitrification + seepage. Diffusion is an internal exchange pathway and not a system loss pathway. We know that denitrification occurs in anaerobic sediment layer, thus nitrate has to be diffused into the soil first, before being denitrified. Also nitrate and ammonia diffuse to lower soil layers before leaving the system via seepage. Consequently, to avoid double counting, part of nitrate pool that is diffused in soil to be lost later (through denitrification and seepage) shouldn't be considered in mass balance error calculations.

The uncertainty associated with inflowing load is relatively small (1.5%) compared to uncertainties involving model processes (like denitrification). Denitrification, as the most important removal process, has the highest uncertainty (largest standard deviation). This

indicates that specific attention has to be given to estimation of parameters related to denitrification process.

Moving from active to passive zones of the wetland (C.2 to C.4) it is generally observed that mass of all exchanges (physical and biogeochemical) decrease along the activity gradient. We know that concentrations of TN and NO<sub>3</sub> are generally smaller in the passive zone (C.4) compared to active zone (C.2), thus one can expect that all masses exchanges in C.4 to be smaller than C.2. However, there are indications in Table 3.4 that point to higher denitrification reaction rates in C.4 compared to C.2. If we calculate the ratio of denitrification to NO<sub>3</sub> diffusion in each compartment ( $\alpha_i = \frac{\text{mass of dinitrification in } C_i}{\text{mass of diffusion in } C_i}$ ), we realize that this ratio grows larger in passive zones compared to active zones ( $\alpha_2 = 1.7 \pm 2.8$ ;  $\alpha_3 = 2.2 \pm 3.3$ ,  $\alpha_4 = 2.9 \pm 3.8$ ). It could be interpreted that despite less availability of NO<sub>3</sub> in passive areas, there is a more favorable environment for denitrification in passive regions of the wetland. This favorability for denitrification could be associated to less availability of oxygen in passive zones.

According to Table 3.5, over the study period, 11861.3± 82.2 kg of allochthonous organic carbon was washed into the wetland through inflow. Out of that amount, 2508.5 ± 518.7 kg of OC (equivalent to 21.1 ± 4.4% of OC loading) was removed/retained via microbial decomposition, deposition of POC and diffusion of DOC to wetland soil. Main removal process was microbial respiration (aerobic+anaerobic), which removed a total of 770.9 ± 584.6 kg of OC, equivalent to 6.5 ± 4.9% of total inflowing TOC load. Diffusion of DOC to the soil retained 286.5± 171.2 kg (2.4 ± 1.4%), deposition of POC removed 242.1 ± 340.7 kg (2.0 ± 2.9%) of TOC and 595.9 ± 36.8 kg of DOC (5.0 ± 0.3% of OC loading) was lost to seepage (GW loss).

Table 3.5: Carbon budgets in the study wetland<sup>y</sup>

	<b>C.1</b>	<b>C.2</b>	<b>C.3</b>	<b>C.4</b>	<b>Total</b>
<i>Run off</i>	0	11861.3 ± 82.2	0	0	11861.3 ± 82.2 (100 ± 0.7%) <sup>z</sup>
<i>Outflow</i>	0	9352.8 ± 436.5	0	0	9352.8 ± 436.5 (78.8 ± 3.7%)
<i>Aerobic respiration</i>	1.6 ± 1.5	234.4 ± 158.8	125.4 ± 99.4	63.4 ± 63	424.8 ± 322.7 (3.6 ± 2.7%)
<i>Anaerobic respiration</i>	15 ± 13.4	109.7 ± 82.3	133.8 ± 98.9	87.6 ± 67.3	346.1 ± 261.9 (2.9 ± 2.2%)
<i>Deposition</i>	12 ± 14.2	78.3 ± 128.4	79.8 ± 92.2	72.0 ± 105.9	242.1 ± 340.7 (2.0 ± 2.9%)
<i>Diffusion</i>	12.5 ± 7.8	98.0 ± 60	110.3 ± 65.8	65.7 ± 37.6	286.5 ± 171.2 (2.4 ± 1.4%)
<i>Seepage (GW loss)</i>	32.1 ± 1.8	188.2 ± 11.9	211.1 ± 13.1	164.5 ± 10	(595.9 ± 36.8) (5.0 ± 0.3%)

<sup>y</sup> Numbers in parentheses are values normalized with runoff loading

<sup>z</sup> All Units are in kg

In general, the uncertainties associated with C processes were smaller than that of N cycle. Largest uncertainty belongs to mass of C lost to aerobic respiration, which has a standard deviation of 322.7 kg, equivalent to 2.7% of TOC loading. However, TOC export had a slightly higher uncertainty compared to TN export (3.7% vs. 2.3%).

Moving from active to passive zones of the wetland (C.2 to C.4), more deposition of OC occurred in active and transient zones (C.2 and C.3) compared to passive zone (C.4). Also similar to earlier findings, in general, mass of all exchanges (physical and biogeochemical) decrease along the activity gradient.

Another observed trend in the wetland is that anaerobic processes become more significant as we move along activity gradient toward passive areas. The ratio of aerobic to anaerobic respiration declines continuously from C.2 to C.4 ( $2.14 \pm 1.93$  to  $0.72 \pm 0.94$ ), indicating that passive zone

has more favorable conditions for denitrification and methanogenesis compared to active zone. This finding is consistent to earlier conclusions from N mass balance analysis.

## **6. Conclusion and summary**

In this chapter, we aimed to expand WetQual model's spatial resolution in order to capture the full spectrum of geochemical interactions in active and passive zones of wetlands. The explained methodology upgraded model resolution in the horizontal domain by discretizing the spatial domain (wetland area) into compartments, and connecting neighboring compartments through advective and dispersive/diffusive exchange. The compartmental model was applied to data collected from a restored wetland in California's Central Valley during growing season of 2007. The study wetland has a formation of a large stagnant zone at the southern end which constitutes more than 50% of the wetland area. The study wetland was divided to 4 compartments along the activity gradient from north to south (most active to most passive). Through a detailed sensitivity and mass balance analysis, we aimed to identify the most important processes engaging nitrogen and carbon constituents along the activity gradient line.

Mass balance analysis revealed that over the course of study period, about  $23.4 \pm 3.9\%$  of the incoming TN load and  $21.1 \pm 4.4\%$  of the TOC load was removed or retained by SJRW. Moving from active to passive zones of the wetland (C.2 to C.4), it was observed that mass of all exchanges (physical and biogeochemical) regarding nitrogen and carbon cycling decreased along the activity gradient. More deposition of OC occurred in active and transient zones (C.2 and C.3) compared to passive zone (C.4). It was also revealed that anaerobic processes become more significant along the activity gradient toward passive areas. Despite less availability of  $\text{NO}_3$  in

passive areas, there was a more favorable environment for denitrification in passive regions of the wetland.

K-S test performed based on model performance on TOC and TN export revealed that the most sensitive parameter for all compartments in the wetland is  $Ef_{act}$  (magnification parameter for the processes of horizontal diffusion and dispersion between compartments). Parameter  $k_{dn}$ , representing denitrification rate, repeatedly shows up as an important parameter in active and passive zones, identifying denitrification is an important loss pathway of nitrogen in the whole study wetland. Decomposition of DOC appeared to be the dominant process within the whole study wetland, as parameters  $k^1_d$ ,  $k^2_d$  and  $k^3_d$  appear at the top of sensitivity list of all compartments. K-S test was not able to reveal information on important processes associated with C and N cycling that are specific to active or passive zones. We think this failure is due to lack of observed data availability for all the compartments of the study wetland.

In the case study presented, using the compartmentalized model we were able to gain insight about deposition patterns of organic material and show that aerobic activity declines in the passive zones. However, capacities of the compartmentalized model were not exploited to its full content, due to lack of observed data for each compartment.

High levels of nitrate and ammonium in the study wetland may indicate that the SJRW wetland is reaching nitrogen saturation. N saturation in wetlands severely impacts biogeochemical cycling of various nutrients. Indicators of an N saturated wetland includes elevated rates of nitrification in soil, increased nitrate leaching to groundwater, acidification of soils and aluminum mobilization to groundwater (Hanson et al. 1994). WetQual model does not directly consider effects of N saturation on biogeochemistry of wetlands. Addition of related relationship

to address such effects may enhance model performance in wetlands similar to SJRW which receive agricultural tailwater with elevated nitrogen levels.

## 7. Appendix

The following table lists model parameters presented through section 2.2, their definitions and equivalent dimensions.

Symbol	Definition & Dimension
<b>Input time series (provided to the model at daily scale)</b>	
$A$	wetland surface area [ $L^2$ ]
$V_w$	water volume of wetland surface water [ $L^3$ ]
$Q_{in}$	volumetric inflow rate [ $L^3T^{-1}$ ]
$Q_g$	groundwater discharge (negative for infiltration) [ $L^3T^{-1}$ ]
$Q_o$	wetland discharge (outflow) rate [ $L^3T^{-1}$ ]
$i_p$	precipitation rate [ $LT^{-1}$ ]
$E_T$	evapotranspiration rate [ $L^3T^{-1}L^{-2}$ ]
<b>Input parameters</b>	
$V_s$	volume of active sediment layer [ $L^3$ ]
$\phi$	wetland soil porosity
$\phi_w$	effective porosity of wetland surface water
$H$	thickness of active soil layer
$m_s$	soil bulk density [ $ML^{-3}$ ]
$\rho_s$	wetland soil particle density [ $ML^{-3}$ ]
<b>Inflow concentrations (daily time series provided to the model)</b>	
$O_{win}, O_p$	concentrations of oxygen in incoming water and precipitation [ $ML^{-3}$ ]
$N_{owin}, N_{awin}, N_{nwin}$	concentrations of organic nitrogen, total ammonia nitrogen and nitrate nitrogen in incoming inflow [ $ML^{-3}$ ]
$N_{ap}, N_{np}$	concentrations of total ammonia nitrogen and nitrate nitrogen in precipitation [ $ML^{-3}$ ]
$q_a, q_n$	dry depositional rates of total ammonia nitrogen and nitrate [ $ML^{-2}T^{-1}$ ]
$N_{aG}, N_{nG}$	total ammonia-nitrogen and nitrate-nitrogen concentration in ground water [ $ML^{-3}$ ]
$m_{win}$	sediment concentration in incoming flow [ $ML^{-3}$ ]

$P_{win}$	inflow total inorganic phosphorus concentration [ML <sup>-3</sup> ]
$C_{Lin}, C_{Rin}, C_{Din}$	concentrations of LPOC, RPOC and DOC in incoming flow [ML <sup>-3</sup> ]

### State variables (simulated by model)

$O_w$	oxygen concentration in free water [ML <sup>-3</sup> ]
$O_{s1}$	oxygen concentration in aerobic sediment [ML <sup>-3</sup> ]
$a$	mass of free floating plant [M <i>Chl a</i> ]
$b$	mass of rooted plants [M <i>Chl a</i> ]
$m_w$	sediment concentration in free water [ML <sup>-3</sup> ]
$m_s$	wetland soil bulk density [ML <sup>-3</sup> ]
$N_{ow}$	particulate organic nitrogen concentration in free water [ML <sup>-3</sup> ]
$N_{aw}$	[NH <sub>4</sub> <sup>+</sup> ] + [NH <sub>3</sub> ] total ammonia-nitrogen concentration in free water [ML <sup>-3</sup> ]
$N_{nw}$	nitrate-nitrogen concentration in free water [ML <sup>-3</sup> ]
$N_{or}$	concentration of rapidly mineralizing organic nitrogen in wetland soil [ML <sup>-3</sup> ]
$N_{or}$	concentration of rapidly mineralizing organic nitrogen in wetland soil [ML <sup>-3</sup> ]
$N_{a2}$	total ammonia-nitrogen pore-water concentration in lower anaerobic layer [ML <sup>-3</sup> ]
$N_{n2}$	nitrate-nitrogen pore-water concentration in lower anaerobic layer [ML <sup>-3</sup> ]
$P_w$	total inorganic phosphorus concentration in free water [ML <sup>-3</sup> ]
$P_1$	total phosphorus concentration in aerobic layer [ML <sup>-3</sup> ]
$P_2$	total phosphorus concentration in anaerobic layer [ML <sup>-3</sup> ]
$C_{Lw}$	concentrations of labile (fast reacting) particulate organic C in free water [ML <sup>-3</sup> ]
$C_{Rw}$	concentrations of refractory (slow reacting) particulate organic C in free water [ML <sup>-3</sup> ]
$C_{Dw}$	concentrations of dissolved organic C in free water [ML <sup>-3</sup> ]
$C_{L1}, C_{R1}, C_{D1}$	pore water concentrations of LPOC, RPOC and DOC in aerobic sediment layer [ML <sup>-3</sup> ]
$C_{L2}, C_{R2}, C_{D2}$	pore water concentrations of LPOC, RPOC and DOC in lower anaerobic sediment layer respectively [ML <sup>-3</sup> ]
$C_{M2}, C_{M1}, C_{Mw}$	methane concentration in anaerobic sediment, aerobic sediment layer and water respectively [ML <sup>-3</sup> ]

### Fixed model parameters

$a_{na}$	gram of nitrogen per gram of chlorophyll-a in plant/algae
$a_{oc}$	gram of oxygen produced per gram of organic carbon synthesized (= 2.67)
$a_{pa}$	gram of phosphorus per gram of Chlorophyll-a
$a_{pn}$	phosphorus to nitrogen mass ratio produced by mineralization of POM (= 1.389)
$r_{c,chl}$	carbon mass ration in <i>chlorophyll a</i>
$r_{on,m}$	gram of oxygen consumed per gram of organic nitrogen mineralized (= 15.29)
$r_{on,n}$	gram of oxygen consumed per gram of total ammonium nitrogen oxidized by nitrification (= 4.57)
$a_{ca}$	ratio of carbon to chlorophyll-a in algae [MM <sup>-1</sup> ]
$a_{mc}$	the stoichiometric yield of Methane from the anaerobic decomposition of gram of organic carbon during methanogenesis [MM <sup>-1</sup> ]

### Model Variables

$l_1$	thickness of aerobic soil layer [L]
$l_2$	thickness of anaerobic soil layer [L]

$v_s$	effective settling velocity [ $LT^{-1}$ ]
$v_r$	resuspension rate [ $LT^{-1}$ ]
$\theta$	Temperature coefficient in Arrhenius equation.
$v_b$	burial velocity [ $LT^{-1}$ ]
$V_1, V_2$	volume of aerobic and anaerobic soil [ $L^3$ ]
$\tau$	wetland soil tortuosity factor
$h$	average depth of water in wetland [L]
$k_{da}$	death rate of free-floating plants [ $T^{-1}$ ]
$k_{db}$	death rate of benthic and rooted plants [ $T^{-1}$ ]
$k_{dn}$	denitrification rate in anaerobic soil layer [ $T^{-1}$ ]
$k_{ga}$	growth rate of free-floating plant [ $T^{-1}$ ]
$k_{gb}$	growth rate of benthic and rooted plant [ $T^{-1}$ ]
$k_{mr}$	first-order rapid mineralization rate in wetland soil [ $T^{-1}$ ]
$k_{ms}$	first-order slow mineralization rate in wetland soil [ $T^{-1}$ ]
$k_{mw}$	first-order mineralization rate in wetland free water [ $T^{-1}$ ]
$k_{ns}$	first-order nitrification rate in aerobic soil layer [ $T^{-1}$ ]
$k_{nw}$	first-order nitrification rate in wetland free water [ $T^{-1}$ ]
$k_s^*$	maximum first-order nitrification rate in wetland soil [ $T^{-1}$ ]
$k_v$	volatilization mass transfer velocity [ $LT^{-1}$ ]
$K_d$	ammonium ion distribution coefficient [ $L^3M^{-1}$ ]
$K_o$	oxygen reaeration mass-transfer velocity [ $LT^{-1}$ ]
$\alpha, \eta$	empirical parameters in the relationship relating oxygen liquid-film transfer velocity to wind speed
$\beta_{a1}, \beta_{n1}$	diffusive mass-transfer rates, respectively, of total ammonia nitrogen and nitrate between wetland water and aerobic soil layer [ $LT^{-1}$ ]
$\beta_{a2}, \beta_{n2}$	diffusive mass-transfer rates, respectively, of total ammonia nitrogen and nitrate between oxygenated soil layer and lower anaerobic layer [ $LT^{-1}$ ]
$\beta_{\pi 1}$	diffusive mass-transfer rate of dissolved phosphorus between wetland water and aerobic soil layer [ $LT^{-1}$ ]
$\beta_{p2}$	diffusive mass-transfer rate of dissolved phosphorus between oxygenated soil layer and lower anaerobic layer [ $LT^{-1}$ ]
$\lambda_\sigma, \lambda_\omega$	empirical coefficients in the relationships limiting nitrification, respectively, in soil and free water to oxygen concentration in wetland water
$S$	rate of nitrogen fixation by microorganisms [ $ML^{-2}T^{-1}$ ]
$f_N$	fraction of total ammonia in ionized form
$R_s$	total ammonia retardation factor in wetland soil
$f_1, f_2$	volumetric fraction of aerobic and reduced soil layers
$O^*$	oxygen concentration in the air (assumed at saturation)[ $ML^{-3}$ ]
$K_o$	oxygen mass-transfer coefficient [ $LT^{-1}$ ]
$S_o$	wetland soil oxygen depletion rate per unit area [ $ML^{-2}T^{-1}$ ]
$S_w$	volumetric oxygen consumption rate in water by other processes [ $ML^{-3}T^{-1}$ ]
$\delta$	thickness of a laminar (diffusive) boundary layer situated on top of the soil-water interface [L]
$\tau_w$	effective tortuosity of the flooded area above soil
$D_o^*$	free-water oxygen diffusion coefficient [ $L^2T^{-1}$ ]
$S_s$	oxygen removal rate per unit volume of aerobic layer by other processes
$K_{s2}$	distribution coefficient in reduced wetland soil [ $L^3M^{-1}$ ].
$F_{Pg}^1$	is net advective groundwater contribution of total phosphorus to the aerobic layer [ $MT^{-1}$ ]

$\phi f_{d,s}$	dissolved fraction of total phosphorus concentration in anaerobic soil layer
$R_0(i)$	solar radiation on day $i$
$r(i)$	earth's eccentricity correction factor for day $i$
$T_d(i)$	total day length on day $i$
$\beta_{D1}, \beta_{M1}$	diffusive mass-transfer rates, respectively, of DOC and CH <sub>4</sub> between wetland water and aerobic soil layer [LT <sup>-1</sup> ]
$\beta_{D2}, \beta_{M2}$	diffusive mass-transfer rates, respectively, of DOC and CH <sub>4</sub> between wetland water and lower anaerobic soil layer [LT <sup>-1</sup> ]
$C^*$	equilibrium concentration of CH <sub>4</sub> in atmosphere [ML <sup>-3</sup> ]
$D^\alpha$	Diffusivity of Methane in air [L <sup>2</sup> T <sup>-1</sup> ]
$D_M^*, D_D^*$	diffusivity of methane and DOC in water, respectively [L <sup>2</sup> T <sup>-1</sup> ]
$J_M$	methane mass exchange coefficient between water and atmosphere [LT <sup>-1</sup> ]
$k_D^1, k_D^2, k_D^3$	maximum dissolved organic C utilization rate for, respectively, aerobic respiration, denitrification and methanogenesis [T <sup>-1</sup> ]
$k_M^1, k_M^2$	maximum methane utilization rate for, respectively, aerobic respiration and denitrification [T <sup>-1</sup> ]
$k_{da}$	death rate of free floating plants [T <sup>-1</sup> ]
$k_{db}$	death rate of rooted and benthic plants [T <sup>-1</sup> ]
$K_O^{in}$	Michaelis–Menten oxygen inhabitation coefficient [ML <sup>-3</sup> ]
$K_N^{in}$	Michaelis–Menten nitrate-N inhibition coefficient [ML <sup>-3</sup> ]
$k_L, k_R$	first order hydrolysis rate of labile particulate organic carbon and refractory particulate organic carbon, respectively [T <sup>-1</sup> ]
$K_N$	Michaelis–Menten nitrate N half saturation concentration required for denitrification [ML <sup>-3</sup> ]
$K_O$	Michaelis–Menten half saturation concentration of dissolved oxygen required for oxic respiration [ML <sup>-3</sup> ]
$Sc_M$	Schmidt number of methane
$S_B$	Bunsen solubility coefficient for methane
$\lambda_r$	specific conductivity of root system [LL <sup>-1</sup> ]
$\beta_{M1}$	methane mass exchange coefficient between aerobic sediment and water [LT <sup>-1</sup> ]
$\beta_{M2}$	methane mass exchange coefficient between aerobic and anaerobic sediment [LT <sup>-1</sup> ]
$\alpha_M$	methane gas transfer velocity between water and atmosphere [LT <sup>-1</sup> ]
$Sc_M$	Schmidt number of methane in a given temperature
$\beta_{o.i,j}, \beta_{a.i,j}, \beta_{n.i,j}$	dispersive/diffusive mass transfer rate across i,j boundary for organic-N, ammonia and nitrate, respectively [LT <sup>-1</sup> ]
$\beta_{m.i,j}, \beta_{o.i,j}, \beta_{p.i,j}$	dispersive/diffusive mass transfer rate across i,j boundary for sediment, oxygen and phosphorus, respectively [LT <sup>-1</sup> ]
$\beta_{L.i,j}, \beta_{R.i,j}, \beta_{D.i,j}, \beta_M$	dispersive/diffusive mass transfer rate across i,j boundary for LPOC, RPOC and DOC and CH <sub>4</sub> , respectively [LT <sup>-1</sup> ]
$f_{act}$	Vertical diffusion magnification factor
$Ef_{act}$	Horizontal diffusion magnification factor

### Explanatory variables

$f_1$	volumetric fraction of the active soil layer that is aerobic
$f_2$	volumetric fraction of the active soil layer that is anaerobic
$f_{a1}$	fraction of mineral nitrogen plant uptake as ammonia-N in the soil aerobic layer.
$f_{a2}$	fraction of mineral nitrogen plant uptake as ammonia-N in the soil anaerobic layer.
$f_{aw}$	fraction of mineral nitrogen plant uptake as ammonia-N in free water
$f_{bs}$	fraction of rooted plant biomass below soil-water interface (within soil layer)
$f_{bw}$	fraction of rooted plant biomass above soil-water interface

$f_{nw}$	fraction of mineral nitrogen plant uptake as nitrate-N in free water
$f_{n1}$	fraction of mineral nitrogen plant uptake as nitrate-N in the aerobic layer
$f_{n2}$	fraction of mineral nitrogen plant uptake as nitrate-N in the anaerobic layer
$f_N$	fraction of total ammonia nitrogen
$f_r$	fraction of rapidly mineralizing particulate organic matter
$f_s$	fraction of slowly mineralizing particulate organic matter
$f_{Sw}$	fraction of nitrogen fixation in water
$F_{N_{ag}}^w, F_{N_{ng}}^w$	groundwater source/loss for total ammonia nitrogen and nitrate nitrogen [ $MT^{-1}$ ]
$F_{N_{ag}}^1, F_{N_{ng}}^1$	groundwater source/loss of total ammonia nitrogen and nitrate in the aerobic layer [ $MT^{-1}$ ]
$F_{N_{ag}}^2, F_{N_{ng}}^2$	groundwater source/loss of total ammonia nitrogen and nitrate in the anaerobic layer [ $MT^{-1}$ ].
$F_{C_{Dg}}^w$	groundwater source/loss for DOC
$F_{C_{Dg}}^1$	groundwater source/loss of DOC from aerobic sediment layer [ $MT^{-1}$ ]
$F_{C_{Dg}}^2$	groundwater source/loss of DOC from anaerobic sediment layer [ $MT^{-1}$ ].
$F_{C_{Mg}}^1, F_{C_{Mg}}^2$	groundwater source/loss for methane [ $MT^{-1}$ ]
$F_{Pg}^w$	advective groundwater contribution of total inorganic phosphorus to the aerobic layer [ $MT^{-1}$ ]
$F_{d,w}$	dissolved fraction of total inorganic phosphorus in free water
$m_w F_{s,w}$	sorbed fraction of total inorganic phosphorus in free water ( $1 - F_{d,w}$ )
$\phi F_{d,s}$	dissolved fraction of total inorganic phosphorus in aerobic layer
$m_s F_{s,s}$	sorbed fraction of total inorganic phosphorus in aerobic layer
$K_{s1}$	distribution coefficient in aerobic layer [ $L^3M^{-1}$ ]
$m_s f_{s,s}$	sorbed fraction of total inorganic phosphorus concentration in anaerobic layer
$f_{aL}, f_{aR}, f_{aD}$	fraction of, respectively, labile particulate, refractory particulate and dissolved organic C produced by death/loss of free floating plants and attached algae ( $f_{aL} + f_{aR} + f_{aD} = 1$ )
$f_{bL}, f_{bR}, f_{bD}$	fraction of, respectively, labile particulate, refractory particulate and dissolved organic C produced by death/loss of rooted and benthic plants ( $f_{bL} + f_{bR} + f_{bD} = 1$ )
$f_{bw}, f_{bs}$	fraction of rooted plant biomass, respectively, above and under soil-water interface

---

## **Chapter 4: Modeling Nitrogen, Carbon and Phosphorus Dynamics in unsaturated wetland soils**

### ***Abstract***

The objective of this study was to extend WetQual capabilities to simulate geochemical reactions in parts of the wetland that are not flooded (unsaturated wetland soil). To accomplish such goal, a comprehensive module for tracking water content in wetland soil was implemented, and model relationships were updated to simulate geochemical reactions of N, C, P related constituents in unsaturated wetland soil. The developed model was applied to a small restored wetland previously introduced in Chapter 2, which is located on Kent Island, Maryland. On average, the ponded compartment of the study wetland covered 65% of the total 1.2 ha area. Through mass balance analysis, it was revealed that denitrification in unsaturated compartment of study wetland was around 3 times higher than that of the ponded compartment ( $32.7 \pm 29.3$  kg vs.  $9.5 \pm 5.5$  kg) whereas ammonia volatilization in unsaturated compartment was a fraction of that of ponded compartment ( $1.2 \pm 1.9$  kg vs.  $11.3 \pm 11.8$  kg). Sensitivity analysis showed that cycling of carbon related constituents in wetland banks (unsaturated soil) had high sensitivity to temperature and available soil moisture.

## 1. Introduction

Hydrology is the main driving force for many physical, chemical, and biological processes in wetlands. In contrast to upland ecosystems, vast majority of biogeochemical properties of soil and wetland biota are governed by hydrology (Mitsch and Gosselink, 2007). Hydrology regulates oxygen availability in wetland soils, consequently governs nutrient availability, pH, GHG gas emissions and toxicity of wetland soil (Reddy and Delaune, 2008; Takatert et al., 1999; Bai et al. 2004). In addition, soil water content controls microbial activity in wetland soil and thus determines rates of microbial respiration (Sleutel et al., 2008; Reddy and Delaune, 2008; Davisson et al., 1998; Ise and Moorcroft, 2006).

There are two aspects of wetland hydrology that need special attention when it comes to wetland biogeochemical modeling. The first aspect is the effect of ground water (GW) fluctuations on wetland soil moisture. Many wetland nutrient cycling models use an internal mass balance module to simulate ground water levels based on precipitation and ET losses. In other words, as Fan and Miguez-Macho (2011) put it, in many large scale models “wetlands are only ‘wetted’ from above, but not from below by the high water table characteristic of wetland conditions”. This results in inadequacies representing the hydrologic cycle of groundwater fed wetlands that are ‘wetted from below’ by groundwater upwelling (Fan and Miguez-Macho, 2011).

Another aspect that requires special consideration in wetland modeling is the seasonal pattern of water level in wetlands and the rise and fall of wetland surface and subsurface water. Consider the hypothetical wetland in Figure 4.1. The presented wetland is seasonally flooded, meaning that it is flooded for extended periods during growing season. As water level falls and rises, the flooded section of the wetland will shrink and expand, respectively. An important drawback of

WetQual model at its earlier state (explained in chapters 2 and 3) – along with many other wetland nutrient cycling models – is its inability to track the dynamics of geochemical reactions in un-inundated sections of the wetland. In other words, the introduced model does not have the capability to track and simulate nutrient balance at the banks (presented with green in Figure 4.1) of the wetland. Consequently, model is not capable of modeling nutrient dynamics in other types of non-flooded wetlands, like “Saturated wetlands”, where substrate is saturated for extended periods during the growing season, but standing water is rarely present.

In this chapter, we aim to address this drawback of the model by extending models capabilities to simulate geochemical reactions in unsaturated wetland soil and to track constituent concentrations in parts of the wetland that are not flooded. To achieve this goal, it is necessary to implement a comprehensive measure for tracking moisture in wetland soil. Once daily soil moisture profile of wetland soil are attained, model relationships are updated to simulate geochemical reactions and track concentrations of N, C, P related constituents in wetland soil.

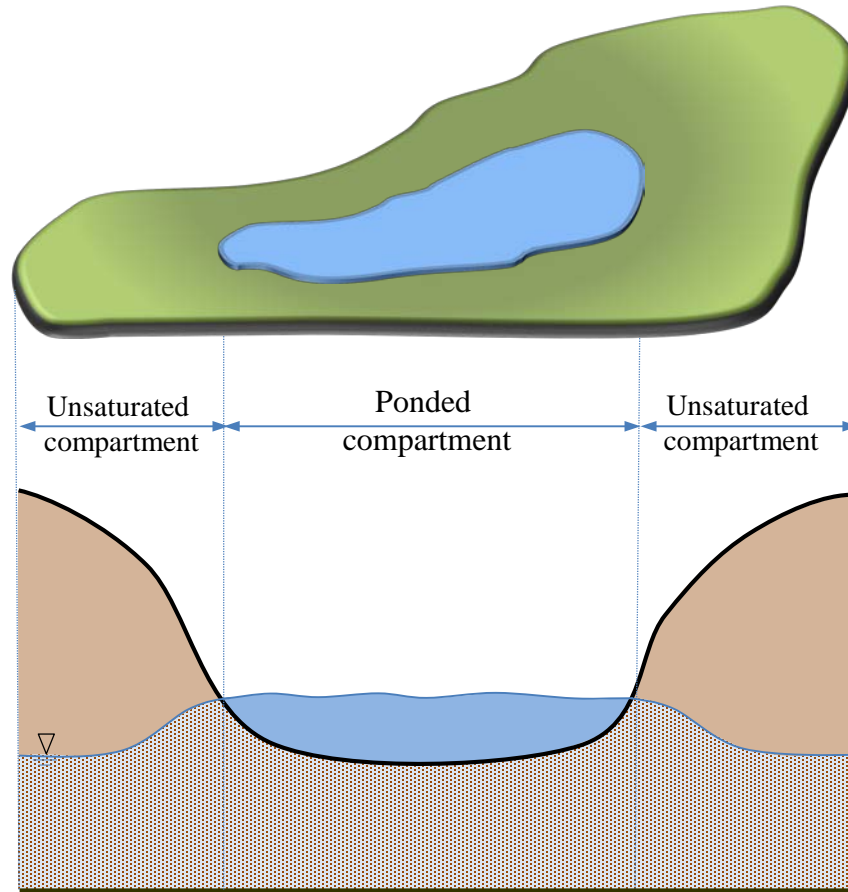


Figure 4.1: Schematics of a hypothetical seasonally flooded wetland

## 2. Modeling moisture redistribution in wetland soil

Simulating soil moisture dynamics in wetland soils can be highly challenging. The challenges that make this task highly uncertain stem from various sources of complexities, such as wetland soil heterogeneity, non-linearity of physical properties in wetland soil and non-uniform root water uptake of wetland plants. In fact, the key to a successful model application in waterlogged environment, such as wetlands, is an accurate simulation of soil moisture content. This means that we need a model that could accurately capture soil moisture redistribution dynamics in wetlands soil. Such a model should consider different sources that provide water to wetland soil

(precipitation, GW upwelling), and sinks that take moisture away (soil evaporation, water extraction by plant roots, and percolation). Having the ability to handle different boundary conditions at the top and the bottom of soil column is another characteristic of the model in mind.

Several analytical solutions were studied for handling simulation of soil moisture redistribution. For instance, we considered estimating infiltration using Green-Ampt (Green and Ampt, 1911) or Horton's equation (Horton, 1940) and calculate soil moisture through mass balance analysis. However, none of the discussed methods were suitable for addressing the water table as a dynamic bottom boundary condition, high non-linearity of soil hydraulic characteristics, vertical variation of physical properties in the soil profile, and irregular soil evaporation demands at the same time. A proper solution to address all the named challenges was found to be a numerical solution of Richards's equation (Richards, 1931). Richards Equation has a clear physical basis; therefore it is generally applicable to soils of different characteristics. In addition, a great number of soil physical physicists have been collecting Soil hydraulic data (e.g. Leij et al., 1996) which enhance the pertinence of the Richards equation.

## **2.1 Richards Equation**

Richards (1931) applied Buckingham's continuity equation to Darcy's law and introduced a differential equation for describing water movement in unsaturated non-swelling soil. A one dimensional Richards' equation could be written as:

$$\frac{\partial \theta}{\partial t} = C(h) \frac{\partial h}{\partial t} = \frac{\partial}{\partial z} \left[ K(h) \left( \frac{\partial h}{\partial z} + 1 \right) \right] - S(z) \quad (4.1)$$

where  $\theta$  is the volumetric water content (dimensionless),  $K$  is the unsaturated hydraulic conductivity ( $LT^{-1}$ ),  $h$  is soil water pressure head (L),  $z$  is the vertical coordinate (L, positively upward),  $t$  is the time (T),  $S$  is the collective term for soil water extraction rate by plant roots and drain discharge ( $T^{-1}$ ) and  $C$  is the specific water content capacity ( $C = \frac{d\theta}{dh}$ ) ( $L^{-1}$ ). Soil hydraulic functions of  $\theta(h)$ ,  $K(\theta)$  and  $C(h)$  could be described by Moalem- van Genuchten model (van Genuchten, 1980):

$$\theta(h) = \theta_{res} + \frac{\theta_{sat} - \theta_{res}}{(1 + |\alpha h|^n)^m} \quad (4.2)$$

$$C(h) = \frac{d\theta}{dh} = \alpha m n |\alpha h|^{n-1} (\theta_{sat} - \theta_{res}) (1 + |\alpha h|^n)^{-(m+1)} \quad (4.3)$$

$$K(\theta) = K_{sat} \left( \frac{\theta - \theta_{res}}{\theta_{sat} - \theta_{res}} \right)^\lambda \left[ 1 - \left( 1 - \left( \frac{\theta - \theta_{res}}{\theta_{sat} - \theta_{res}} \right)^{\frac{1}{m}} \right)^m \right]^2 \quad (4.4)$$

Where  $\theta_{sat}$  and  $\theta_{res}$  are, respectively, saturated and residual water content (dimensionless),  $K_{sat}$  is the saturated hydraulic conductivity ( $LT^{-1}$ ) and  $\alpha$  ( $L^{-1}$ ),  $n$  (dimensionless),  $m$  (dimensionless) and  $\lambda$  (dimensionless) are fitting parameters which can be extracted from soil databases ( $m = 1 - 1/n$ ).

## 2.2 Finite difference solution to Richard's equation

In a search for a theoretically correct, rapidly converging solution to the one-dimensional Richards equation with an accurate mass balance, we adopted the methodology presented in van Dam and Feddes (2000) with slight modifications. This methodology is similar to what is applied in SWAP model, which is a field scale model for simulating transport of water, solutes and heat in the vadose zone (Kroes et al., 1999). Following van Dam and Feddes (2000), for an implicit backward finite difference solution to Richard's equation, the active soil layer is divided into compartments with thickness of  $\Delta z$  with each compartment containing a node in the middle (Figure 4.2). Equation (4.1) is discretized to the following form (van Dam and Feddes, 2000):

$$C_i^{j+1,p-1}(h_i^{j+1,p} - h_i^{j+1,p-1}) + \theta_i^{j+1,p-1} - \theta_i^j = \frac{\Delta t}{\Delta z} \left[ K_{i-(0.5)}^j \left( \frac{h_{i-1}^{j+1,p} - h_i^{j+1,p}}{\Delta z} \right) + K_{i-(0.5)}^j - K_{i+(0.5)}^j \left( \frac{h_i^{j+1,p} - h_{i+1}^{j+1,p}}{\Delta z} \right) - K_{i+(0.5)}^j \right] - \Delta t S_i^j \quad (4.5)$$

where subscript  $i$  is the node number, superscript  $j$  is the time step,  $\Delta t$  is length of each timestep and  $\Delta z$  is compartment thickness (see Figure 4.2) . Superscript  $p$  is the picard iteration level, thus  $C_i^{j+1,p-1}$  is the specific water content capacity evaluated at the pressure head value of the last picard iteration,  $h_i^{j+1,p-1}$ .  $K_{i-0.5}^j$  and  $K_{i+0.5}^j$  are internodal hydraulic conductivity for  $i^{th}$  node. Hydraulic conductivity ( $K$ ) and soil water extractions ( $S$ ) are evaluated at the old time level  $j$ , which according to van Dam and Feddes (2000), gives a good approximation at time steps of  $10^{-6} < \Delta t < 0.2$  days. Once Equation (4.5) is written for all nodes, the series on  $n$  equations



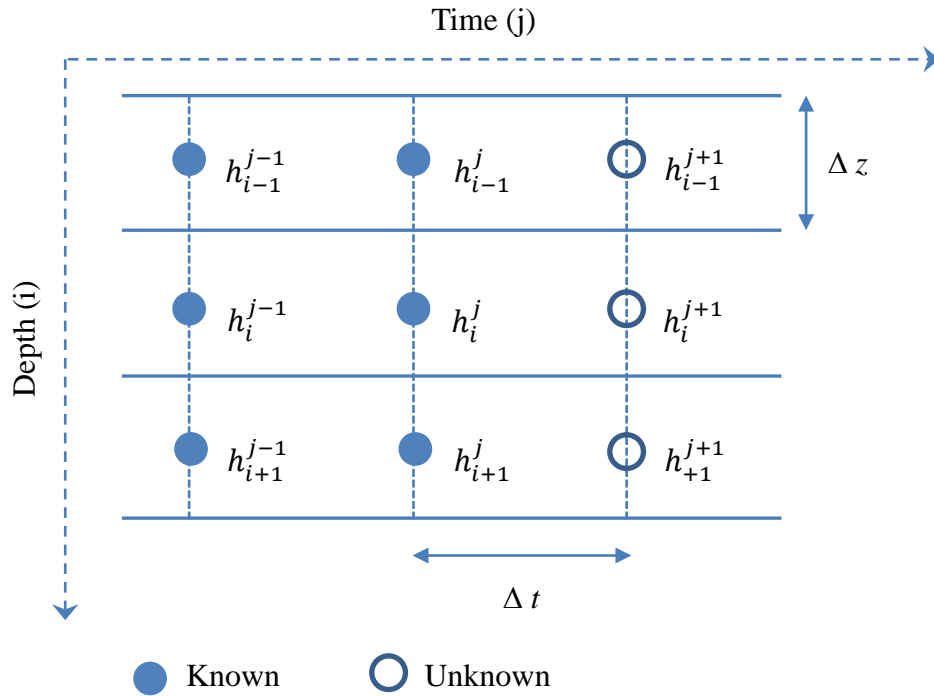


Figure 4.2: Spatial and temporal discretization of Richard's Equation

### 2.3 Upper and lower boundary conditions

In the finite difference method adopted from van Dam and Feddes (2000), special attention is paid to the procedure of selecting the right top and bottom boundary conditions. The right conditions for top and bottom boundaries become very important for situations with intense rainfall (specifically where rainfall intensity is greater than soil infiltration capacity) or with fluctuating groundwater levels close to the soil surface. The steps to determine the top boundary condition is presented in Appendix (see section 9.2). The top boundary condition could be flux-controlled or head-controlled. Top boundary condition is flux-controlled at moderate weather and soil wetness conditions. In case of wet weather or prolonged dry weather, the soil water pressure head at the soil surface governs the boundary condition. The bottom boundary conditions vary depending on presence of GW table at the bottom of soil column. If there is an existing GW

table, the bottom boundary is head controlled, with  $h=0$  at GW level. When GW table is non-existent, or is very deep, the bottom flux controls the bottom boundary conditions. In such circumstances, the head pressure gradient equals zero and bottom flux is only motivated by gravity; thus  $q_{bot} = -K_{n+\frac{1}{2}}^{j+1}$ . See appendix (section 9.2) for derivation of coefficients  $\alpha, \beta, \gamma$  and  $f$  for top and bottom boundary nodes.

### 3. Compartmentalization of unsaturated soil

In this study we have employed a compartmentalization scheme that is slightly different from compartment arrangements of chapter 3. The new compartmentalization approach keeps track of constituents mass in wetland soil and water more accurately, thus reducing the overall mass balance error. In the new compartmentalization scheme, which will be referred to as Sat/Unsat scheme, wetland is divided into two compartments: ponded compartment and unsaturated compartment. Like before, the ponded compartment has a pool of standing water (W) at the top; a thin layer of aerobic soil in the middle ( $S_1$ ) and a thick column of reduced soil at the bottom ( $S_2$ ). The unsaturated compartment has three layers of soil standing on the top of each other. At the top, there is a column of soil which extends from soil surface down to the top of water table ( $S_0$  in Figure 4.3). This column ( $S_0$ ) is not saturated and is assumed to be completely aerobic. Extending from the water table to some depth below, lays a thin aerobic layer ( $S_1$ ). Below this depth, where oxygen is practically negligible, the soil is saturated but anaerobic, with thickness extending from the depth of zero oxygen concentration to the depth of the active sediment layer ( $S_2$ ).

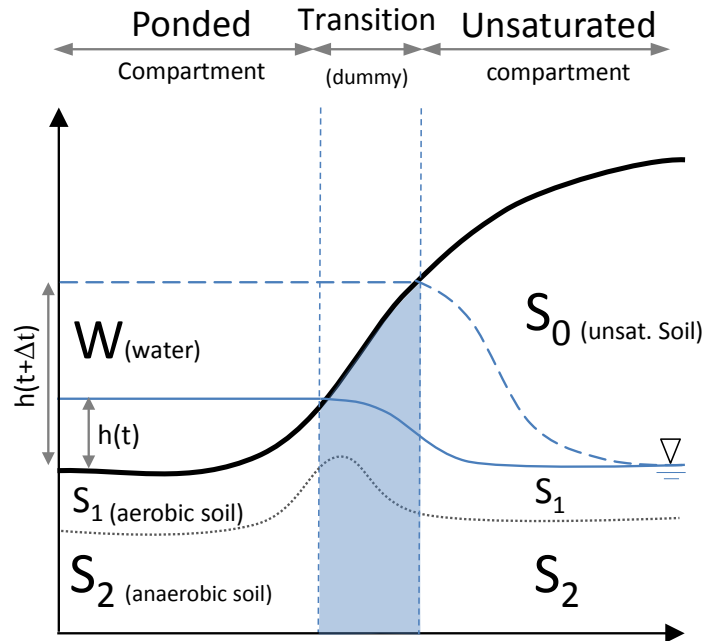


Figure 4.3: Schematic representation for new Sat/Unsat compartmentalization scheme

In the Sat/Unsat scheme, the total area of the wetland is kept constant, as opposed to earlier versions of WetQual (Chapters 2 and 3) where the area of the wetland was allowed to shrink and expand. The total wetland area (which is fixed) is distributed between ponded and unsaturated compartments. However, the area of ponded compartment is allowed to shrink and expand dynamically, with fall and rise of water level. Since the total area of the wetland is fixed, this shrinking and expanding will be at the expense of unsaturated compartment, meaning that when the ponded compartment expands, the unsaturated compartment shrinks, and vice versa. To track the mass exchange between the two compartments, it was necessary to define a temporary compartment at the middle, called the dummy compartment. At each time step, the dummy compartment will form and will adopt the concentrations of either ponded or unsaturated compartments (depending on whether water level is falling or rising). The constituent

concentrations of ponded or unsaturated compartments will be updated at the end of the time step as one or the other incorporates the dummy compartment.

Figure 4.3 presents schematics of a case where water level of the ponded compartment (on the left) has risen over one time step ( $h(t + \Delta t) > h(t)$ ). Consequently, ponded compartment has taken over an area which previously belonged to the unsaturated compartment. In such case, the dummy compartment (in the middle) adopts the concentration of the unsaturated compartment. However, because of rise in water level, the empty pore spaces of soil in dummy compartment have been filled with water. Thus the constituent concentration in dummy compartment soil could be approximated through volumetric averaging between the two concentrations (concentration in water pool of ponded compartment and concentration of unsaturated compartment soil). For a generic constituent ( $C$ ) we have:

$$C_1(d) = \frac{\theta_u C_{1,u} + (\phi_u - \theta_u) C_{w,p}}{\phi_u} \tag{4.7}$$

$$C_2(d) = \frac{\theta_u C_{2,u} + (\phi_u - \theta_u) C_{w,p}}{\phi_u}$$

where  $C_1(d)$  and  $C_2(d)$  represent constituent concentration in aerobic and anaerobic soil of the dummy compartment. Subscript  $p$  and  $u$ , respectively, refer to ponded and unsaturated compartments, thus  $\phi_u$  and  $\theta_u$  are porosity and water content of the unsaturated compartment. Accordingly, at the end of time step, the dummy compartment is incorporated into the ponded compartment. In other words, mass of constituents in dummy compartment is transferred to the ponded compartment, and the concentrations in aerobic and anaerobic soil of ponded compartment are updated such that:

$$\begin{aligned}\bar{C}_{1.p} &= \frac{C_{1.p} \times A_p(i) + C_1(d) \times (A_p(i+1) - A_p(i))}{A_p(i+1)} \\ \bar{C}_{2.p} &= \frac{C_{2.p} \times A_p(i) + C_1(d) \times (A_p(i+1) - A_p(i))}{A_p(i+1)}\end{aligned}\quad (4.8)$$

where  $i$  denotes time,  $A_p$  is area of ponded compartment and  $\bar{C}_{1.p}$  and  $\bar{C}_{2.p}$  are the updated concentrations in ponded compartment's aerobic and anaerobic soil layers respectively.

Similarly, in case of falling water level in the ponded compartment ( $h(t + \Delta t) < h(t)$ ), the unsaturated compartment will take over an area which previously belonged to the ponded compartment. In such case, the dummy compartment (in the middle) adopts the concentration of the ponded compartment, thus:

$$\begin{aligned}C_1(d) &= C_{1.p} \\ C_2(d) &= C_{2.p}\end{aligned}\quad (4.9)$$

And at the end of time step, the dummy compartment is incorporated into the unsaturated compartment. The concentrations in the unsaturated soil compartment are updated such that:

$$\begin{aligned}\bar{C}_{0.u} &= \frac{\phi_p(A_p(i+1) - A_p(i))\Delta h_p C_{1.p} + L_{0.u}\theta_u A_u(i)C_{0.u}}{A_u(i+1)L_{0.u}\theta_u} \\ \bar{C}_{1.u} &= \frac{\phi_p(A_p(i+1) - A_p(i))C_{1.p} + \phi_u A_u(i)C_{1.u}}{A_u(i+1)\phi_u} \\ \bar{C}_{2.u} &= \frac{\phi_p(A_p(i+1) - A_p(i))C_{2.p} + \phi_u A_u(i)C_{2.u}}{A_u(i+1)\phi_u}\end{aligned}\quad (4.10)$$

where  $\bar{C}_{0.u}$ ,  $\bar{C}_{1.u}$  and  $\bar{C}_{2.u}$  are the updated concentrations in unsaturated compartment,  $L_{0,u}$  represents depth of layer  $S_0$  of unsaturated compartment,  $\theta_u$  stands for average moisture content

of column  $S_0$  and  $\Delta h_p$  is variation of water depth in ponded compartment during time step  $i$ . In addition to concentrations, moisture content of column  $S_0$  requires updating:

$$\bar{\theta}_{0,u} = \frac{\phi_p \Delta A_p \Delta h_p + L_{0,u} \theta_u A_u(i)}{A_u(i+1) L_{0,u}} \quad (4.11)$$

where  $\bar{\theta}_{0,u}$  is the updated moisture content of  $S_0$ .

#### 4. Updated relationships for N, P and C cycling in unsaturated wetland soil

Model relationships for C, N and P related constituents were adjusted to reflect physical and geochemical dynamics in unsaturated soil conditions. Since there is no standing water in the unsaturated compartment, processes of burial and settling are non-existent, thus are removed from the equations. Other reaction rates were adjusted for available soil moisture in the unsaturated soil column. Many studies have shown that moisture deficiency slows soil respiration reactions (Reddy and Delaune, 2008; Davisson et al., 1998; Ise and Moorcroft, 2006). The common practice in ecological models is to adjust reaction rates based on the ratio of soil water content to soil moisture at field capacity or at wilting point. For instance, SWAT model (Neitsch et al., 2005) adjusts mineralization rate in agricultural soil by multiplying the following adjustment factor (Neitsch et al., 2005):

$$\eta_{sw} = \frac{SW}{FC} \quad (4.12)$$

where  $\eta_{sw}$  is mineralization adjustment factor for soil moisture,  $SW$  is soil water content on a given day (mm), and  $FC$  is amount of water held in soil at field capacity water content (mm).

For the case of this study, we employed a generic correction factor to adjust reaction rates according to available soil moisture in the unsaturated soil column. Since  $\theta_{sat}$  and  $\theta_{res}$  (saturation

and residual moisture content) were already employed in model, they were used as substitutes to  $SW$  and  $WP$  to form the following relationship:

$$\eta_{sw,x} = \frac{\theta}{\theta + \xi_x(\theta_{sat} - \theta_{res})} \quad (4.13)$$

where  $\eta_{sw,x}$  is reaction  $x$  adjustment factor for soil moisture,  $\theta$  is available soil moisture in unsaturated soil and  $\xi_x$  is a calibration parameter ( $0.01 < \xi_x < 1$ ) which adjusts the shape of the correction factor. In the relationships to follow, reaction rates that are adjusted for soil moisture have been marked with  $(\theta)$  sign. Adjusted model relationships for unsaturated soil compartment are presented by Equations (4.14) to (4.36). Please refer to Table 4.1 for definition of new model parameters. For definition of previously defined parameters please refer to Section 7 of Chapter 3. Note that model parameters/variables followed by subscript  $i$  represent reaction rates/concentrations specific to  $i^{\text{th}}$  compartment.

#### 4.1 Organic Nitrogen

$$V_{s,i} \frac{dN_{or,i}}{dt} = f_r a_{na} k_{ab,i}(\theta) f_{bs} b_i - V_{s,i} k_{mr,i}(\theta) N_{or,i} + f_r (1 - f_{sw}) A_i S_i \quad (4.14)$$

$$V_{s,i} \frac{dN_{os,i}}{dt} = f_s a_{na} k_{ab,i}(\theta) f_{bs} b_i - V_{s,i} k_{ms,i}(\theta) N_{os,i} + f_s (1 - f_{sw}) A_i S_i \quad (4.15)$$

## 4.2 Ammonia-N

$$\begin{aligned}
K_h(1 - f_N) \frac{d\pi_i V_{0.i} N_{a0.i}}{dt} + R_{s.i} \frac{d\theta_i V_{0.i} N_{a0.i}}{dt} \\
= -A_i \pi_i k_v (K_H(1 - f_N) N_{a0.i} - N^*) + F_{N_{ag.i}}^0 - f_{a0} a_{na} k_{gb.i}(\theta) f_0 b_i \\
+ V_{0.i} k_{mr.i}(\theta) N_{or.i} + V_{0.i} k_{ms.i}(\theta) N_{os.i} - \theta_i V_{0.i} f_N k_{ns.i}(\theta) N_{a0.i} \\
+ A_i \beta_{ax} (N_{a1.i} - N_{a0.i})
\end{aligned} \tag{4.16}$$

$$\begin{aligned}
\phi_i R_{s.i} \frac{dV_{1.i} N_{a1.i}}{dt} \\
= F_{N_{ag.i}}^1 - f_{a1} a_{na} k_{gb.i}(\theta) f_1 b_i + V_{1.i} k_{mr.i}(\theta) N_{or.i} + V_{1.i} k_{ms.i}(\theta) N_{os.i} \\
+ A_i \beta_{ax} (N_{a0.i} - N_{a1.i}) - \phi_i V_{1.i} f_N k_{ns.i} N_{a1.i} + A_i \beta_{n2} (N_{a2.i} - N_{a1.i})
\end{aligned} \tag{4.17}$$

$$\begin{aligned}
\phi_i R_{s.i} \frac{dV_{2.i} N_{a2.i}}{dt} \\
= F_{N_{ag.i}}^2 - f_{a2} a_{na} k_{gb.i}(\theta) f_2 b_i + V_{2.i} k_{mr.i}(\theta) N_{or.i} + V_{2.i} k_{ms.i}(\theta) N_{os.i} \\
+ A_i \beta_{n2} (N_{a1.i} - N_{a2.i})
\end{aligned} \tag{4.18}$$

## 4.3 NO<sub>3</sub>-N

$$\begin{aligned}
V_{0.i} \frac{d\theta_i N_{n0.i}}{dt} = F_{N_{ng.i}}^0 + \phi_i V_{0.i} f_N k_{ns.i}(\theta) N_{a0.i} - A_i \beta_{nx} (N_{n0.i} - N_{n1.i}) \\
- f_{n1} a_{na} k_{gb.i}(\theta) f_1 b_i
\end{aligned} \tag{4.19}$$

$$\begin{aligned}
\phi_i V_{1.i} \frac{dN_{n1.i}}{dt} = A_i \beta_{nx} (N_{n0.i} - N_{n1.i}) - A_i \beta_{n2} (N_{n1} - N_{n2}) + \phi_i V_{1.i} f_N k_{ns.i} N_{a1.i} + F_{N_{ng.i}}^1 \\
- f_{n1} a_{na} k_{gb.i}(\theta) f_1 b_i
\end{aligned} \tag{4.20}$$

$$\phi_i V_{2.i} \frac{dN_{n2.i}}{dt} = A_i \beta_{n2} (N_{n1.i} - N_{n2.i}) - \phi_i V_{2.i} k_{dn.i} N_{n2.i} + F_{N_{ng.i}}^2 - f_{n2} a_{na} k_{gb.i}(\theta) f_2 b_i \tag{4.21}$$

#### 4.4 Phosphorus

$$V_{0.i} \frac{dP_{0.i}}{dt} = \beta_{px} A_i (F_{ds} P_{1.i} - F_{xds} P_{0.i}) + F_{Pg.i}^0 - a_{pa} k_{gb.i}(\theta) f_0 b_i + V_{0.i} a_{pn} k_{mr.i}(\theta) N_{or.i} \\ + V_{0.i} a_{pn} k_{ms.i}(\theta) N_{os.i} \quad (4.22)$$

$$V_{0.i} \frac{dP_{1.i}}{dt} = \beta_{px} A_i (F_{xds} P_{0.i} - F_{ds} P_{1.i}) + F_{Pg.i}^1 - a_{pa} k_{gb}(\theta) f_1 b_i + V_{1.i} a_{pn} k_{mr.i}(\theta) N_{or.i} \\ + V_{1.i} a_{pn} k_{ms.i}(\theta) N_{os} + \beta_{p2} A_i (f_{ds} P_{2.i} - F_{ds} P_{1.i}) \quad (4.23)$$

$$V_{2.i} \frac{dP_{2.i}}{dt} = V_{2.i} a_{pn} k_{mr.i}(\theta) N_{or.i} + V_{2.i} a_{pn} k_{ms}(\theta) N_{os.i} - \beta_{p2} A_i (f_{ds} P_{2.i} - F_{ds} P_{1.i}) + F_{Pg.i}^2 \\ - a_{pa} k_{gb}(\theta) f_2 b_i \quad (4.24)$$

#### 4.5 LPOC

$$V_0 \frac{dC_{L0.i}}{dt} = a_{ca} k_{db.i}(\theta) f_0 f_{bs} f_{bL} b_i - V_{0.i} k_{L.i}(\theta) C_{L0.i} \quad (4.25)$$

$$V_{1.i} \frac{dC_{L1.i}}{dt} = a_{ca} k_{db.i}(\theta) f_1 f_{bs} f_{bL} b_i - V_{1.i} k_{L.i} C_{L1.i} \quad (4.26)$$

$$V_{2.i} \frac{dC_{L2.i}}{dt} = a_{ca} k_{db.i}(\theta) f_2 f_{bs} f_{bL} b_i - V_{2.i} k_{L.i} C_{L2.i} \quad (4.27)$$

#### 4.6 RPOC

$$V_{0.i} \frac{dC_{R0.i}}{dt} = a_{ca} k_{db.i}(\theta) f_0 f_{bs} f_{bR} b_i - V_{0.i} k_{R.i}(\theta) C_{R0.i} \quad (4.28)$$

$$V_{1.i} \frac{dC_{R1.i}}{dt} = a_{ca} k_{db.i}(\theta) f_1 f_{bs} f_{bR} b_i - V_{1.i} k_{R.i} C_{R1.i} \quad (4.29)$$

$$V_{2.i} \frac{dC_{R2.i}}{dt} = a_{ca} k_{db.i}(\theta) f_2 f_{bs} f_{bR} b_i - V_{2.i} k_{R.i} C_{R2.i} \quad (4.30)$$

#### 4.7 DOC

$$\begin{aligned}
V_{0.i} \frac{d\theta_i C_{D0.i}}{dt} &= a_{ca} k_{db.i}(\theta) f_0 f_{bs} F_{bD} b_i + V_{0.i} k_{L.i}(\theta) C_{L0.i} + V_{0.i} k_{R.i}(\theta) C_{R0.i} \\
&\quad - \beta_{Dx} A_i (C_{D0.i} - C_{D1.i}) + F_{C_{Dg.i}}^0 - \phi_i V_{0.i} k_{D.i}^1(\theta) C_{D0.i}
\end{aligned} \tag{4.31}$$

$$\begin{aligned}
\phi_i V_{1.i} \frac{dC_{D1.i}}{dt} &= a_{ca} k_{db.i}(\theta) f_1 f_{bs} F_{bD} b_i + V_{1.i} k_{L.i} C_{L1.i} + V_{1.i} k_{R.i} C_{R1.i} \\
&\quad - \beta_{D2} A_i (C_{D1.i} - C_{D2.i}) + F_{C_{Dg.i}}^1 - \beta_{Dx} A_i (C_{D1.i} - C_{D0.i}) \\
&\quad - \phi_i V_{1.i} \frac{O_{s1}}{O_{s1} + K_o} k_{D.i}^1 C_{D1.i}
\end{aligned} \tag{4.32}$$

$$\begin{aligned}
\phi_i V_{2.i} \frac{dC_{D2.i}}{dt} &= a_{ca} k_{db.i}(\theta) f_2 f_{bs} f_{bD} b_i + V_{2.i} k_{L.i} C_{L2.i} + V_{2.i} k_{R.i} C_{R2.i} - \beta_{D2} A_i (C_{D2.i} - C_{D1.i}) \\
&\quad + F_{C_{Dg.i}}^2 - \phi_i V_{2.i} \frac{N_{n2.i}}{N_{n2.i} + K_N} k_{D.i}^2 C_{D2.i} - \phi_i V_{2.i} \frac{K_N^{in}}{N_{n2.i} + K_N^{in}} k_{D.i}^3 C_{D2.i}
\end{aligned} \tag{4.33}$$

#### 4.8 CH<sub>4</sub>

$$\begin{aligned}
K_h \frac{d\pi_i V_{0.i} C_{M0.i}}{dt} + \frac{d\theta_i V_{0.i} C_{M0.i}}{dt} &= -A_i \pi_i k_v (K_H C_{M0.i} - C_M^*) + \beta_{Mx} A_i (C_{M1.i} - C_{M0.i}) - \theta_i V_{0.i} k_{M.i}^1(\theta) C_{M0.i} \\
&\quad + F_{C_{Mg.i}}^0 + \lambda_r f_0 f_{bs} b_i R_v D^\sigma (C^* - C_{M0.i})
\end{aligned} \tag{4.34}$$

$$\begin{aligned}
\phi V_{1.i} \frac{dC_{M1.i}}{dt} &= -\beta_{M2} A_i (C_{M1.i} - C_{M2.i}) - \phi_i V_{1.i} \frac{O_{s1}}{O_{s1} + K_o} k_{M.i}^1 C_{M1.i} + F_{C_{Mg.i}}^1 \\
&\quad + \lambda_r f_1 f_{bs} b_i R_v D^\sigma (C^* - C_{M1.i}) + \beta_{Mx} A_i (C_{M1.i} - C_{M0.i})
\end{aligned} \tag{4.35}$$

$$\begin{aligned} \phi V_{2.i} \frac{dC_{M2.i}}{dt} = & \phi_i V_{2.i} \frac{K_N^{in}}{N_{n2.i} + K_N^{in}} k_{D2.i}^3 C_{D2.i} + \beta_{M2} A_i (C_{M1.i} - C_{M2.i}) \\ & - \phi_i V_{2.i} \frac{N_{n2.i}}{N_{n2.i} + K_N} k_{M2.i}^2 C_{M2.i} + F_{C_{Mg}.i}^2 + \lambda_r f_2 f_{bs} b_i R_v D^\sigma (C^* - C_{M2.i}) \end{aligned} \quad (4.36)$$

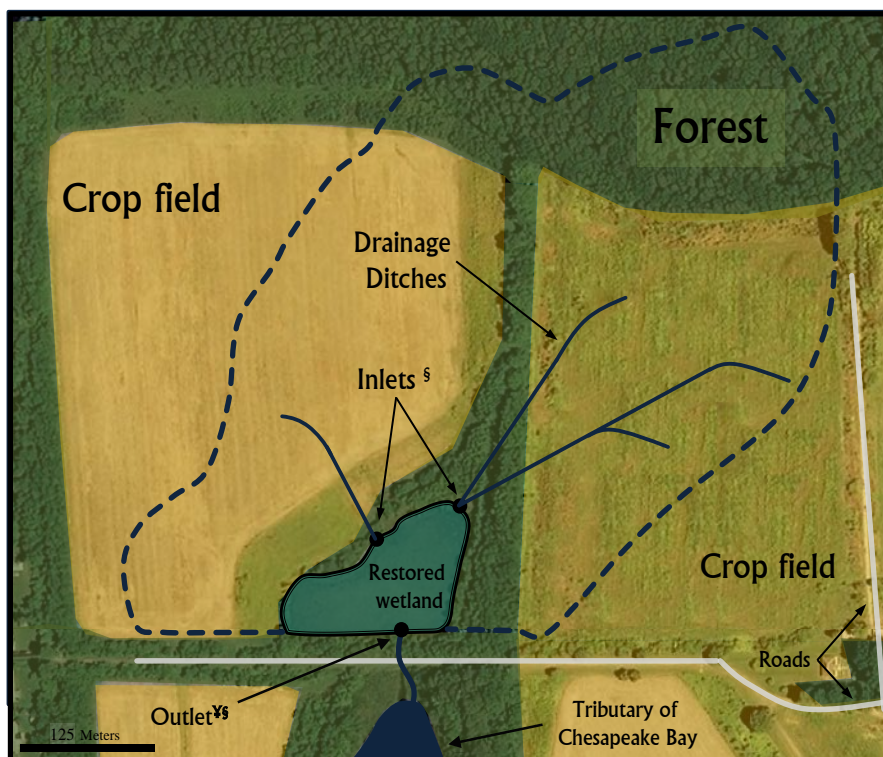
Table 4.1: Definition and dimation of new model parameters

Symbol	Definition & Dimension
$V_0$	Volume of wetland unsaturated soil column
$N_{a0}$	$[\text{NH}_4^+] + [\text{NH}_3]$ total ammonia-nitrogen concentration in unsaturated soil $[\text{ML}^{-3}]$
$N_{n0}$	nitrate-nitrogen concentration in unsaturated soil $[\text{ML}^{-3}]$
$P_0$	total inorganic phosphorus concentration in unsaturated soil $[\text{ML}^{-3}]$
$C_{L0}$	concentrations of labile (fast reacting) particulate organic C in unsaturated soil $[\text{ML}^{-3}]$
$C_{R0}$	concentrations of refractory (slow reacting) particulate organic C in unsaturated soil $[\text{ML}^{-3}]$
$C_{D0}$	concentrations of dissolved organic C in unsaturated soil $[\text{ML}^{-3}]$
$C_{M0}$	methane concentration in anaerobic sediment, aerobic sediment layer and water respectively $[\text{ML}^{-3}]$
$K_h$	Ratio of $\text{NH}_3$ in gas form to $\text{NH}_3$ in liquid form
$\theta$	Soil water content ( $\text{L}^0$ )
$\xi_D$	adjustment factor for aerobic respiration of DOC in reference to available soil moisture
$\pi$	Portion of soil volume that is filled with air ( $\pi = \phi - \theta$ )
$\theta_{sat}, \theta_{res}$	Soil saturated and residual water content
$\beta_{nx}, \beta_{ax}, \beta_{px}, \beta_{Dx}, \beta_{Mx}$	diffusive mass-transfer rates, respectively, of total ammonia, nitrate, inorganic phosphorus, DOC and methane between unsaturated wetland soil and saturated aerobic soil layer $[\text{LT}^{-1}]$
$F_{C_{Mg}}^0, F_{C_{Dg}}^0, F_{N_{ng}}^0, F_{N_{ag}}^0$	groundwater source/loss of methane, DOC, nitrate and total ammonia nitrogen in the unsaturated soil layer $[\text{MT}^{-1}]$

## 5. Case study application

The developed model was applied to a study wetland, previously introduced in Chapter 2. The study wetland, described thoroughly by Jordan et al. (2003), is a small restored wetland located on Kent Island, Maryland (Figure 2.2) which was monitored for flow and water quality data for approximately 2 years (Figure 4.6). The study wetland, called Barnstable wetland, was restored from an artificially drained cropland by the Chesapeake Wildlife Heritage with the intention to provide wildlife habitat and improve the quality of runoff from surrounding crop fields. During

the study period (May 1995 - May 1997), a maximum 90% of the wetland surface was covered by emergent vegetation through growing season; this portion dropped to a minimum of 10% during non-growing season. Water entered the wetland through ditches draining surface runoff from surrounding catchment and outflowed via a standpipe connected to a 120° V-notch weir. The entire 1.3-ha area of the wetland was submerged and lacked well-defined flow channels when the water was deep enough to flow out of the weir. An impermeable layer of clay, within 0.5 m of soil surface during wetland restoration blocked groundwater exchanges and infiltration. Automated instruments were used to measure unregulated water inflows and to sample water entering and leaving the wetland from 8 May 1995 through 12 May 1997. Weekly (typically 5 to 8 days) flow averaged nitrate N, total ammonia N, organic N, inorganic P, and TSS and TOC (total organic carbon) concentrations in runoff were available from Jordan et al. (2003). Figure 4.6 exhibits the hydrology of the study wetland (inflow, outflow and average water depth in ponded compartment) in addition to inflow concentrations of TOC, NH<sub>4</sub>, NO<sub>3</sub>, TSS and inorganic P to the study wetland from May 1995 to May 1997. Details of data collection and analysis can be found in Jordan et al. (2003). Sources for other input data (precipitation, temperature, etc.) used in the model could be found in Kalin et al. (2013) who validated the N and P cycles of WetQual model on the same study wetland. Later in the results section, we will compare findings of Kalin et al. (2013) to the results obtained from the updated model, presented in this chapter.



<sup>∇</sup> Outflow structure consisted of a standpipe connected to a 120° V-notch weir.  
<sup>§</sup> Automated samplers were installed to sample water entering and leaving the wetland.

Figure 4.4: Study wetland and its watershed outlined by dashed lines (regenerated from Jordan et al., 2003).

As mentioned earlier, in this chapter, we aimed to extend our models capabilities to simulate geochemical reactions in unsaturated wetland soil and to track constituent concentrations in parts of the wetland that are not flooded. A proper validation procedure for the developed model requires us to have a study wetland with field measurements of soil moisture and constituent concentration in unsaturated soil for a period of time. Finding such dataset was not an easy task and we were not able to secure such dataset; consequently, we were forced to turn to available datasets for model validation purposes. Applying the newly developed model to Barnstable wetland will not allow us to completely validate the new developments in the model. However,

using the newly developed model, we can gain insight about mass exchanges through microbial activities in the unsaturated banks of the study wetland.

The model applied to Barnstable wetland was divided into two compartments, a ponded compartment in the middle, surrounded by an unsaturated compartment (similar to Figure 4.1). As mentioned earlier the total area of the wetland is kept constant. The area of ponded compartment is allowed to shrink and expand dynamically at the expense of unsaturated compartment, meaning that when the ponded compartment expands, the unsaturated compartment shrinks, and vice versa. On average, the ponded compartment covers 65% of the total 1.2 ha area of the wetland. Figure 4.5 shows the percentage of total wetland area covered by ponded compartment over study period.

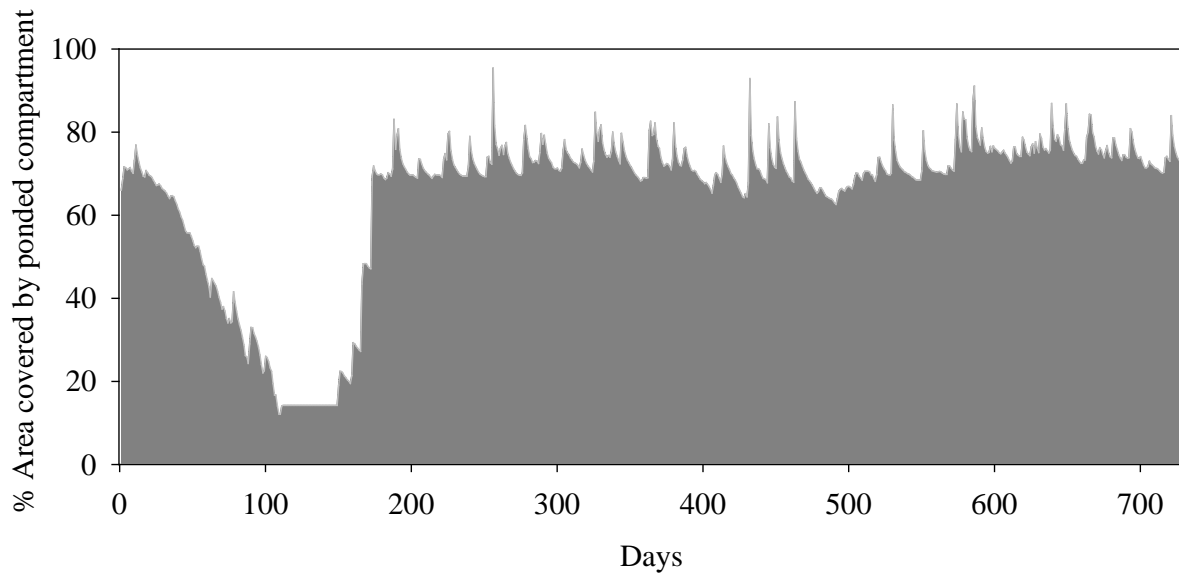


Figure 4.5: % Area covered by ponded compartment in Barnstable wetland over study period

According to Jordan et al. (2003), the study wetland is underlain by a silty clay loam subsurface horizon which forms an extensive and continuous aquiclude. Given this information, it was safe to assume presence of a perched water table below wetland surface, sustaining the study wetland during dry periods. Since we had no records on the depth of such perched water table, it was assumed that the water table resides at a depth equivalent to the bottom of ponded compartment (similar to Figure 4.3).

In sections to follow, results from the model presented in chapter 2, in addition to the results of Kalin et al (2012) will be used for comparison purposes. To avoid confusion, we will refer to the earlier model as “Lumped model” whereas the newly developed model in this chapter will be referenced as “Expanded model”.

## **6. Model Assessment**

Model assessment performed in this chapter is similar to the process applied in chapters 2 and 3. A combination of both GLUE and GSA methods (Beven and Binley, 1992; Spear and Hornberger ,1980) were employed to assess model prediction uncertainty and quantitative sensitivity to model parameters. Please see Figure 2.4 for a brief portrayal of the GSA/GLUE methodology applied in this chapter.

In brief, we generated 100,000 statistically independent parameter sets for each compartment (ponded and unsaturated compartments), sampled randomly from previously defined distributions which were extracted from literature values/tabulations.

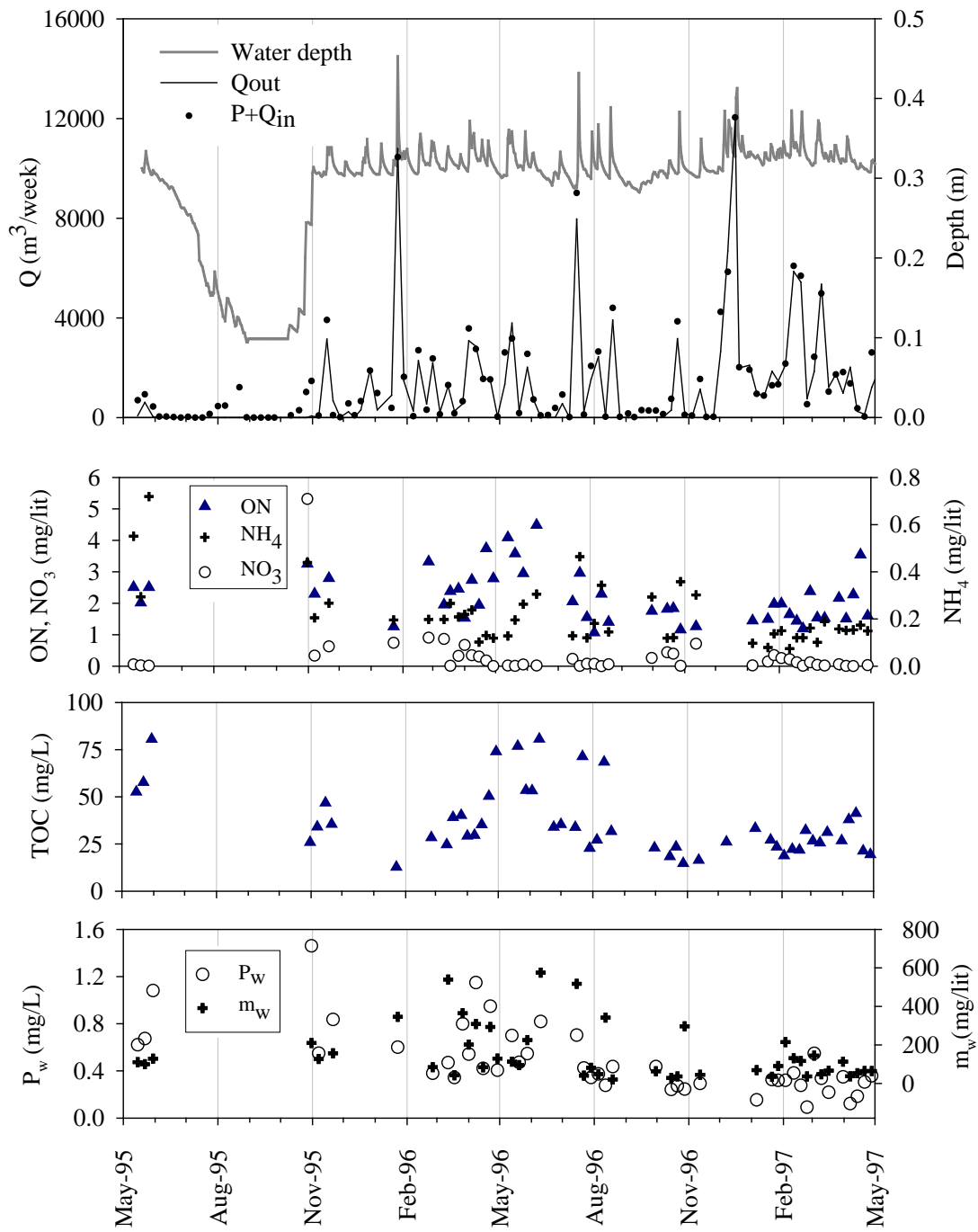


Figure 4.6: Hydrology of the study wetland (inflow, outflow and average water depth in ponded compartment) in addition to inflow concentrations of TOC,  $\text{NH}_4$ ,  $\text{NO}_3$ , TSS and inorganic P from May 1995 to May 1997

Model parameter distribution and their respective upper and lower bounds (quantities) for carbon cycle could be found in Table 2.3. For N, P and sediment cycles, reader is referred to Kalin et al. (2013). To perform Monte Carlo (MC) simulations, the model was run 100,000 times, each time with one set of parameters to yield an ensemble of 100,000 time series for constituent concentrations. Two performance criteria ( $MBE$  and  $E_{ns}$ ) were used to construct a likelihood function that evaluates the goodness of fit between model-predicted concentrations and observed data for each MC simulation (Equation 2.23). For each compartment, parameter sets were sorted based on their likelihoods and the top 1% datasets with the highest likelihoods were separated as behavioral dataset ( $\mathbf{B}$ ) from the rest of the parameter sets (non-behavioral datasets,  $\mathbf{B}'$ ).

Subsequently, quantitative sensitivity analysis was performed using Kolmogorov-Smirnov test (Massey Jr, 1951) to reveal the most sensitive parameters. Kolmogorov-Smirnov test is a nonparametric test that is used to quantify a distance between the reference cumulative distribution function (CDF) – generated from non-behavioral parameter values or  $\mathbf{B}'$ – and posterior CDF of a parameter generated from behavioral datasets (or  $\mathbf{B}$ ). If such distance – referred to as  $D_{max}$  – is significant at a certain confidence level ( $\alpha$ ), the parameter is declared sensitive. Prior and posterior prediction uncertainty were next obtained by using model predictions generated respectively from the whole spectrum of model parameter distributions ( $\mathbf{B} \cup \mathbf{B}'$ ), and from behavioral parameters only ( $\mathbf{B}$ ).

## 7. Results and discussion

Model fitness was gauged by comparing simulated loading (export) of TSS, TN,  $\text{NO}_3$ , ON,  $\text{NH}_4$ , TOC and  $\text{PO}_4$  with observed data collected at the outlet using two performance criteria of Mass Balance Error ( $MBE$ ) and Nash-Sutcliffe efficiency ( $E_{ns}$ ). Table 4.2 exhibits average model

performances ( $E_{ns}$  and  $MBE$ ) for behavioral simulations (top 1%). As mentioned earlier, contents of Chapter 2, in addition to Kalin et al. (2013) present application of an earlier version of WetQual model to the same study site. The earlier model will be referred to as “Lumped model” whereas the newly developed model in this chapter will be referenced as “Expanded model”.

Table 4.2: Average model performances (MBE and  $E_{ns}$ ) for behavioral simulations based on observed and simulated loadings (mass of export)

	PO <sub>4</sub>	TN	Onw	NH <sub>4</sub>	NO <sub>3</sub>	TSS	TOC
$MBE$ (%)	47.3	-8.2	-13.7	-0.27	29.1	-46.3	-4.1
$E_{ns}$	0.54	0.61	0.46	0.91	0.96	0.58	0.88

As showed in Table 4.2, model performs exceptionally well in capturing dynamics of TOC, NO<sub>3</sub> and NH<sub>4</sub> loadings (mass export) from study wetland with small mass balance error (except for NO<sub>3</sub> and TSS) and large  $E_{ns}$  ( $E_{ns}>0.88$ ). Model performed fairly well in predicting TN, TSS and PO<sub>4</sub> exports from the study wetland, with  $E_{ns}$  ranging from 0.54 to 0.61. Despite increased complexity, model performance of the distributed model is very close to that of the simpler Lumped model (see Chapter 2 and Kalin et al., 2013). Given that there were no additional data points to further fine-tune the Expanded model of this chapter, we can claim that the Expanded model exceeds the Lumped model in functionality. For the sake of brevity, we will keep the analysis limited to carbon and nitrogen constituents throughout the rest of this chapter.

## 7.1 Soil moisture redistribution in Barnstable wetland

In practice, solving Richard’s equation was more complicated than expected. Due to hyperbolic nature of Richard’s equation, high non-linearity of soil hydraulic functions of  $\theta(h)$ ,  $K(\theta)$  and

$C(h)$ , (described by Moalem- van Genuchten model, see section 2.1) and rapidly changing boundary conditions near the soil surface, the numerical solution crashes easily, specifically when soil is close to saturation. We had initially considered assessing model sensitivity to parameters embedded in Richard equation. This required us to generate a number of independent parameter sets and perform MC simulations on the soil moisture module. However, because of the stated problem (frequent crashes), we were forced to just assume a fixed set of parameters and run the soil moisture model deterministically. These fixed parameters (listed in Table 4.3) were extracted from literature (Kroes et al., 2008) for soils thought to be close to Jordan et al.’s (2003) description of soil in our study site.

Table 4.3: Assumed parameter values for Richard’s equation

$\theta_{sat}$	$\theta_{res}$	$K_{sat}$ (cm.sec <sup>-1</sup> )	$\lambda$	$\alpha$ (cm <sup>-1</sup> )	$n$
0.43	0.001	$2.02 \times 10^{-5}$	-0.14	0.0249	1.507

Figure 4.7 exhibits model simulated soil moisture content in unsaturated compartment of Barnstable wetland, averaged vertically over the whole soil column. Barnstable wetland has no records of soil moisture during the study period, thus the simulated results can’t be validated directly. However, the general validity of soil moisture component of the model could be verified with side by side comparison of soil moisture time series (in banks of wetland) with depth of ponding (in the center). Depth of standing water is a representative of wetland hydroperiod, and a direct function of rainfall. Similarly, soil moisture in the banks is directly a function of precipitation, thus one could expect that the local minima and maxima of the two graphs to coincide.

The explained logic is evident in Figure 4.7, specifically during the long dry period between days 100 to 160 where depth of ponding is at its minimum. During the simulation period, soil moisture in the banks of the wetland had an average moisture content ( $\theta$ ) of 0.41 which is close to soil saturated water content ( $\theta_{sat} = \phi = 0.43$ ).

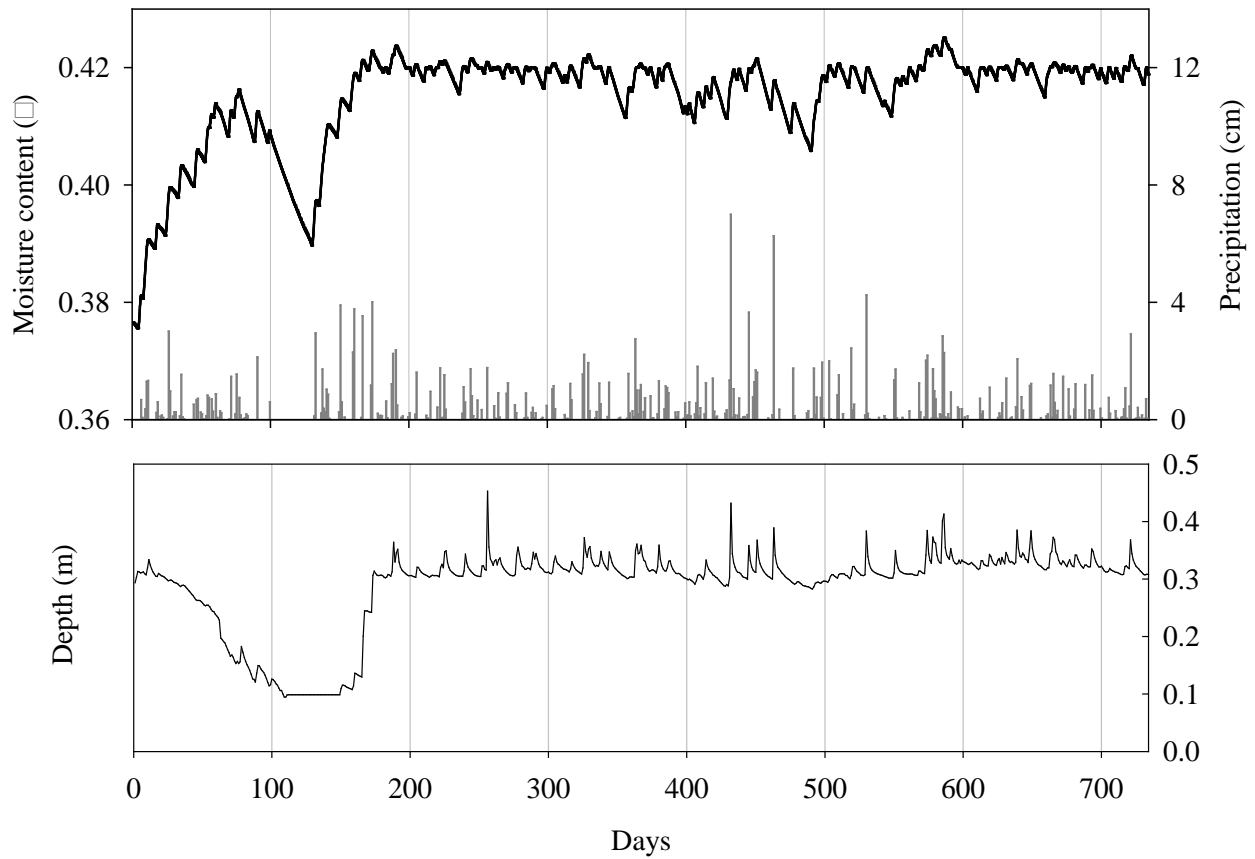


Figure 4.7: Average soil moisture content in unsaturated compartment of Barnstable wetland +daily precipitation records (top) along with average depth of water in the ponded compartment (bottom)

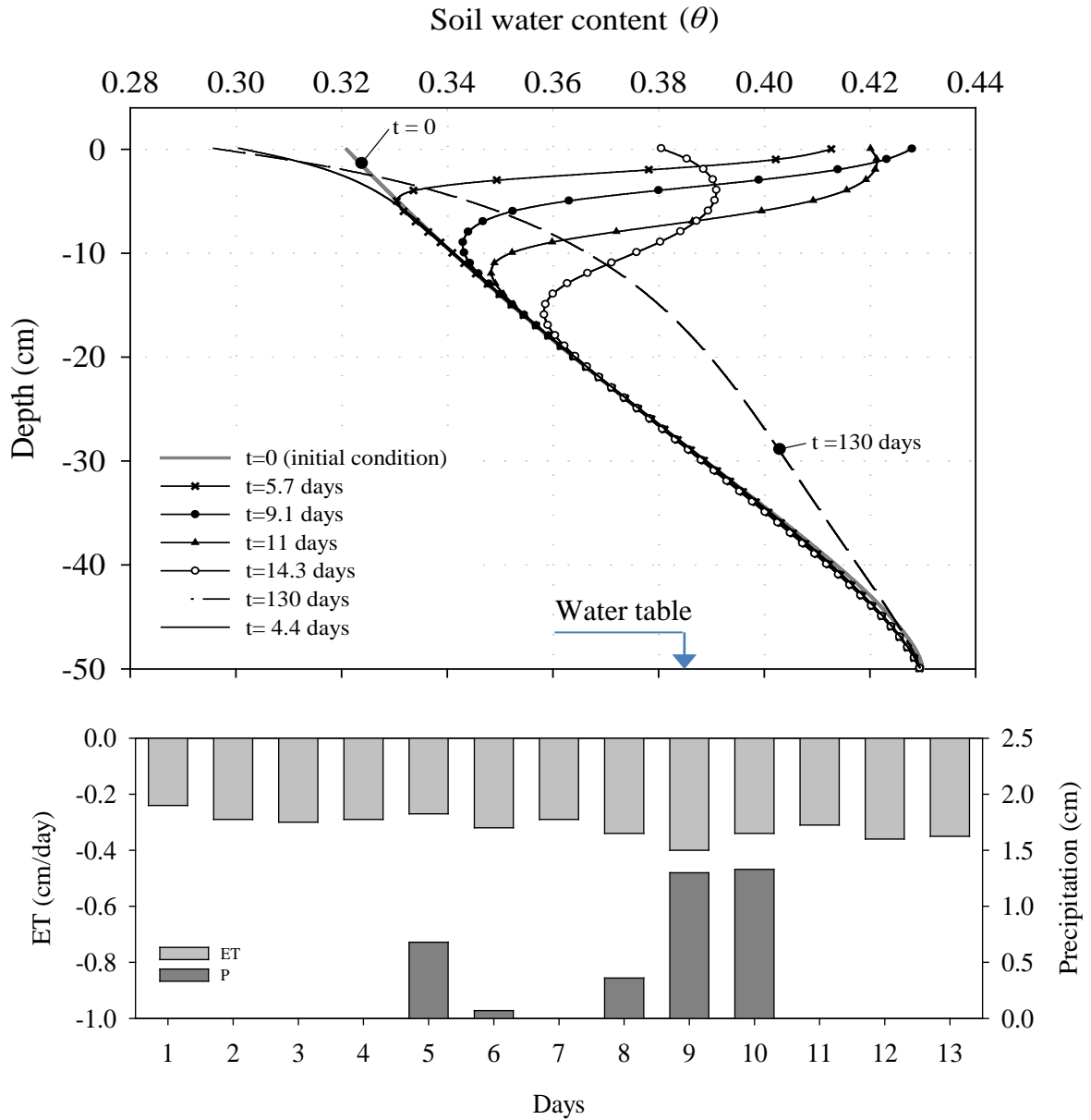


Figure 4.8: Simulated soil moisture profile in the banks of Barnstable wetland (top) in addition to evapotranspiration rate and precipitation records (bottom) during first two weeks of study period.

To further explore validity of the employed numerical scheme, soil moisture profiles were drawn for the first two weeks of simulation period (Figure 4.8). As shown in Figure 4.8, the bottom

node that coincides with perched water table (depth = -50 cm) remains saturated during simulation period due to defined bottom boundary conditions (head controlled, with  $h=0$  at GW level). During the first 5 days, where there is no record of precipitation, soil becomes drier at the top few centimeters. Between days 5 to 10, where a sum of 3.75 cm of rainfall occurs, soil becomes saturated at the top; and afterwards, soil moisture starts to redistribute downwards. In general, due to existence of a shallow perched water table and excessive rainfall, soil moisture at banks of Barnstable wetland remains close to saturation. At driest conditions ( $t=130$  days), the average soil moisture does not drop below 0.39 (Figure 4.8).

## 7.2 Sensitivity analysis

The Kolmogorov-Smirnov (K-S) test was applied to the behavioral (**B**) and non-behavioral (**B'**) datasets of each compartment, to statistically quantify the sensitive and insensitive parameters. Figure 4.9 to Figure 4.11 summarize the most sensitive parameters for ponded and unsaturated compartments of the study wetland in order of sensitivity based on  $\text{NH}_4$ ,  $\text{NO}_3$  and TOC loading respectively. On the vertical axes of the presented graphs is  $D_{\max}$  resulted from K-S test, and sensitive parameters are listed on horizontal axis in order of sensitivity. For the ponded compartment, the sensitivity was gauged at 5% significance level, whereas for the unsaturated compartment, significance level was set to 20%, simply because not too many parameters showed sensitive at 5% level. The reason behind this remark stems from the fact that there are no observations available for direct validation of unsaturated compartment. Bottom panels of Figure 4.9 to Figure 4.11 exhibit the sensitive parameters of the Lumped model for the represented constituent. These extra panels were borrowed from chapter 2 and from Kalin et al. (2013) for comparison purposes.

Comparing top and bottom panels of Figure 4.9, it is observed that the parameters for  $\text{NH}_4$  that appear sensitive for ponded compartment more or less conform to the sensitive parameters of the Lumped model. However, the order of sensitivity is not necessarily the same. Another observation is that the total numbers of sensitive parameters for the Lumped and Expanded model (Ponded+unsaturated) are more or less equal. The same observations could be made for  $\text{NO}_3$  in Figure 4.10.

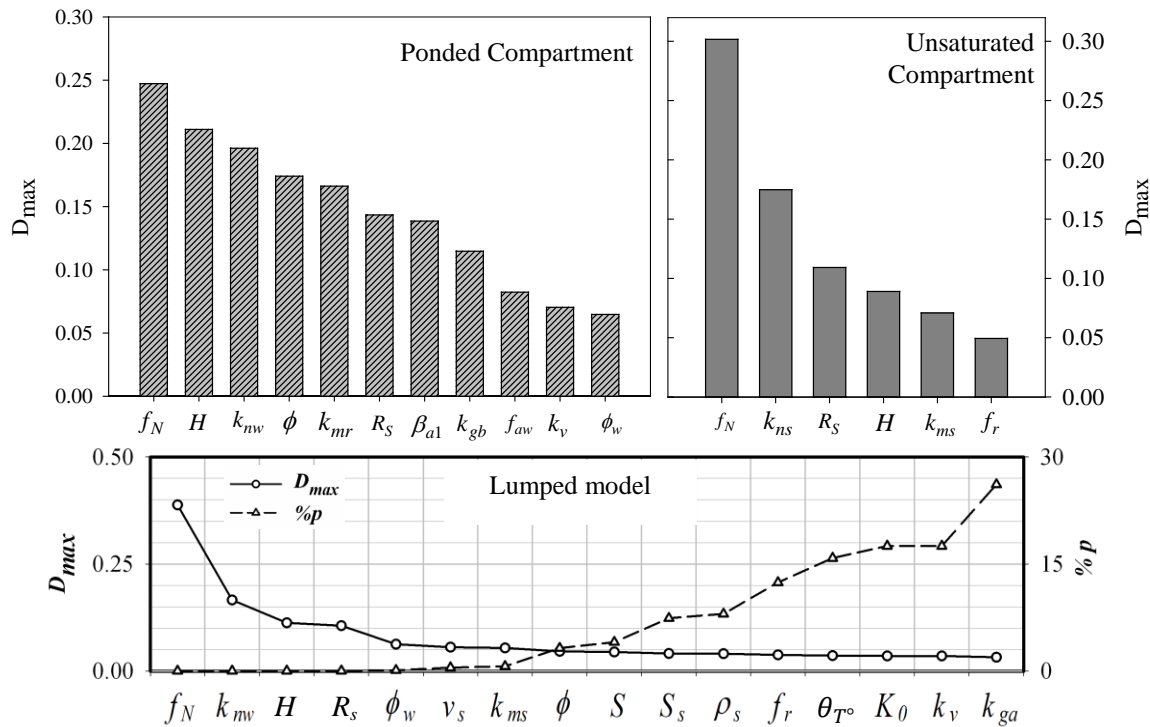


Figure 4.9: Summary of the K-S test and order of sensitivities based on  $\text{NH}_4$  loading for ponded and unsaturated compartments (top) and Lumped model (bottom, borrowed from Kalin et al., 2013)

Looking at top panels of Figure 4.9, in both ponded and unsaturated compartments, parameter  $f_N$  which captures the effects of  $pH$  and temperature on fraction of total ammonia in ionized form (Hantush et al., 2013) appears as the most sensitive parameter. Depth of active sediment layer

( $H$ ) also appears sensitive for both compartments. Parameter  $k_{ns}$  (nitrification rate in aerobic soil) followed by  $R_s$  (ammonia retardation factor in wetland soil) represent the second and third sensitive parameters for unsaturated compartment. Judging from the sensitive parameter, it appears that loss of ammonia to nitrification is the most important process in the unsaturated compartment, which is not unexpected due to abundance of oxygen in the top soil layer. The relatively high sensitivity of ammonia retardation factor in wetland soil,  $R_s$  indicates the importance of adsorption of ammonium ions onto negatively charged particles in unsaturated compartment.

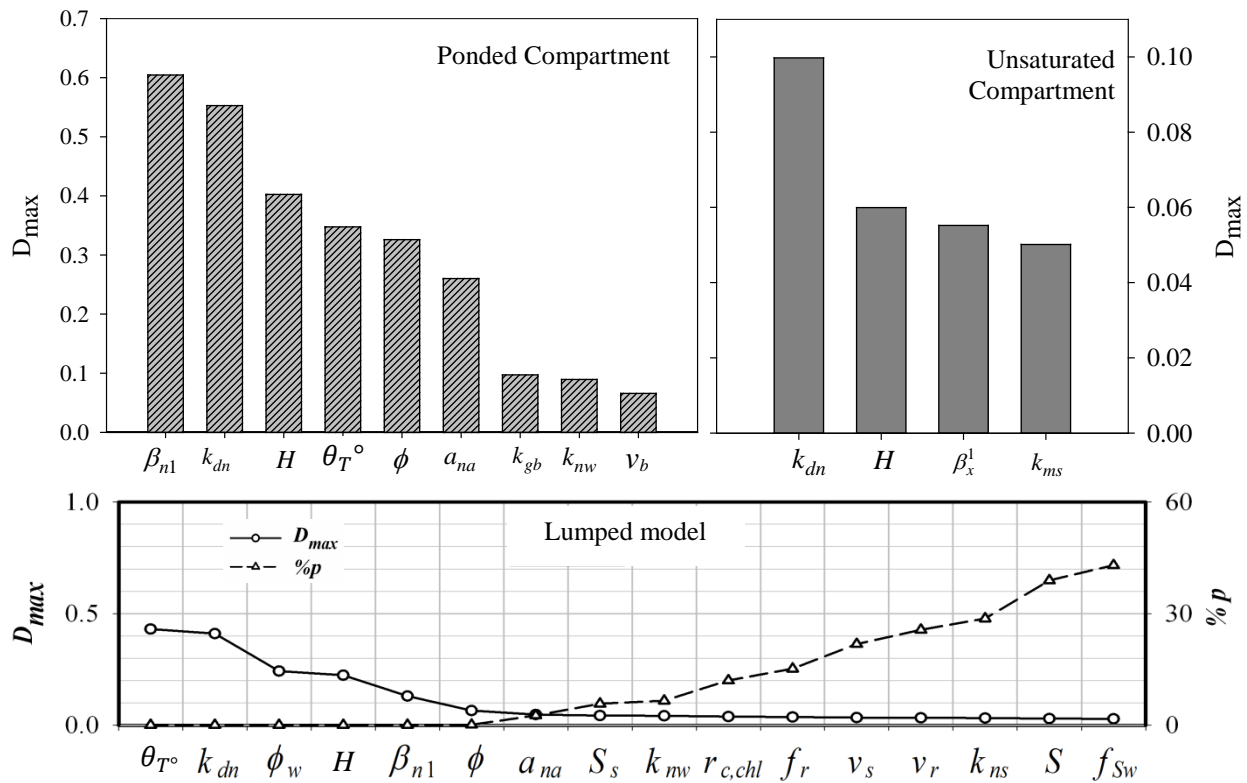


Figure 4.10: Summary of the K-S test and order of sensitivities based on  $\text{NO}_3$  loading for ponded and unsaturated compartments (top) and Lumped model (bottom, borrowed from Kalin et al., 2013)

From top right panel of Figure 4.10, with appearance of  $k_{dn}$  and  $H$  (denitrification rate and depth of active sediment layer) as top sensitive parameters, one could conclude that denitrification is the most important loss pathway of nitrate in unsaturated compartment. An explanation for this phenomenon could be that soil aeration in the unsaturated compartment promotes more nitrification in the unsaturated zone. Once nitrate is diffused into lower soil layers, denitrification is promoted in reduced soil column.

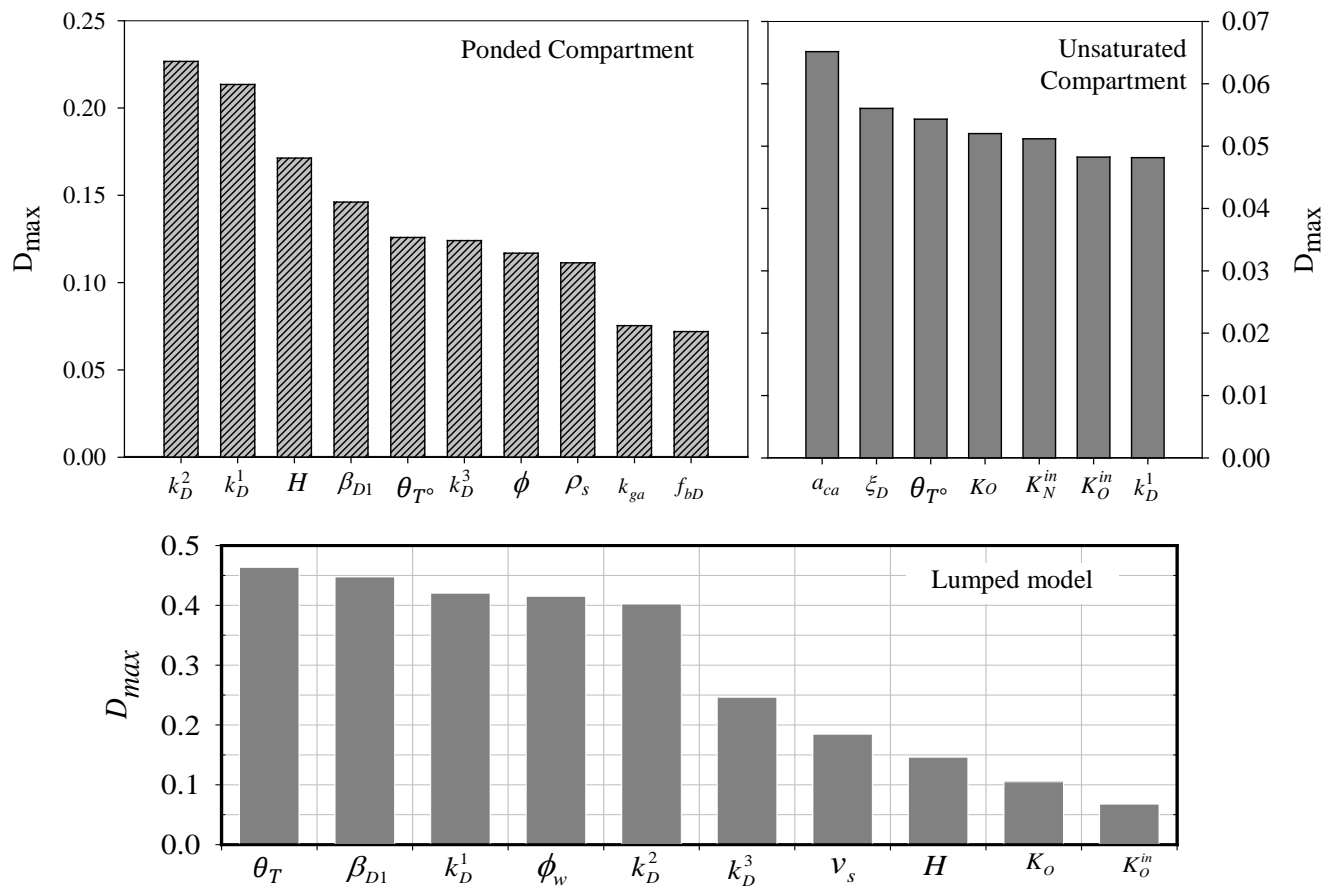


Figure 4.11: Summary of the K-S test and order of sensitivities based on TOC loading for ponded and unsaturated compartments (top) and Lumped model (bottom, borrowed from Chapter 2 )

From top right panel of Figure 4.11, an interesting observation that could be made is the appearance of  $\xi_D$  as second most sensitive parameter. Parameter  $\xi_D$  is the adjustment factor for aerobic respiration of DOC in reference to available soil moisture. Appearance of  $\xi_D$  in a sequence with  $\theta_T^\circ$  (Temperature coefficient in Arrhenius equation, Hantush et al., 2013) reveals that cycling of carbon related constituents in wetland banks (unsaturated soil) has high sensitivity to temperature and available soil moisture. Parameter  $a_{ca}$  (ratio of carbon to chlorophyll a in plants) appears as most sensitive parameter for carbon cycling of unsaturated compartment, indicating important effect of plant decomposition on C cycling in wetland banks.

### 7.3 Mass balance analysis

Table 4.4 and Table 4.5 summarize the N and C budgets and the major retention and removal pathways for ponded and unsaturated compartments during the study period. Last columns of the two tables represent earlier findings from the Lumped model (borrowed from Chapter 2 and Kalin et al., 2013). For the last two columns of both tables, all the numbers are normalized with the incoming load (shown in parentheses) to demonstrate a better picture of all the sources and sinks relative to loading. Values shown are the means +/- one standard deviation obtained from the behavioral set simulations.

According to Table 4.4, over the two year period about  $75 \pm 16\%$  of the incoming TN load left the wetland through hydrologic export. Deposition of organic N retained about  $25.5 \pm 7.0\%$  of the incoming TN load over the study period. Denitrification of nitrate in the bottom sediments and ammonia volatilization were responsible for  $12.0 \pm 9.9\%$  and  $3.6 \pm 3.9\%$  removal of TN loading, respectively. Comparing last two columns of Table 4.4, it is observable that Lumped and Expanded models have minimal differences in their nitrogen budget.

Table 4.4: Nitrogen budget in the study wetland<sup>z</sup>

	Ponded compartment	Unsaturated Compartment	<b>Total</b>	<i>Lumped model</i> <sup>y</sup>
<i>Run off</i>	336.3	N.A.	336.3 (95.8)	336.3 (95.8%) <sup>¥</sup>
<i>Atmospheric Deposition</i>	14.6	N.A.	14.6 (4.2)	14.6 (4.2%)
<i>Outflow</i>	262.3 ± 55.9	N.A.	262.3 ± 55.9 (74.7 ± 15.9%)	269.2 ± 36.7 (76.7 ± 10.5%)
<i>Net Deposition</i>	89.4 ± 24.5	N.A.	89.4 ± 24.5 (25.5 ± 7.0%)	64.6 ± 31.3 (18.4 ± 8.9%)
<i>Volatilization</i>	11.3 ± 11.8	1.2 ± 1.9	12.5 ± 13.7 (3.6 ± 3.9%)	8.1 ± 6.8 (2.3 ± 1.9%)
<i>Denitrification</i>	9.5 ± 5.5	32.7 ± 29.3	42.2 ± 34.8 (12.0 ± 9.9%)	27.9 ± 5.8 (7.9 ± 1.6%)
<i>NH<sub>4</sub> diffusion</i>	-10.1 ± 28.1	N.A.	-10.1 ± 28.1 (-2.88 ± 8.0%)	-1.1 ± 2.8 (-0.3 ± 0.8%)
<i>NO<sub>3</sub> diffusion</i>	14.7 ± 3.3	N.A.	14.7 ± 3.3 (4.19 ± 0.94%)	31.6 ± 5.0 (9.0 ± 1.4%)

<sup>z</sup>All Units are in kg

<sup>y</sup>Results of the Lumped model are borrowed from Kalin et al. (2013)

<sup>¥</sup>Numbers in parentheses are values normalized with runoff loading+atmospheric deposition

The most notable difference is in the mass of denitrification, where the Expanded model reports almost 50% more denitrification than the Lumped model (42.2 ± 34.8 kg vs. 27.9 ± 5.8 kg). It is also notable that the uncertainty related to denitrification in the Expanded model is much higher than that of the Lumped model, with the large uncertainty stemming from the unsaturated compartment. Denitrification in unsaturated compartment is reported around 3 times higher than that of the ponded compartment (32.7 ± 29.3 kg vs. 9.5 ± 5.5 kg) whereas ammonia volatilization in unsaturated compartment was a fraction of that of ponded compartment (1.2 ± 1.9 kg vs. 11.3 ± 11.8 kg). The latter observation could be a result of higher nitrification activity in aerobic wetland soil and less availability of ammonia. In general, the Expanded model has a higher

uncertainty compared to Lumped model. This was not unexpected given that the unsaturated model has a larger number of parameters, and lack of field observations for direct validation of the unsaturated compartment results.

Table 4.5 presents the carbon mass exchanges and exports for the study wetland, averaged over behavioral model outputs over the simulation period. During the study period, 3849 kg of organic carbon was washed into the wetland through inflow and  $360.3 \pm 177.6$  kg of atmospheric C was fixed by plants. Over the two year period,  $1398.5 \pm 302.8$  kg of OC ( $36.3 \pm 7.7\%$  of OC loading) was removed via microbial decomposition processes and eventually emitted to the atmosphere in inorganic form (Gaseous loss). Diffusion of DOC to soil layers retained  $312.9 \pm 118$  kg ( $8.1 \pm 3.1\%$ ) and a minimal amount ( $180.8 \pm 88.4$  kg, equivalent to  $4.7 \pm 2.3\%$  of OC load) was retained in the soil as a result of settling.

Similar to earlier findings, the Lumped and Expanded models are in agreement and report close numbers for carbon budget in the study wetland. The most prominent difference is in the mass of accumulated biomass where the Expanded model reports twice as much biomass accumulation compared to the Lumped model. This difference lies in the structural difference between the two models. As explained earlier in the Sat/Unsat scheme of Expanded model, the total area of the wetland is monitored (ponded + unsaturated compartments), as opposed to the Lumped where the area of the wetland shrinks and expands with rise and fall of water level in ponded sections of the wetland. In other words, the Lumped model ignores plants that grow out of the ponded boundary whereas the Expanded model considers both ponded and unsaturated areas. The model reports minimal gaseous losses from unsaturated compartments which might be due to low availability of labile OC in those areas.

Table 4.5: Carbon budgets in the study wetland<sup>z</sup>

	Ponded compartment	Unsaturated Compartment	<b>Total</b>	<i>Lumped model</i> <sup>y</sup>
<i>Run off</i>	3849	N.A.	3849	3849
<i>Outflow</i>	2338.1 ± 173.4	N.A.	2338.1 ± 173.4 (60.7 ± 4.5%)	2430±152 (63.1 ± 4.0%)
<i>Gaseous losses</i>	1328.7 ± 261.3	69.8 ± 41.5	1398.5 ± 302.8 (36.3 ± 7.9%)	1350± 269 (35.1 ± 7.0%)
<i>Deposition</i>	180.8 ± 88.4	N.A.	180.8 ± 88.4 (4.7 ± 2.3%)	172±79 (4.5 ± 2.1%)
<i>Biomass accumulation</i> <sup>ξ</sup>	180.6 ± 89.0	179.7 ± 88.6	360.3 ± 177.6 (9.4 ± 4.6%)	176±88 (4.6 ± 2.3%)
<i>Diffusion</i>	312.9 ± 118	N.A.	312.9 ± 118 (8.1 ± 3.1%)	269 122 (7.0 ± 3.2%)

<sup>z</sup> All Units are in kg

<sup>y</sup> Results of the Lumped model are borrowed from Chapter 2

<sup>¥</sup> Numbers in parentheses are values normalized with runoff loading

<sup>ξ</sup> Biomass accumulation is equivalent to net primary productivity multiplied by area

## 8. Summary and Conclusion

In this chapter, we aimed to extending WetQual models capabilities to simulate geochemical reactions in parts of the wetland that are not flooded (unsaturated wetland soil). To accomplish these goals, we first implemented a comprehensive module for tracking moisture in wetland soil. The rapidly converging finite difference solution to Richard's equation, introduced by van Dam and Feddes (2000), was coded in the model to trace soil moisture in unsaturated wetland soil. Once daily soil moisture profile of wetland soil were attained, model relationships were updated to simulate geochemical reactions and track concentrations of N, C, P related constituents in wetland soil. A proper model validation required field measurements of soil moisture and constituent concentration in wetland soil for a period of time. Such data were not available to us, thus we turned to available datasets for model validation. The developed model was applied to a study wetland, previously introduced in Chapter 2. The study wetland is a small restored wetland

located on Kent Island, Maryland which was monitored flow and water quality data for approximately 2 years. Although we were not able to completely validate the new developments in the model, we were able to quantify mass exchanges through microbial activities in the unsaturated banks of the study wetland, a task which was not possible before.

Although we initially considered assessing model sensitivity to parameters embedded in Richard equation, multiple crashes of the numerical model forced us to run the soil moisture model deterministically. A side by side comparison of simulated soil moisture time series (in banks of wetland) with depth of ponding (in the center) showed that local minima and maxima of the two graphs to coincide, indicating the validity of soil moisture module.

The parameters that appeared sensitive for ponded compartment (through KS test) more or less conformed to the sensitive parameters of the Lumped model; however, the order of sensitivity was not necessarily the same. KS test also revealed that carbon cycling in the unsaturated zone has high sensitivity to temperature and available soil moisture. Mass balance analysis revealed that Lumped and Expanded models have minimal differences in their nitrogen and carbon budget. For N budget, the most notable difference appeared in the mass of denitrification, where the Expanded model reported almost 50% more denitrification than the Lumped model. Denitrification in unsaturated compartment was reported around 3 times higher than that of the ponded compartment whereas ammonia volatilization in unsaturated compartment was a fraction of that of ponded compartment. Regarding carbon mass balance, model reported minimal gaseous losses from unsaturated compartments which could have been due to low availability of labile OC in those areas. Expanded model reported twice as much biomass accumulation in the study wetland compared to the Lumped model.

## 9. Appendix

This appendix shows derivation of coefficients required for numerical solution of Richard's equation. In addition, the methodology of defining top and bottom boundary conditions are explained. Material presented in Appendix are mainly adopted from van Dame and Feddes (2000).

### 9.1 Intermediate nodes

As mentioned earlier, Equation (4.1) could be re-arranged to form a tri-diagonal system of matrices (see Equations (4.5) and (4.6)). For intermediate nodes, coefficients  $\alpha$ ,  $\beta$ ,  $\gamma$  and  $f$  could be derived as:

$$\begin{aligned}\alpha_i &= -\frac{\Delta t}{\Delta Z^2} K_{i-0.5}^j \\ \beta_i &= C_i^{j+1,p-1} + \frac{\Delta t}{\Delta Z^2} (K_{i-0.5}^j + K_{i+0.5}^j) \\ \gamma_i &= -\frac{\Delta t}{\Delta Z^2} K_{i+0.5}^j\end{aligned}\tag{4.37}$$

$$f_i = C_i^{j+1,p-1} h_i^{j+1,p-1} - \theta_i^{j+1,p-1} + \theta_i^j + \frac{\Delta t}{\Delta Z} (K_{i-0.5}^j + K_{i+0.5}^j) - \Delta t^j S_i^j$$

where subscript  $i$  is the node number, superscript  $j$  is the time level,  $\Delta t$  is length of each timestep and  $\Delta z$  is compartment thickness. Superscript  $p$  is the picard iteration level, thus  $C_i^{j+1,p-1}$  is the water capacity evaluated at the pressure head value of the last picard iteration,  $h_i^{j+1,p-1}$ .

$K_{i-0.5}^j$  and  $K_{i+0.5}^j$  are internodal hydraulic conductivity for  $i^{th}$  node such that:

$$K_{i-0.5}^j = \frac{1}{2}(K_{i-1}^j + K_i^j) \quad (4.38)$$

$$K_{i+0.5}^j = \frac{1}{2}(K_{i+1}^j + K_i^j)$$

Hydraulic conductivity ( $K$ ) and soil water extractions ( $S$ ) are evaluated at the old time level  $j$ ,

## 9.2 Top node

The following figure exhibits the procedure for selecting top boundary conditions through the iterative solution of the Richards equation (Redrawn from van Dam and Feddes, 2000):

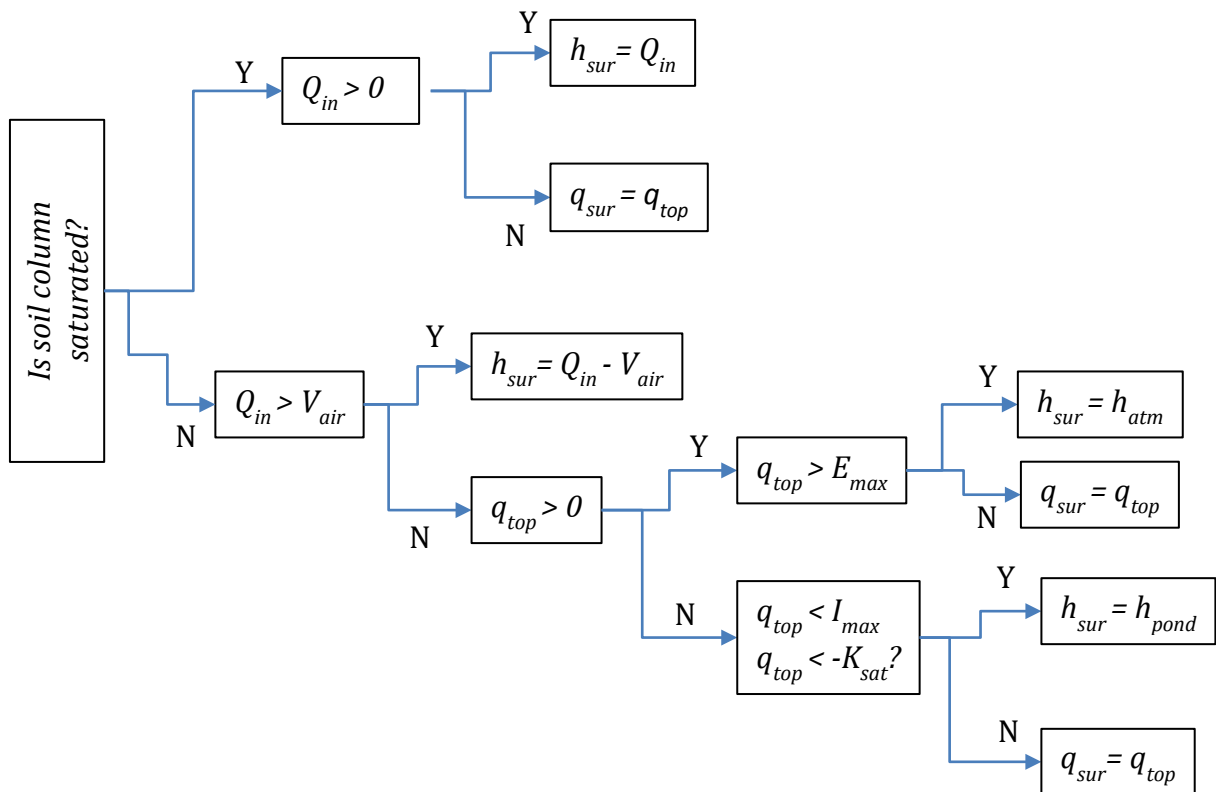


Figure 4.12: The procedure for selecting top boundary conditions through the iterative solution of the Richards equation (van Dam and Feddes, 2000)

where

$$Q_{in} = (q_{bot} - q_{top} - q_{root})\Delta t$$

$$q_{top} = q_{ET} - q_{prec} - \frac{h_{pond}}{\Delta t}$$

$$I_{max} = K_{\left(\frac{1}{2}\right)} \left( \frac{h_{pond} - 1}{2} \right) \quad (4.39)$$

$$E_{max} = K_{\left(\frac{1}{2}\right)} \left( \frac{h_{atm} - h_1^{j+1,p-1} - z_1}{z_1} \right)$$

in which  $q_{bot}$  is the flux at the soil profile bottom ( $LT^{-1}$ ),  $q_{top}$  is the potential flux at the soil surface ( $LT^{-1}$ ),  $q_{root}$  is the rate of extraction of water by roots ( $LT^{-1}$ ),  $q_{ET}$  is the actual soil surface evaporation ( $LT^{-1}$ ),  $q_{prec}$  is the precipitation rate at the soil surface ( $LT^{-1}$ ),  $h_{pond}$  is the height of the water ponding at soil surface (L),  $I_{max}$  is maximum infiltration rate at the soil surface ( $LT^{-1}$ ),  $V_{air}$  is the pore volume in soil profile which is filled with air,  $E_{max}$  is the maximum ET flux that soil can sustain ( $LT^{-1}$ ).

### 9.2.1 Flux boundary condition (flux controlled, $q_{sur}$ )

For the top node under flux control, coefficients  $\beta$ ,  $\gamma$  and  $f$  could be derived as:

$$\beta_1 = C_1^{j+1,p-1} + \frac{\Delta t}{\Delta Z^2} K_{1.5}^j$$

$$\gamma_1 = -\frac{\Delta t}{\Delta Z^2} K_{1.5}^j \quad (4.40)$$

$$f_1 = C_1^{j+1,p-1} h_1^{j+1,p-1} - \theta_1^{j+1,p-1} + \theta_1^j + \frac{\Delta t}{\Delta Z} (q_{sur} - K_{1.5}^j) - \Delta t^j S_i^j$$

### 9.2.2 Head boundary condition (head controlled, $h_{sur}$ )

For the top node under head control, coefficients  $\beta$ ,  $\gamma$  and  $f$  could be derived as:

$$\beta_1 = C_1^{j+1,p-1} + \frac{\Delta t}{\Delta Z^2} (K_{0.5}^j + K_{1.5}^j)$$

$$\gamma_1 = -\frac{\Delta t}{\Delta Z^2} K_{1.5}^j \quad (4.41)$$

$$f_1 = C_1^{j+1,p-1} h_1^{j+1,p-1} - \theta_1^{j+1,p-1} + \theta_1^j + \frac{\Delta t}{\Delta Z} (K_{0.5}^j - K_{1.5}^j) + \frac{\Delta t}{\Delta Z^2} K_{0.5}^j h_{sur} - \Delta t^j S_i^j$$

### 9.3 Bottom node

As mentioned earlier, bottom boundary conditions vary depending on presence of GW table. If there is an existing GW table, the bottom boundary is head controlled, with  $h=0$  at GW level.

When GW table is non-existent, the bottom flux ( $q_{bot} = -K_{n+\frac{1}{2}}^{j+1}$ ) controls the bottom boundary conditions.

#### 9.3.1 Flux boundary condition (flux controlled, $q_{bot}$ )

For the bottom node under flux control, coefficients  $\beta$ ,  $\alpha$  and  $f$  could be derived as:

$$\alpha_n = -\frac{\Delta t}{\Delta Z^2} K_{n-0.5}^j$$

$$\beta_n = C_n^{j+1,p-1} + \frac{\Delta t}{\Delta Z^2} K_{n-0.5}^j \quad (4.42)$$

$$f_n = C_n^{j+1,p-1} h_n^{j+1,p-1} - \theta_n^{j+1,p-1} + \theta_n^j + \frac{\Delta t}{\Delta Z} (q_{bot} + K_{n-0.5}^j) - \Delta t^j S_n^j$$

### 9.3.2 Head boundary condition (head controlled, $h_{bot}$ )

For the bottom node under head control, coefficients  $\beta$ ,  $\alpha$  and  $f$  could be derived as:

$$\begin{aligned}\alpha_n &= -\frac{\Delta t}{\Delta Z^2} K_{n-0.5}^j \\ \beta_n &= C_n^{j+1,p-1} + \frac{\Delta t}{\Delta Z^2} (K_{n-0.5}^j + K_{n+1.5}^j) \\ f_n &= C_n^{j+1,p-1} h_n^{j+1,p-1} - \theta_n^{j+1,p-1} + \theta_n^j + \frac{\Delta t}{\Delta Z} (K_{n-0.5}^j - K_{n+0.5}^j) \\ &\quad + \frac{\Delta t}{\Delta Z^2} K_{n+0.5}^j h_{bot} - \Delta t^j S_n^j\end{aligned}\tag{4.43}$$

## **Chapter 5: Conclusions**

### **1. Summary and Conclusions**

Wetlands possess qualities that distinguish them as the most important influencer of the global C budgets. They have the highest carbon density among all terrestrial ecosystems and are known as the greatest individual source of methane emission to the atmosphere. Wetlands are also the primary source of humic substances to freshwater aquatic systems. In this study, the overall objective was to advance the current state of wetland modeling by introducing a comprehensive mechanistic wetland carbon cycling model. In Chapter 1, three main objectives were presented. Each of these objectives is summarized below, and following that, the most important findings are listed.

#### **1.1 Objective 1**

To develop a mechanistic wetland carbon cycling model that reflects various physical and biogeochemical interactions affecting C cycling in flooded wetlands, and is capable of simulating the dynamics of OC retention, OC export and GHG emissions on the same platform.

Using field collected data from a small restored wetland on the eastern shore of the Chesapeake Bay, model credibility was evaluated and a thorough sensitivity and uncertainty analysis was carried out. It was found that:

- 1- Model performed well in capturing TOC export fluctuations and dynamics from the study wetland. Model appeared to be more reliable and less uncertain when it's predictions on

TOC mass export is used; nevertheless, model performance on concentration simulations was shown to be relatively acceptable too.

- 2- Model showed a narrow behavioral uncertainty in predicting TOC export, however, overall model uncertainty peaked substantially when outflow was high.
- 3- Over the period of 2 years, the study wetland removed equivalent to  $35.1 \pm 7.0\%$  of the OC carbon intake via OC decomposition, and retained equivalent to  $11.5 \pm 5.3\%$  mainly through DOC diffusion to sediment. Thus, the study wetland appeared as a carbon sink rather than source

## 1.2 Objective 2

To improve model's spatial resolution in the horizontal domain (x-y plain) through compartmentalization, enabling it to capture the spatial variability of geochemical reactions along different zones of the wetland.

The compartmental model was applied to data collected from a restored wetland in California's Central Valley. The study wetland had a formation of a large stagnant zone, constituting more than 50% of its area. It was found that:

- 1- Over the course of the study period, about  $23.4 \pm 3.9\%$  of the incoming TN load and  $21.1 \pm 4.4\%$  of the TOC load was removed or retained by study wetland
  - 2- Mass of all exchanges (physical and biogeochemical) regarding nitrogen and carbon cycling decreased along the activity gradient (from active to passive zones)
  - 3- More deposition of OC occurred in active and transient zones compared to passive zone.
- It was also revealed that anaerobic processes become more significant along activity gradient toward passive areas.

- 4- Capacities of the compartmentalized model were not exploited to its full content, due to lack of observed data for each compartment.

### **1.3 Objective 3**

To extend model's capabilities to simulate geochemical reactions in unsaturated wetland soil and to track constituent concentrations in parts of the wetland that are not flooded.

A comprehensive module for tracking moisture in wetland soil was implemented and model relationships were updated to simulate geochemical reactions and track concentrations of N, C, P related constituents in wetland soil. The developed model was applied to the study wetland previously introduced in Chapter 2, and results of the two models were compared. It was found that:

- 1- Lumped and Expanded models (models developed for objective 1 and 3, respectively) had minimal differences in their nitrogen and carbon budget. For N budget, the most notable difference appeared in the mass of denitrification, where the Expanded model reported almost 50% more denitrification than the Lumped model.
- 2- Denitrification in unsaturated compartment was reported around 3 times higher than that of the ponded compartment whereas ammonia volatilization in unsaturated compartment was a fraction of that of ponded compartment.
- 3- Expanded model reported twice as much biomass accumulation in the study wetland compared to the Lumped model.

## 2. Future research

There are several sources of uncertainties in current model (structural uncertainty+ parameter uncertainty) which need to be addressed in future studies. For second objective of this study, we expanded the model to capture the spatial variability of geochemical reactions along different zones of the wetland; however, due to lack of a proper dataset, we were not able to assess model's uncertainty to its full content. Similarly, uncertainty of model developed for the third objective was not assessed completely since we were missing a dataset containing constituent concentrations in wetland soil. For future research, I suggest evaluation of the developed model by applying it to different case studies. For instance, in case of the model developed for objective 2, a study wetland which has been sampled in several locations (along activity gradient) for a period of time would be ideal for assessing model uncertainty.

WetQual model does not possess a standalone hydrologic module and is currently dependable on observed hydrologic data. This is a major drawback of the model and needs to be addressed. For future research, development of a comprehensive hydrologic module that is capable of simulating water levels in ponded compartments, outflow discharge, infiltration losses and advective exchanges between ponded compartments is suggested.

The model developed in this study (WetQual model) provides a useful tool for quantifying and predicting impacts of climate change or management alternatives on N, P and C cycling in wetlands. For future research, a joint application of WetQual model along with a watershed model could be useful for understanding effects of different scenarios on water quality and geochemistry of wetlands.

Many popular watershed scale water quality models fail to explain wetland specific biogeochemical processes and mostly ignore the role of wetlands in recycling nutrients. Wetland soils are treated the same as upland soils and flooded wetlands are not distinguished from other impoundments. A future study could be designed around incorporating WetQual model in to a well-known watershed model such as SWAT (Neitsch et al., 2005) in order to enhance SWAT's performance in simulating wetlands nutrient cycling functions.

My other suggestions for future studies are:

- To enhance the primary productivity component in the model. Currently WetQual uses a simple mass balance model for plant biomass growth and death (Chapra, 1997). The current NPP model is too simple to simulate plant growth in more complicated environments, like forested wetlands.
- To design a GUI (Graphical user interface) for the model. WetQual model at this stage is consisted of a few thousand lines of codes, and too complicated for public release. A GUI would help to extend the model's accessibility for public use.

## References

- Akaike, H., 1974. A new look at the statistical model identification. *Automatic Control, IEEE Transactions on* 19, 716-723
- Anderson, C.J., Mitsch, W.J., 2006. Sediment, carbon, and nutrient accumulation at two 10-year-old created riverine marshes. *Wetlands* 26, 779-792
- Arabi, M., Govindaraju, R.S., Hantush, M.M., 2007. A probabilistic approach for analysis of uncertainty in the evaluation of watershed management practices. *Journal of Hydrology* 333, 459-471
- Arah, J., Stephen, K., 1998. A model of the processes leading to methane emission from peatland. *Atmospheric Environment* 32, 3257-3264
- Aselmann, I., Crutzen, P.J., 1989. Global distribution of natural freshwater wetlands and rice paddies, their net primary productivity, seasonality and possible methane emissions. *Journal of Atmospheric chemistry* 8, 307-358
- Bade, D., 2009. Gas exchange at the air-water interface. *Encyclopedia of Inland Waters* 26, 70-78
- Bai, J., Deng, W., Zhu, Y., Wang, Q., 2004. Spatial variability of nitrogen in soils from land/inland water ecotones. *Communications in soil science and plant analysis* 35, 735-749
- Barker, J., Fritz, P., 1981. The occurrence and origin of methane in some groundwater flow systems. *Canadian Journal of Earth Sciences* 18, 1802-1816
- Beven, K., Binley, A., 1992. The future of distributed models: model calibration and uncertainty prediction. *Hydrological processes* 6, 279-298
- Beven, K., Freer, J., 2001. Equifinality, data assimilation, and uncertainty estimation in mechanistic modelling of complex environmental systems using the GLUE methodology. *Journal of Hydrology* 249, 11-29
- Boudreau, B.P., 1997. *Diagenetic models and their implementation: modelling transport and reactions in aquatic sediments*. Springer.
- Bradford, M., Ineson, P., Wookey, P., Lappin-Scott, H., 2001. Role of CH<sub>4</sub> oxidation, production and transport in forest soil CH<sub>4</sub> flux. *Soil Biology and Biochemistry* 33, 1625-1631
- Byrnes, B., Austin, E., Tays, B., 1995. Methane emissions from flooded rice soils and plants under controlled conditions. *Soil Biology and Biochemistry* 27, 331-339
- Canário, J., Vale, C., Nogueira, M., 2008. The pathway of mercury in contaminated waters determined by association with organic carbon (Tagus estuary, Portugal). *Applied Geochemistry* 23, 519-528

- Cao, M., Marshall, S., Gregson, K., 1996. Global carbon exchange and methane emissions from natural wetlands: Application of a process-based model. *Journal of Geophysical Research* 101, 14399-14414
- Cerco, C.F., Cole, T., 1995. User's Guide to the CE-QUAL-ICM Three-dimensional Eutrophication Model: Release Version 1.0. US Army Engineer Waterways Experiment Station.
- Chan, A., Parkin, T., 2000. Evaluation of potential inhibitors of methanogenesis and methane oxidation in a landfill cover soil. *Soil Biology and Biochemistry* 32, 1581-1590
- Chapra, S.C., 1997. Surface water-quality modeling. McGraw-Hill New York.
- Chow, A.T., Tanji, K.K., Gao, S., 2003. Production of dissolved organic carbon (DOC) and trihalomethane (THM) precursor from peat soils. *Water Research* 37, 4475-4485
- CIMIS, C.I.M.I.S., 2007. Climate data obtained from <http://www.cimis.water.ca.gov/cimis/welcome.jsp>
- Cui, J., Li, C., Sun, G., Trettin, C., 2005a. Linkage of MIKE SHE to Wetland-DNDC for carbon budgeting and anaerobic biogeochemistry simulation. *Biogeochemistry* 72, 147-167
- Cui, J., Li, C., Trettin, C., 2005b. Analyzing the ecosystem carbon and hydrologic characteristics of forested wetland using a biogeochemical process model. *Global Change Biology* 11, 278-289
- Dam, J.v., Huygen, J., Wesseling, J., Feddes, R., Kabat, P., Walsum, P.v., Groenendijk, P., Diepen, C.v., 1997. Theory of SWAP version 2.0; simulation of water flow, solute transport and plant growth in the soil-water-atmosphere-plant environment.
- Davidson, E., Belk, E., Boone, R.D., 1998. Soil water content and temperature as independent or confounded factors controlling soil respiration in a temperate mixed hardwood forest. *Global change biology* 4, 217-227
- Denman, K., Brasseur, G., Chidthaisong, A., Ciais, P., Cox, P., Dickinson, R., Hauglustaine, D., Heinze, C., Holland, E.J., al., e., 2007. Couplings Between Changes in the Climate System and Biogeochemistry, in: Solomon et al. (2007), pp. 499-588.
- DHI, 2004. Coastal Hydraulics and Oceanography User Guide. Danish Hydraulic Institute, Hørsholm, Denmark.
- Di Toro, D.M., 2001. Sediment flux modeling. Wiley-Interscience New York.
- Dongquan, Z., Jining, C., Haozheng, W., Qingyuan, T., 2012. Application of a sampling based the combined objective to parameter identification and uncertainty analysis of an urban rainfall-runoff modeling. *Journal of Irrigation and Drainage Engineering*
- Dunne, T., 1978. Water in environmental planning. Macmillan.
- Fan, Y., Miguez-Macho, G., 2011. A simple hydrologic framework for simulating wetlands in climate and earth system models. *Climate dynamics* 37, 253-278
- Fischer, H.B., 1979. Mixing in inland and coastal waters. Access Online via Elsevier.

- Green, W.H., Ampt, G., 1911. Studies on soil physics, 1. The flow of air and water through soils. *J. Agric. Sci* 4, 1-24
- Hanson, G.C., Groffman, P.M., Gold, A.J., 1994. Symptoms of nitrogen saturation in a riparian wetland. *Ecological Applications*, 750-756
- Hantush, M.M., Kalin, L., Isik, S., Yucekaya, A., 2013. Nutrient dynamics in flooded wetlands: I. Model development. *Journal of Hydrologic Engineering* 10.1061/(ASCE)HE.1943-5584.0000741
- Hedges, J., Keil, R., Benner, R., 1997. What happens to terrestrial organic matter in the ocean? *Organic Geochemistry* 27, 195-212
- Hornberger, G., Spear, R., 1980. Eutrophication in Peel Inlet—I. The problem-defining behavior and a mathematical model for the phosphorus scenario. *Water Research* 14, 29-42
- Horton, R.E., 1941. An approach toward a physical interpretation of infiltration-capacity. *Soil Science Society of America Journal* 5, 399-417
- Huang, Y., Zhang, W., Zheng, X., Li, J., Yu, Y., 2004. Modeling methane emission from rice paddies with various agricultural practices. *Journal of Geophysical Research* 109, D08113
- IPCC, 2007. Climate change 2007-the physical science basis: Working group I contribution to the fourth assessment report of the IPCC. Cambridge University Press.
- Ise, T., Moorcroft, P.R., 2006. The global-scale temperature and moisture dependencies of soil organic carbon decomposition: an analysis using a mechanistic decomposition model. *Biogeochemistry* 80, 217-231
- Jähne, B., Heinz, G., Dietrich, W., 1987. Measurement of the diffusion coefficients of sparingly soluble gases in water. *Journal of Geophysical Research* 92, 10767-10710,10776
- Ji, Z.-G., 2008. Hydrodynamics and water quality: modeling rivers, lakes, and estuaries. Wiley-Interscience.
- Jordan, T.E., Pittek, M.A., Hofmockel, K.H., Whigham, D.F., 2003. Nutrient and sediment removal by a restored wetland receiving agricultural runoff. *Journal of Environmental Quality* 32, 1534-1547
- Jordan, T.E., Whigham, D.F., Hofmockel, K., Gerber, N., 1999. Restored wetlands in crop fields control nutrient runoff. *Nutrient Cycling and Retention in Natural and Constructed Wetlands*. Backhuys Publishers, Leiden, The Netherlands, 49-60
- Kadlec, R.H., Wallace, S., 2008. Treatment wetlands. CRC press.
- Kalin, L., Hantush, M.M., 2006. Hydrologic modeling of an eastern Pennsylvania watershed with NEXRAD and rain gauge data. *Journal of Hydrologic Engineering* 11, 555-569
- Kalin, L., Hantush, M.M., Isik, S., Yucekaya, A., Jordan, T., 2013. Nutrient dynamics in flooded wetlands: II. Model evaluation. *Journal of Hydrologic Engineering* 10.1061/(ASCE)HE.1943-5584.0000750

- Kayranli, B., Scholz, M., Mustafa, A., Hedmark, Å., 2010. Carbon storage and fluxes within freshwater wetlands: a critical review. *Wetlands* 30, 111-124
- Keller, J.K., 2011. Wetlands and the global carbon cycle: what might the simulated past tell us about the future? *New Phytologist* 192, 789-792
- Kellner, E., Baird, A., Oosterwoud, M., Harrison, K., Waddington, J., 2006. Effect of temperature and atmospheric pressure on methane (CH<sub>4</sub>) ebullition from near-surface peats. *Geophysical research letters* 33, L18405
- King, E., Bottrell, S., Sapsford, D., Raiswell, R., 2003. Modelling carbon fluxes in a constructed wetland. *Land Contamination and Reclamation* 11, 199-204
- King, G., 1992. Ecological aspects of methane oxidation, a key determinant of global methane dynamics. *Advances in microbial ecology* 12, 431-468
- Knorr, W., Heimann, M., 2001. Uncertainties in global terrestrial biosphere modeling: 1. A comprehensive sensitivity analysis with a new photosynthesis and energy balance scheme. *Global Biogeochemical Cycles* 15, 207-225
- Kutner, M.H., Nachtsheim, C.J., Neter, J., Li, W., 2005. *Applied linear statistical models*. McGraw-Hill New York.
- Leij, F.J., 1996. UNSODA unsaturated soil hydraulic database.
- Li, T., Huang, Y., Zhang, W., Song, C., 2010a. CH<sub>4</sub>MOD- wetland: A biogeophysical model for simulating methane emissions from natural wetlands. *Ecological Modelling* 221, 666-680
- Li, T., Huang, Y., Zhang, W., Song, C., 2010b. CH<sub>4</sub>MODwetland: A biogeophysical model for simulating methane emissions from natural wetlands. *Ecological Modelling* 221, 666-680
- Little, K.W., 2012. *Environmental fate and transport analysis with compartment modeling*. CRC Press.
- Lloyd, C.R., Rebelo, L.-M., Finlayson, C.M., 2013. Providing low-budget estimations of carbon sequestration and greenhouse gas emissions in agricultural wetlands. *Environmental Research Letters* 8, 015010
- Massey Jr, F.J., 1951. The Kolmogorov-Smirnov test for goodness of fit. *Journal of the American statistical Association*, 68-78
- Maynard, J., 2009. Biogeochemical cycling and retention of carbon and nutrients in a constructed wetland receiving agricultural runoff in the San Joaquin Valley, California.
- Maynard, J.J., O'Geen, A.T., Dahlgren, R.A., 2011. Sulfide induced mobilization of wetland phosphorus depends strongly on redox and iron geochemistry. *Soil Science Society of America Journal* 75, 1986-1999
- Min, J.H., Wise, W.R., 2009. Simulating short-circuiting flow in a constructed wetland: the implications of bathymetry and vegetation effects. *Hydrological Processes* 23, 830-841
- Mitchell, D., 1994. Floodplain wetlands of the Murray-Darling Basin: management issues and challenges. *Murray-Darling Basin floodplain wetlands management*

- Mitsch, W.J., Gosselink, J.G., 2007. *Wetlands*, 4th ed. Wiley, Hoboken, N.J. xi, 582 p. pp.
- Mitsch, W.J., Straškraba, M., Jrgensen, S.E., 1988. *Wetland modelling (Developments in Environmental Modelling, v.12)*. Elsevier Science Publishers.
- Mitsch, W.J.G.J.G., 2007. *Wetlands*. Wiley, Hoboken.
- Neitsch, S., Arnold, J., Kiniry, J., Williams, J., King, K., 2005. *Soil and water assessment tool: theoretical documentation, version 2005*. Texas, USA
- Penha-Lopes, G., Flindt, M.R., Ommen, B., Kristensen, E., Garret, P., Paula, J., 2012. Organic carbon dynamics in a constructed mangrove wastewater wetland populated with benthic fauna: A modelling approach. *Ecological Modelling* 232, 97-108
- Potter, C.S., 1997. An ecosystem simulation model for methane production and emission from wetlands. *Global Biogeochemical Cycles* 11, 495-506
- Raghoebarsing, A.A., Pol, A., Van de Pas-Schoonen, K.T., Smolders, A.J., Ettwig, K.F., Rijpstra, W.I.C., Schouten, S., Damsté, J.S.S., den Camp, H.J.O., Jetten, M.S., 2006. A microbial consortium couples anaerobic methane oxidation to denitrification. *Nature* 440, 918-921
- Raich, J.W., Rastetter, E.B., Melillo, J.M., Kicklighter, D.W., Steudler, P.A., Peterson, B.J., Grace, A.L., Moore, B., Vorosmarty, C.J., 1991. Potential Net Primary Productivity in South America: Application of a Global Model. *Ecological Applications* 1, 399-429.10.2307/1941899
- Reddy, K., Schipper, L.A., 1996. Determination of methane oxidation in the rhizosphere of *Sagittaria lancifolia* using methyl fluoride. *Soil Science Society of America Journal* 60, 611-616
- Reddy, K.R., DeLaune, R.D., 2004. *Biogeochemistry of wetlands: science and applications*. Crc Press.
- Reddy, K.R., DeLaune, R.D., 2008. *Biogeochemistry of wetlands: science and applications*, 1 ed. CRC Press, Taylor & Francis Group, Boca Raton, FL
- Richards, L.A., 1931. Capillary conduction of liquids through porous mediums. *Physics* 1, 318-333
- Riera, J.L., Schindler, J.E., Kratz, T.K., 1999. Seasonal dynamics of carbon dioxide and methane in two clear-water lakes and two bog lakes in northern Wisconsin, USA. *Canadian Journal of Fisheries and Aquatic Sciences* 56, 265-274
- Runkel, R.L., Crawford, C.G., Cohn, T.A., 2004. *Load Estimator (LOADEST): A FORTRAN program for estimating constituent loads in streams and rivers*. US Department of the Interior, US Geological Survey.
- Saltelli, A., Sobol, I.M., 1995. About the use of rank transformation in sensitivity analysis of model output. *Reliability Engineering & System Safety* 50, 225-239
- Sander, R., 1999. *Compilation of Henry's law constants for inorganic and organic species of potential importance in environmental chemistry*. Max-Planck Institute of Chemistry, Air Chemistry Department

- Schnoor, J.L., 1996. Environmental modeling: fate and transport of pollutants in water, air, and soil. John Wiley and Sons.
- Sharifi, A., Kalin, L., Hantush, M.M., Isik, S., Jordan, T.E., 2013. Carbon dynamics and export from flooded wetlands: A modeling approach. *Ecological Modelling* 263, 196-210
- Sitch, S., Smith, B., Prentice, I.C., Arneth, A., Bondeau, A., Cramer, W., Kaplan, J., Levis, S., Lucht, W., Sykes, M., 2003. Evaluation of ecosystem dynamics, plant geography and terrestrial carbon cycling in the LPJ dynamic global vegetation model. *Global Change Biology* 9, 161-185
- Sleutel, S., Moeskops, B., Huybrechts, W., Vandenbossche, A., Salomez, J., De Bolle, S., Buchan, D., De Neve, S., 2008. Modeling soil moisture effects on net nitrogen mineralization in loamy wetland soils. *Wetlands* 28, 724-734
- Solomon, S., Qin, D., Manning, M., Chen, Z., Marquis, M., Averyt, K., Tignor, M., Miller, H., 2007. *Climate Change 2007: The Scientific Basis. Contribution of Working Group I to the Fourth Assessment Report of the Intergovernmental Panel on Climate Change*. Cambridge: Cambridge University Press.
- Spear, R., Hornberger, G., 1980. Eutrophication in peel inlet--II. Identification of critical uncertainties via generalized sensitivity analysis. *Water Research* 14, 43-49
- Steinberg, C., 2003. *Ecology of humic substances in freshwaters: determinants from geochemistry to ecological niches*. Springer Verlag.
- Stern, J., Wang, Y., Gu, B., Newman, J., 2007. Distribution and turnover of carbon in natural and constructed wetlands in the Florida Everglades. *Applied Geochemistry* 22, 1936-1948
- Takatert, N., Sanchez-Pérez, J.M., Trémolières, M., 1999. Spatial and temporal variations of nutrient concentration in the groundwater of a floodplain: effect of hydrology, vegetation and substrate. *Hydrological Processes* 13, 1511-1526
- Tang, J., Zhuang, Q., Shannon, R., White, J., 2010. Quantifying wetland methane emissions with process-based models of different complexities. *Biogeosciences* 7, 3817-3837
- Tranvik, L., Jansson, M., 2002. Climate change (Communication arising): Terrestrial export of organic carbon. *Nature* 415, 861-862
- Van Dam, J.C., Feddes, R.A., 2000. Numerical simulation of infiltration, evaporation and shallow groundwater levels with the Richards equation. *Journal of Hydrology* 233, 72-85
- Walter, B.P., Heimann, M., 2000. A process-based, climate-sensitive model to derive methane emissions from natural wetlands: Application to five wetland sites, sensitivity to model parameters, and climate. *Global Biogeochemical Cycles* 14, 745-765
- Walter, B.P., Heimann, M., Matthews, E., 2001. Modeling modern methane emissions from natural wetlands: 1. Model description and results. *Journal of Geophysical Research: Atmospheres* (1984–2012) 106, 34189-34206
- Walter, B.P., Heimann, M., Shannon, R., White, J., 1996. A process-based model to derive methane emissions from natural wetlands. *Geophysical Research Letters* 23, 3731-3734

- Wania, R., 2007. Modelling northern peatland land surface processes, vegetation dynamics and methane emissions, Department of Earth Sciences. University of Bristol
- Wania, R., Ross, I., Prentice, I., 2010. Implementation and evaluation of a new methane model within a dynamic global vegetation model: LPJ-WHyMe v1. 3.1. *Geosci. Model Dev* 3, 565-584
- Wanninkhof, R., Asher, W.E., Ho, D.T., Sweeney, C., McGillis, W.R., 2009. Advances in quantifying air-sea gas exchange and environmental forcing\*. *Marine Science* 1
- Worrall, F., Burt, T., Shedden, R., 2003. Long term records of riverine dissolved organic matter. *Biogeochemistry* 64, 165-178
- Yamamoto, S., Alcauskas, J.B., Crozier, T.E., 1976. Solubility of methane in distilled water and seawater. *Journal of Chemical and Engineering Data* 21, 78-80
- Yu, K., Wang, Z., Chen, G., 1997. Nitrous oxide and methane transport through rice plants. *Biology and fertility of soils* 24, 341-343
- Zhang, Y., Li, C., Trettin, C.C., Li, H., Sun, G., 2002. An integrated model of soil, hydrology, and vegetation for carbon dynamics in wetland ecosystems. *Global Biogeochemical Cycles* 16, 1061
- Zhuang, Q., McGuire, A., O'Neill, K., Harden, J., Romanovsky, V., Yarie, J., 2002. Modeling soil thermal and carbon dynamics of a fire chronosequence in interior Alaska. *Journal of Geophysical Research: Atmospheres* (1984–2012) 107, FFR 3-1-FFR 3-26
- Zhuang, Q., Melillo, J.M., Kicklighter, D.W., Prinn, R.G., McGuire, A.D., Steudler, P.A., Felzer, B.S., Hu, S., 2004a. Methane fluxes between terrestrial ecosystems and the atmosphere at northern high latitudes during the past century: A retrospective analysis with a process-based biogeochemistry model. *Global Biogeochem. Cycles* 18, GB3010.10.1029/2004gb002239
- Zhuang, Q., Melillo, J.M., Kicklighter, D.W., Prinn, R.G., McGuire, A.D., Steudler, P.A., Felzer, B.S., Hu, S., 2004b. Methane fluxes between terrestrial ecosystems and the atmosphere at northern high latitudes during the past century: A retrospective analysis with a process-based biogeochemistry model. *Global Biogeochemical Cycles* 18
- Ziegler, S.E., Fogel, M.L., 2003. Seasonal and diel relationships between the isotopic compositions of dissolved and particulate organic matter in freshwater ecosystems. *Biogeochemistry* 64, 25-52